2020

In Vivo Data Capture Using HSSR for Calibration of Computational Models

Thor Erik Andreassen

In Vivo Data Capture Using HSSR for Calibration of Computational Models

_____

A Thesis

Presented to

the Faculty of the Daniel Felix Ritchie School of Engineering and Computer Science

University of Denver

_____

In Partial Fulfillment

of the Requirements for the Degree

Master of Science

_____

by

Thor Andreassen

June 2020

Advisor: Dr. Kevin Shelburne

Author: Thor Andreassen
Title: In Vivo Data Capture Using HSSR for Calibration of Computational Models
Advisor: Dr. Kevin Shelburne
Degree Date: June 2020

Abstract

Computational modeling is a vital tool for understanding and evaluating healthy and unhealthy function of the musculoskeletal aspects of the human body. However, the accuracy of the musculoskeletal models depends significantly on the accuracy of the input data used to calibrate various behavioral parameters of the model. To date, most computational models have been built using generic *in vitro* data, mostly because of a lack of accurate and meaningful datasets from *in vivo* testing. The next major step in computational modeling is to create subject-specific computational models using calibration data taken from *in vivo* testing. The overall goal was to develop custom devices that when combined with high-speed stereo radiography (HSSR) techniques allow the measurement of *in vivo* subject data for use in the calibration of computational models. A leg press, and a knee laxity apparatus, were designed, built, and validated for use with HSSR for *in vivo* subject-specific data collection.

Acknowledgments

There is a long list of people that I would like to thank for their contributions and support in helping make this thesis and the larger work as a whole possible. Firstly, I would like to show my utmost appreciation to my advisor, Dr. Kevin Shelburne, for his unending teaching, guidance, expertise, and support through the entire process, for which this work would not exist without. Not to mention, for being the reason that I came to the Center for Orthopaedic Biomechanics at the University of Denver in the first place. Secondly, I would sincerely like to thank Dr. Landon Hamilton, for his integral part in designing and building all the custom devices and his countless hours spent aiding in the data collections. I would also like to thank Dr. Chadd Clary for his numerous contributions and guidance in cadaveric testing and data processing, as well as for participating in my defense committee. I would additionally like to thank Dr. Dinah Loerke for participating in my defense committee. I would also like to thank Dr. Donald Hume, Sean Higinbotham, and Yashar Behnam, for all their help in data collections, and their advice at different stages of the work. I would like to thank Stormy Hegg, and Ryan Knowles for their help in tracking and segmenting. Last but certainly not least, to my family, girlfriend, and all my friends and colleagues at the Ritchie School of Engineering and Computer Science at the University of Denver, I would like to thank you all for your never-ending support and for keeping me sane, none of this would have been possible without you.

Table of Contents

List of Figures

Chapter 1: Introduction

1.1. Motivation

Precision medicine seeks to improve healthcare by tailoring treatment of individuals and groups to their specific characteristics and anatomy. Following this new trend, computer models of people that inform the understanding of pathology and treatment must become more patient-specific. Historically, computer models have been generic, that is, designed to simulate average individuals and populations based on tissue geometry and properties most often derived from in vitro measurements from a variety of sources in the literature. More recently, computer models of the lower limbs and knee have been made specimen-specific to mimic the mechanics of individual cadaveric specimens. The next step is to develop patient-specific models of the knee. In particular, knee joint motion and joint stiffness must be measured in vivo to enable the calibration of patient-specific models of the knee. Moreover, these measurements of motion and stiffness have their value in the diagnosis and evaluation of joint pathology and repair.

Therefore, the overall goal of this research was to design, build, and validate methods of gathering accurate and useful quantitative subject-specific in vivo measurements for use in future calibration of subject-specific knee models. The hope is that this work will inform future individuals on the means and viability of in vivo assessment for model calibration.

1.2. Objectives

The overall goal was accomplished through three specific aims:

1. Design and build a device capable of measuring an individual's passive and weight-bearing knee range of motion (ROM) kinematics under known loads through the entire flexion cycle using HSSR.
2. Design, build, and evaluate a device capable of accurately measuring an individual's anterior-posterior (AP) and internal-external (IE) knee laxity at several knee flexion angles under a range of loads using HSSR. This aim has been the focus of the work.
3. Evaluate the performance of the knee laxity measurement device from Aim 2 against measurements taken from a validated laxity device.

1.3. Overall Format

This thesis will begin in Chapter 2 with a literature review of the different aspects of in vivo measurements for ROM, and laxity measurements, and then a review of in vivo data capture for use in model calibration. Chapter 3 will then layout the design of a leg press capable of ROM data capture sufficient for Aim 1 of the work, followed by an in-depth design of a novel device for in vivo laxity assessment for Aim 2 of the work. Chapter 4 will then briefly reiterate the design of the laxity assessment device, and then use captured specimen and subject data to validate the use of the device in vivo. Lastly, Chapter 5 will discuss and conclude on the validity and lessons learned of devices for in vivo data capture, as well as discuss future work possibilities surrounding the use of these devices for in vivo data capture for computational modeling.

Chapter 2: Literature Review

2.1. Passive Range of Motion

Range of motion is a crucial part of the evaluation of joint health. In general, there are two types of range of motion: passive and active. Active ROM is generally defined as the ROM that can be achieved by the subject using their muscle force production; while, Passive ROM is generally defined as the ROM that an evaluator can cause the joint to go through [1]. Individuals with adequate muscle force production, usually have little difference between the Passive and the Active ROM, while individuals with discrepancy may indicate muscle weakness.

In the knee joint, in particular, ROM is a key feature used by clinicians in the evaluation of general knee healthy. Evidence has shown that knee ROM is affected after ACL injuries, joint arthroplasty, and general knee injuries [2]. In computational modeling, knee ROM is used to calibrate passive ligament parameters, as well as to evaluate the validity of the ligament stiffness models [3]. As such, a means of accurately gathering kinematic data through the full knee ROM is needed.

The most common method to measure knee ROM still used today, is to use a goniometer, such as the one shown in Figure 2-1 and manually measure the angle of the tibia relative to the femur at the full extension pose of the patient, as well as the pose of the patient at the fully flexed position, for both the active and passive positions [1,4].

Figure 2-1 Goniometer Knee Flexion Angle Setup from Hancock et al. [5]

However, work has shown that the accuracy of these methods has a great deal of inter and intratester variability in the final measurements [5]. Another means of measuring ROM is to flex the knee and capture an Xray image of the knee and then draw lines on the Tibia and Femur in the Xray to determine the knee angle, which has shown to have improved accuracy over surface goniometer measurements [6]. However, both of these methods are limited to only determining the total extrema of the ROM, and thus are unable to determine or observe any kinematic patterns that occur through the flexion cycle, which is the most useful for computational model calibration.

Recent work has focused on using MRI measurements and Xray fluoroscopy as a means of accurately capturing the knee kinematics at a range of flexion angles through the ROM. MRI measurements an MRI, to first capture detailed geometry of the bones and tissue at full extension to create 3D bone geometry [7]. Then shorter/lower fidelity scans are taken at different flexion angles through the ROM. Then the 3D bone

geometries are mapped to these scans to calculate the position of the bones at various flexion angles, shown in Figure 2-2. This method is advantageous as it does not subject the subject to any radiation, and captures the exact position of the soft tissues at various portions of the flexion cycle. The soft tissue geometry is particularly useful for calibration and validation of computational models, as the exact locations of the ligaments and geometry can be compared through the flexion cycle to the positions in the computational model. However, there are also a few drawbacks to this method. The first is that the analysis can only be done for static shots, and thus the more substantial inertial effects cannot be taken into account. The flexion will skip from one angle to the next without observing the motion in between. The other is that process takes a significant amount of time to gather enough MRI scans at each flexion angle to allow for post alignment.

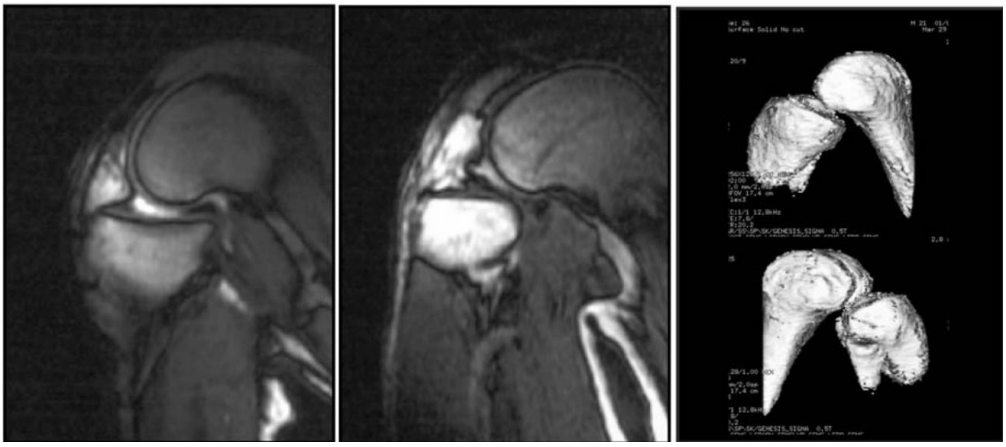

Figure 2-2 Interventional MRI scans for Knee ROM from Johal et al. [7]

Fluoroscopic based methods use a series of Xrays and bone geometries of the subject taken from CT and MRI, to match the 3D bone geometries to the projection of the bones in the Xrays during the activity. Several studies have performed single-plane fluoroscopy,

which uses a single Xray source and observes the knee motion from extension to deep flexion of up to 150°, shown below in Figure 2-3 [8,9]. These have the advantage that they can capture inertial effects as there is effectively no time stuck at a single angle like in the MRI case. They also work significantly faster, allowing for repeats of trials or other datasets to be gathered in the same amount of time that the MRI methods would take. However, work has shown that the error of single-plane can be upwards of 4 mm for translation DOF and 3° for rotational DOF, especially for specific viewing planes [10].

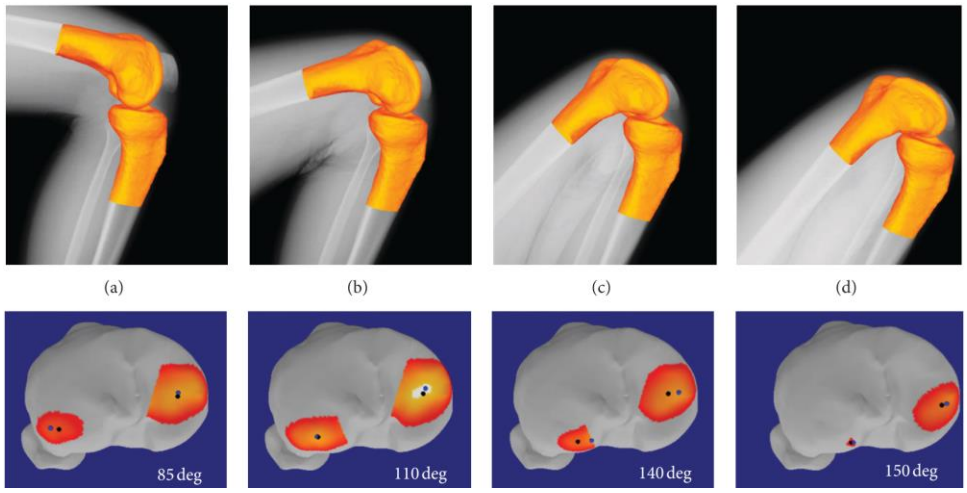

Figure 2-3 Deep Knee ROM Captured from Single Plane Fluoroscopy from Hamai et al. [9]

In Contrast, bi-plane fluoroscopy or High-Speed Stereo Radiography (HSSR) can be used to more accurately capture the kinematics. HSSR uses two offset radiograph images to more accurately calculate the location of the bones in 3D space. In 2001, Hasano et al. used HSSR techniques to capture passive knee ROM characteristics from hyperextension to 120° of knee flexion. However, their work was limited to only measuring passive ROM, which is known to often be less than the active ROM, particularly in people with muscle weakness. This limitation to only passive ROM, exists because it becomes

challenging to have an evaluator create the motion necessary for the observation of the full active ROM without exposing the evaluator to the Xray radiation; as well as the motion would be challenging to create a natural fluid motion of the knee through this active ROM. As such, different motion activities are used to observe the knee behavior in the deeper active flexion regions, such as the knee lunge.

The lunge is a commonly performed trial in *in vivo* studies to capture deep active ROM behaviors [11–13]. It provides a manner of loaded activity, through the person's body weight to pull the knee through the ROM, shown below in Figure 2-4.

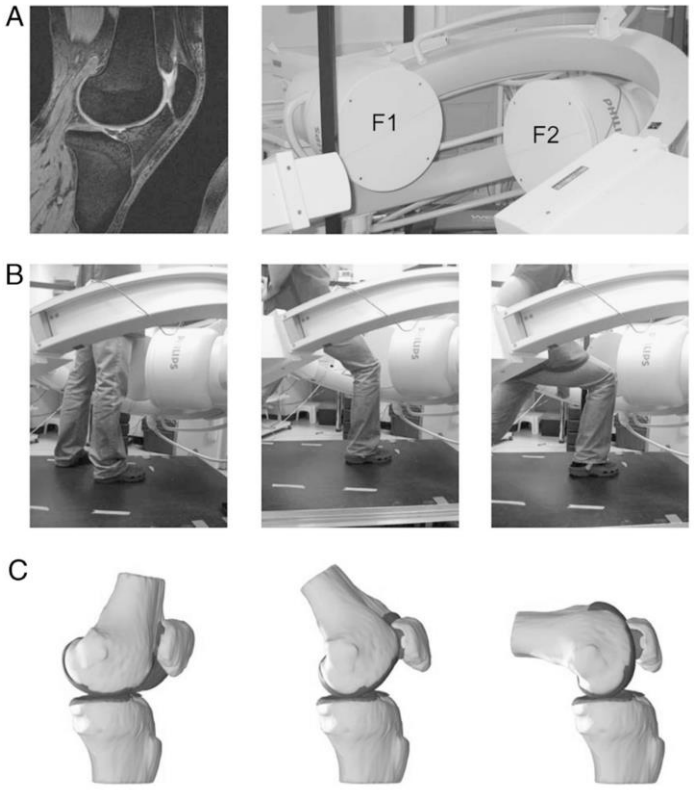

Figure 2-4 Knee Lunge Activity Setup, Activity, and Model Kinematics from Van De Velde et al. [12]

However, these same studies mention that many subjects are unable to perform these motions, and that the consistency in the motion compared to the desired motion for the

task is iffy. At the same time, the deepest flexion angles observed are often less than 90°. In theory, the lunge should be capable of observing the deep flexion ROM that the activity is designed to observe, but the lunge task often falls short. As such, passive ROM trials are commonly the only data used and captured. The discrepancy that exists between the passive ROM and the active ROM trials is a crucial feature in evaluating muscle strength, and can be useful in informing muscle parameters in subject-specific computational models. However, without accurately gathering the active ROM data, computational models are missing out on critical information that could be useful in informing subject model muscle strength. What is needed is a means of capturing the active ROM of the knee joint, like the passive ROM trials, with the ability to adjust the amount of load applied.

2.2. Joint Laxity

2.2.1. Laxity Definition and Introduction

Joint laxity is a term that is not well defined and has no generally accepted meaning. Different definitions exist while primarily describing various aspects of the same underlying phenomena. This thesis will use a definition of laxity that is most correlated to fundamental engineering concepts; joint laxity represents the relative motion of a joint that results from the passive force-displacement relationships due to the non-linear interactions of the underlying tissues [14]. Put more simply, joint laxity is an overarching term for the interactions of underlying soft-tissue structures to create a complicated relationship between an applied force at a joint and the resulting motion of one bone relative to the other.

The following discussion has been sub-divided into the following sections: a brief review of the clinical understanding and use of laxity, a brief overview of the use of laxity assessment in computational models, a more detailed review of three fundamental laxity studies to date, and lastly an in-depth look into the historical methods/designs/uses of instrumented knee laxity measurement, both in vitro and then in vivo.

2.2.2. Importance of Laxity in Clinical Aspects

Joint laxity is a surrogate measure of ligament sufficiency that is key for the evaluation of all joints in the body. Clinical definitions of joint laxity vary and have shifted over time. However, the generally agreed-upon meaning of joint laxity in clinical settings refers to the abnormal looseness of a joint in an unnatural movement direction, such as knee anterior/posterior (AP) motion, with increased laxity described as an increased looseness [15]. Joint laxity assessments are commonplace at every stage in the clinical evaluation of joint stability. In the knee, manual laxity assessments - measurements made by hand manipulations of the joint, are regularly used to evaluate the integrity of the ACL, PCL, MCL, and LCL [16].

In 1995, Kim et al. showed a comparison of the three most common manual laxity assessments for ACL integrity: Pivot Shift, Anterior Drawer Test, and the Lachman test, and showed high accuracy in the prediction of ACL injuries from side to side differences in joint laxity [17]. This study and many more have solidified joint laxity assessments as standard practice for evaluation of soft tissue integrity in the knee [18–21].

Manual Laxity assessments are highly accurate and integral to determining ligament sufficiency in clinical settings. However, they have little carryover to computational

modeling and broader engineering as a whole, where objective quantitative measurements are essential for proper calibration of models. For this calibration, devices capable of gathering quantitative laxity assessments are necessary.

2.2.3. Laxity Measurements for Computational Model Calibration

Laxity measurements are useful for calibrating and validating the various ligamentous properties in computational models. In 1996, Blankevoort et al. developed a knee model that used axial connector spring elements to represent each of the ligament bundles [22]. They then used previously published values for the stiffness of the ligaments, and applied them to each of the ligaments. They then changed the reference strains applied to each of the ligament bundles, to optimize the resulting kinematics of the model to experimental kinematics data. After the model ligament properties were calibrated, they performed a laxity test on the computational model, and compared the resulting AP and VV displacements with values from previous laxity examinations. In this case, the laxity measurements were used to validate the overall motion of the knee model, and did not act to create the initial model.

In contrast, in 2017, Ali et al. used a similarly created model of the knee shown below in Figure 2-5, with ligaments again represented by axial connector spring elements [23].

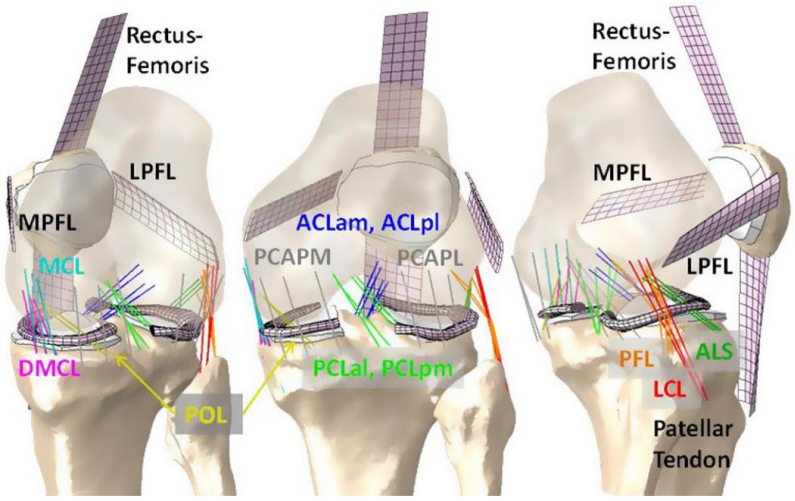

Figure 2-5 Computational Knee Model with Axial Connector Spring Elements for Ligaments from Ali et al. [23]

The model used experimental data from *in vitro* testing, which included AP, IE, and VV laxity measurements. The properties of the ligaments, namely attachment sites, reference strain, and ligament stiffness, were optimized until the model of the laxity trials reproduced the same *in vitro* laxity experiments. The model was then validated against the simulated gait data to determine validity.

Laxity data is used to validate the performance of a model in motions beyond the ones it was calibrated for, or the laxity data can be used to perform the calibration of the ligamentous parameters directly.

2.2.4. Key Laxity Studies

Laxity measurements, particularly of the knee, have been made accurately since the early 70's. Historically, laxity research has been dominated by the evaluation/creation of a new apparatus for laxity measurement and the resulting dataset of laxity data resulting therein. Markolf et al. were primarily the first to measure knee laxity in cadaveric specimens accurately [24]. They began by segmenting the femurs and tibias of 35

cadaveric knees, potting the knees, and then fixing the femur to a reference. Loads were measured using a custom load cell and goniometer rigidly attached to the tibia. They then applied loads via a handle and observed the displacements of the tibia relative to the femur shown in Figure 2-6.

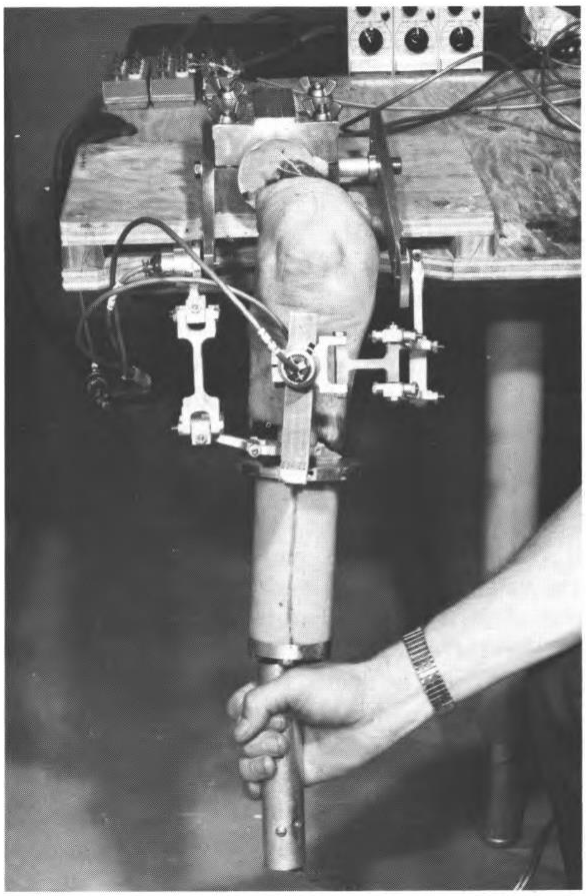

Figure 2-6 Cadaveric Knee Laxity Apparatus from Markolf et al. [24]

They then applied various loads in the anterior-posterior (AP), internal-external (IE), and varus-valgus (VV) directions at different degrees of knee flexion and recorded the resulting displacements. A three-segment linear approximation was fit to the non-linear curve to quantify the approximate slope in 3 different regions of the stiffness of the joint at a corresponding flexion angle. They then calculated the intersection of the fit lines to

create “breakpoints.” These breakpoint regions defined the region where the joint stiffened, and the total displacement between breakpoints defined the laxity quantity shown in Figure 2-7. They then created graphs by taking the three stiffness values across all specimens and averaging them together, generating three fit lines up to the chosen “breakpoints” and then refitting a curve to the tangent to these slope averages of the data, repeating at different flexion angles.

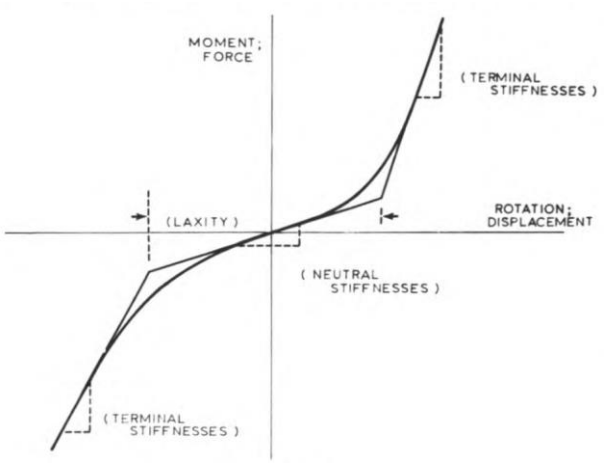

Figure 2-7 Markolf Laxity Definition Segment Fitting from Markolf et al. [24]

The research demonstrates one of the first studies to gather quantitative knee laxity measurements on both healthy and simulated ailment populations *in vitro*. They showed that there is a non-linear relationship between the force and displacement of the joint, with increasing stiffness occurring at higher displacements. They also showed a general trend of increased laxity, based on their definition of laxity, with increased flexion angle for VV and IE moments, shown in Figure 2-8 below. In contrast to IE and VV, however, they showed that there was an increase in AP laxity, followed by a decrease in laxity at various flexion angles, with the transition occurring around 45 degrees of knee flexion.

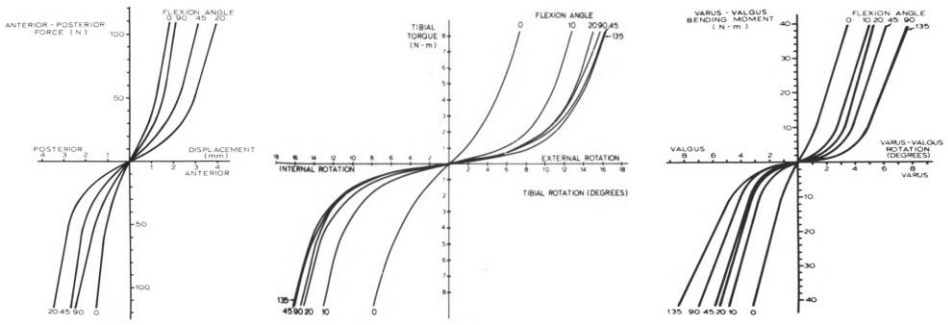

Figure 2-8 AP, IE, and VV Laxity Curves from Markolf et al. [24]

They also identified relative contributions as a percent change between changes to the ligaments and other soft tissues, and the effects on various laxity plane measurements, shown in Figure 2-9. These contributions are useful as a reference, both for clinical use and for computational model calibration. This chart allows for the individual soft-tissue contributions on the joint laxity to be understood and to aid in the reverse process of calibrating the individual tissues. For example, that the Varus-Valgus test is the best at identifying the Medial Collateral Ligament damage.

	Stiffness												Laxity			
	External Rotation — Terminal (Knee Flexion)				Internal Rotation — Terminal (Knee Flexion)				Neutral (Knee Flexion)				Rotatory (Knee Flexion)			
	0°	20°	45°	90°	0°	20°	45°	90°	0°	20°	45°	90°	0°	20°	45°	90°
Menisci removed (9)	—	—	—	—	—	—	—	—	0.59	0.71	0.76	0.75	1.31	—	—	—
Cruciate ligaments																
Anterior (4)	—	—	—	—	—	—	—	—	0.71	—	—	—	1.38	—	—	—
Posterior (4)	—	—	—	—	—	—	—	—	0.71	—	—	0.73	—	—	—	—
Both (8)	—	—	—	—	—	—	—	—	0.58	—	0.62	0.46	1.54	—	—	—
Collateral ligaments																
Medial (6)	—	—	—	—	0.71	0.74	0.65	—	0.43	—	—	0.65	2.05	1.44	1.40	1.44
Lateral (7)	—	—	—	—	—	—	—	—	0.52	0.40	0.38	—	1.35	—	—	—
Combinations																
Ant. cruc. and medial collat. (3)	—	—	—	—	—	—	—	—	0.51	—	—	—	2.81	1.82	1.67	1.65
Ant. cruc. and lateral collat. (3)	—	—	—	—	—	—	—	—	0.34	—	—	—	1.68	—	—	—
Post. capsule and medial collat. (3)	—	—	—	—	0.54	0.64	0.65	—	0.36	0.75	—	0.23	2.07	1.72	1.63	1.67
Post. capsule and lateral collat. (3)	—	—	—	0.68	—	—	—	—	0.16	—	0.27	—	1.90	1.30	1.33	—

Figure 2-9 IE Rotation Stiffness Ratio Changes from Resection of various Soft Tissue, from Markolf et al. [24]

However, the limitations of their work resulted mainly from the fitting of the three-line segments to the curve. The curve fitting relied on arbitrarily chosen force values to

identify the breakpoints for the transition, resulting in laxity measurements difficult for repetition by later studies. Since these values required the creation of the entire force-displacement curve to identify singular quantities of laxity or stiffness, as opposed to merely reporting the total displacement at a given load, helping to add to the confusion of what “laxity” is.

In 1988, Blankevoort et al. built a device that utilized a system of cables and pulleys to remove the manual manipulation present in Markolf’s design [25]. The device shown in Figure 2-10 was capable of creating loads in all 6 DOF simultaneously via known weights on pulleys rigidly attached to different mechanics fixed to each bone. The resulting displacements of the bones were measured using a biplane fluoroscopy system and tantalum beads implanted into the bone. This study like several since used Roentgenography based measurements to determine the relative motion of the bones.

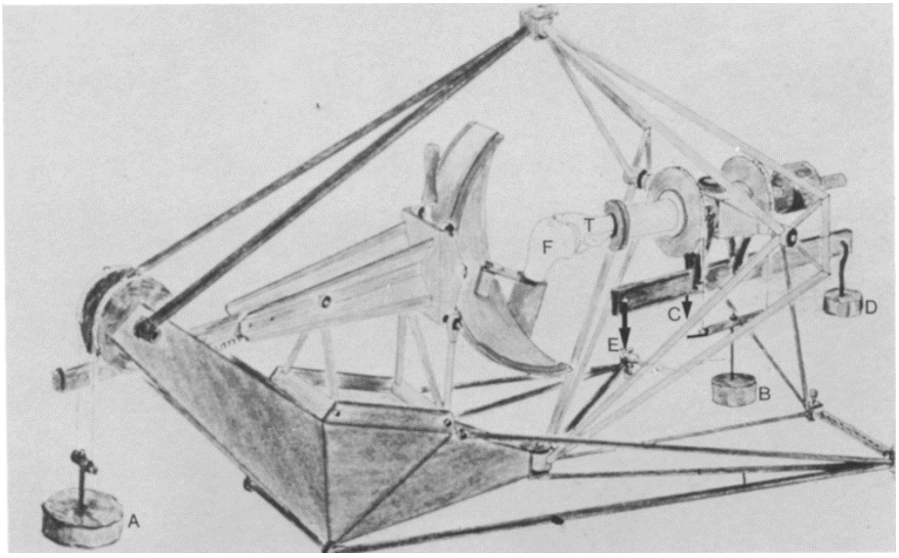

Figure 2-10 Blankevoort Knee Laxity Apparatus, from Blankevoort et al. [25]

As part of their testing and evaluation, they emphasized that there exists an "envelope" region of passive motion within the knee. This envelope region is near zero load, and the exact motion of the knee is highly dependent on the specific external loads applied to the knee.

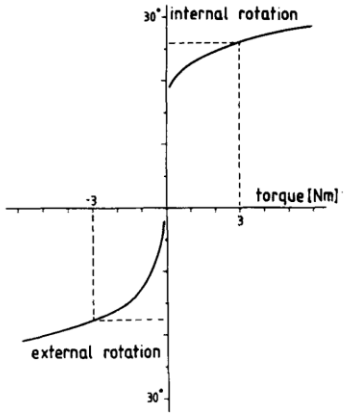

Figure 2-11 IE Laxity Curve with Discontinuous Envelope region from Blankevoort et al. [25]

They observed that at higher axial loads of around 300N, the motion pathway of the knee is relatively consistent; however, at smaller magnitudes of load, a small change could create a significant change in the exact motion path in an almost chaotic manner. The envelope region is the area where the ligaments provide little resistance to the resulting displacements, shown in Figure 2-11 as the vertical line. In contrast, the region outside of the passive envelope is affected by the ligament stiffness. In their paper, they maintain that within this envelope region, the knee is an "unstable system." Critically, they mention that the total displacement for various laxity measurements at different flexion angles is repeatable, but that the exact motion pathway is unpredictable. They also mention that changes in the axial load for magnitudes less than around 300N have little effect on the limits of tibial rotation. This observation is in stark contrast with

Markolf, which showed that differences in axial loads measured up to 900N showed significant differences in tibial rotation limits.

Another critical feature of Blankevoort's work, as mentioned previously, is that these measurements, along with other measurements from similar studies, were used to inform and provide inputs for calibrating ligament parameters for subsequent work [22]. This work validates that custom devices using biplane fluoroscopy, with loads applied via pulleys, are sufficient to calibrate inputs into complex computational models.

Markolf and Blankevoort built custom devices to measure knee laxity, which, while useful for research settings, have little carryover to use in clinical practice. In contrast, Daniel et al. created a custom device that later became the commercially available KT-1000 arthrometer to measure the anterior laxity of the knee [19,26]. This device was designed for clinical use, and as such, has the unique capability of performing both *in vivo* and *in vitro* data capture. The KT-1000 was primarily the first commercially available laxity device for large scale clinical use, and has since become the standard device for clinicians to measure knee laxity in a repeatable and objective manner [27]. The device enabled them to gather a large cohort of subjects, both healthy controls and injured knee subjects [19]. The KT1000, shown in Figure 2-12, works by first placing the ankle on a block and flexing the knee to around 30 degrees. Then a contact pressure is applied to the patella to hold the patella/femur relatively fixed while simultaneously using a spring-loaded handle to apply an anterior displacement to the tibia via a system of cuffs. The device is capable of measuring the displacement of the tibia relative to the femur, at three standard loads: 15 lbf (67 N), 20 lbf (89 N), and 30 lbf (134 N). The measurement

is often repeated on the contralateral side to compare side to side differences in anterior laxity of the knee.

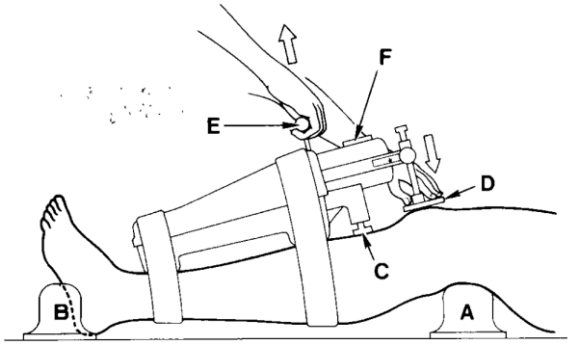

Figure 2-12 KT1000 Knee Laxity Tester from Daniel et al. [19]

In 1985, Daniel et al. showed that at 30° of knee flexion, healthy individuals have on average a 7.2 mm anterior displacement with a standard deviation of 1.9 mm of the tibia relative to the Femur for a 20 lbf anterior load applied [19]. They also showed that there is, on average, a side to side anterior knee laxity difference of 0.8 mm, with a standard deviation of 0.7 mm.

Their work represents one of the first high subject count studies on healthy individuals, and introduced a novel laxity device used in clinics to this day. With the device being so popular, that it has since prompted the creation of 2 newer models: KT2000, and the KT3000. Since its creation in the 1980s, any laxity device created for clinical use in measuring AP laxity is benchmarked against this device. Anyone choosing to create a new knee laxity device is unofficially required to have an understanding of the KT1000, as it acts as the standard tool for quantitative knee laxity measurements to this day.

2.2.5. Knee Laxity Devices

The accuracy and availability of quantitative laxity measurements are primarily based on the device used to measure it. In the last 50 years, there have been a vast number of devices with a wide range of designs created for measuring different aspects of knee laxity. Despite the significant differences in designs, these laxity devices broadly fall into two categories: *in vivo* and *in vitro*.

2.2.5.1. In Vitro Devices

Historically the majority of accurate and detailed knee laxity data has come from *in vitro* testing. Many devices have been built since the original devices by Markolf et al. and Blankevoort et al., with varying designs, but the vast majority of them have similar design features.

Many laxity testing designs allow a testing operator to apply loads through the use of handles rigidly attached to the bones to simulate the tests performed by clinicians shown in Figure 2-13 and Figure 2-14 below [28–32]. These devices allow the tester to apply motions similar to those applied manually by clinicians. As such, they are the best option for reproducing traditional manual laxity measurements, while being able to measure the resulting laxity curves accurately. This has the advantage that the measurements and results are the most directly transferable to the clinical setting.

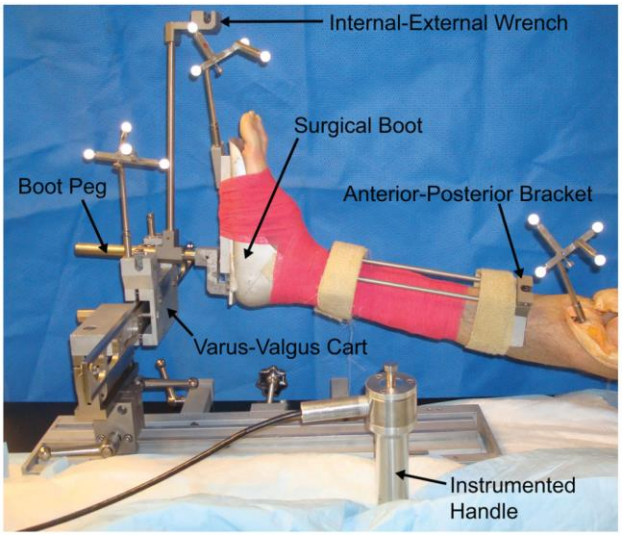

Figure 2-13 Manual AP, IE and VV Knee Laxity Tester from Siston et al. [31]

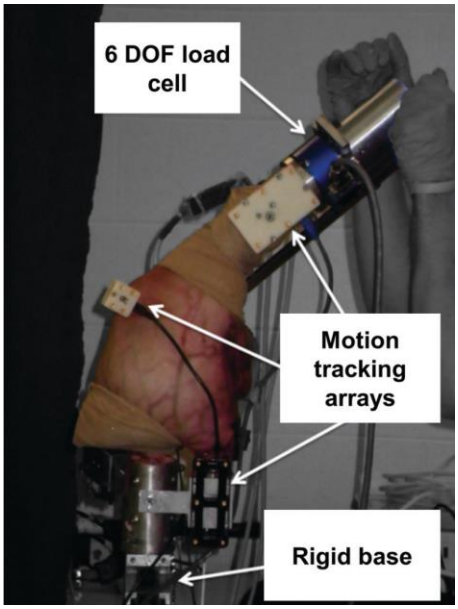

Figure 2-14 Knee Laxity Testing Setup from Harris et al. [29]

However, they have two significant disadvantages. The first being that loads are applied by hand, resulting in less control and accuracy. As such, load profiles are difficult to prescribe and make it near impossible to create a load in a single DOF. The second

issue is that with the loads being applied manually, these devices become highly specialized and difficult to perform other measurements.

Other *in vitro* devices can apply the loads automatically. These devices, such as the one shown in Figure 2-15, generally use some combination of a load frame, rotary table, CNC style axis, or other similar mechanics, along with a controller of some kind to apply a pre-determined load profile in either a single or multiple DOF simultaneously [33,34]. Of these devices, some are custom created by research labs such as the Kansas Knee Simulator in Figure 2-16 below, or the Purdue Knee Simulator [35]. While other laxity devices can be purchased commercially, such as the AMTI Vivo, the Kuka Robotics robots, and other similar devices [36–39]. These automatic devices allow for easier prescription of loads, and subsequently easier transfer/validation of the experimental data to the computational model data, of one is desired [37,40,41].

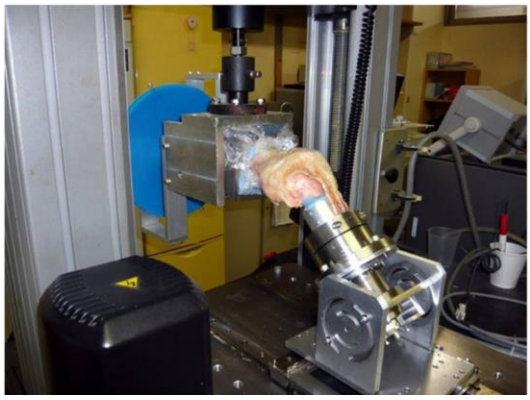

Figure 2-15 AP drawer laxity test using axial load frame from Nohmi et al. [33]

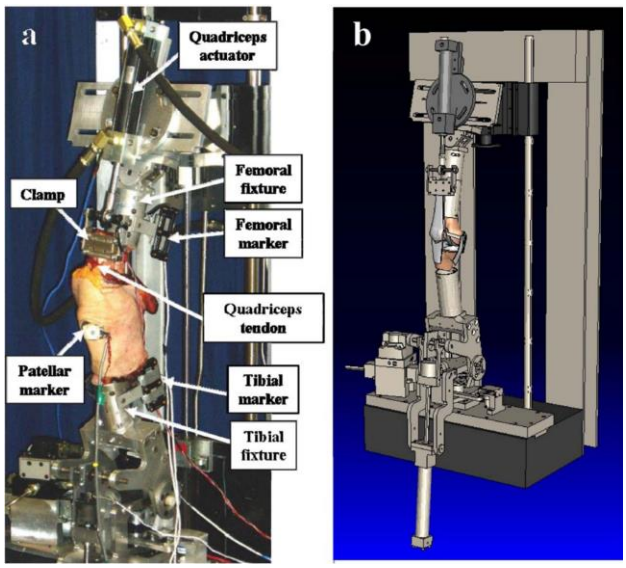

Figure 2-16 Kansas Knee Simulator and Corresponding Computational Knee Model for Knee Extension from Baldwin et al. [42]

These types of designs enable complicated load profiles, and can allow for more complicated laxity measurements, such as hysteresis effects or strain rate measurements. These automatic devices are more versatile than their manual counterparts, allowing users to perform other tests: Range of Motion (ROM) tests, simulated loading from *in vivo* measurement data, fatigue/reliability testing. With their increased functionality, these are becoming more and more popular as they are more a more cost-efficient solution for *in vitro* measurement.

The critical aspect of these *in vitro* designs is that the loads and displacements are applied directly to the bones. *I*n *vitro* based methods are inherently performed on cadaveric tissue, and thus do not need to be non-invasive. This invasive nature gives them the advantage that bones can be rigidly fixed to the load cells, and displacements can be measured directly on the bones of interest via high accuracy methods. With this rigid

measurement, there is no ambiguity in the resulting measurements, and as such, *in vitro* data capture is the gold standard for accurate laxity measurements.

2.2.5.2. In Vivo Devices

In vivo measurements have historically been made to compare differences in the laxity of healthy and post-injury individuals, with particular emphasis on ACL injuries [19,43,44]. Studies have also been interested in understanding differences in knee laxity between men and women, and the potential hormonal causes that may explain the differences [45–49]. *In vivo* measurements have also been used to understand the effects and contributions of muscle activity on the resulting knee laxity measurements [50,51]. All of these studies cannot be performed *in vitro*, and as such, require an accurate means of measurement that can work *in vivo*.

In vivo measurements have overwhelmingly been made by clinicians/researchers using commercially available arthrometers; among these are the KT1000, KT2000, KT3000, Genourob, Rolimeter, Stryker Knee Laxity Tester, Genucom Knee Analysis System, Dyonics Dynamic Cruciate Tester, and many more. These devices work by using a surface-based force probe, a system of straps to restrain the appendages, and a system of displacement probes to perform the measurement, such as the setup in Figure 2-17 below.

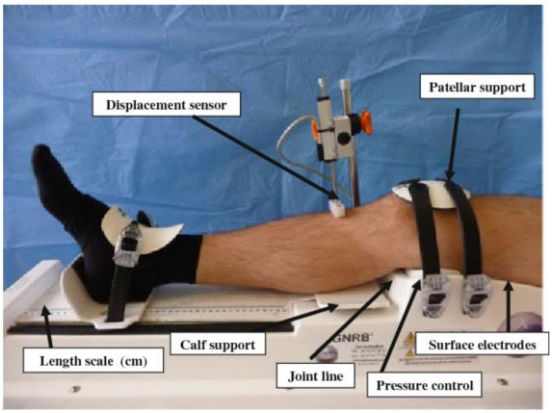

Figure 2-17 Example setup of Commercial Genourob device from Collete et al. [52]

However work has shown that the variability of these devices amongst one another is quite significant as shown below in Figure 2-18 [44]

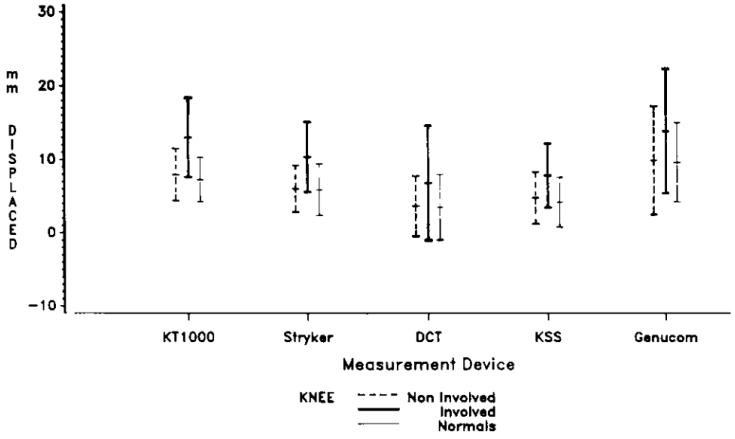

Figure 2-18 Graph of Anterior Displacement Mean and Standard Deviations for Different Arthrometers, from Anderson et al. [44]

While these errors are relatively small for clinical measurements, they can be large enough to cause issues for computational models [53]. Making their use for calibration of computational models very limited. As a result, there have been a significant number of laxity devices designed in recent years to try and improve accuracy, ease of use,

repeatability, and the functionality of laxity measurements, with the hopes of allowing for better input data for the creation of subject-specific models.

All sorts of knee laxity devices have been designed in recent years to try and improve *in vivo* knee laxity measurements, with the majority of *in vivo* devices being very different from *in vitro* devices [31,54]. Unlike the *in vitro* devices where almost all loads are applied via load cells rigidly attached to the bones, non-invasive *in vivo* laxity measurement devices are incapable of applying loads directly to the bones.

Several different means of load application have been used previously for *in vivo* knee laxity measurement. While some devices for AP laxity measurement are made to apply loads similarly to manual evaluations of clinicians, the majority of laxity devices for AP and VV loads, are applied via a combination of cables, pulleys and cuffs to apply the loads in various directions [55–59]. With the most advanced/comprehensive knee laxity device of this kind to date, being the Vermont Knee Laxity device shown in Figure 2-19 below. These have the advantage that they are relatively easy to design and can be made to apply multiple loads simultaneously.

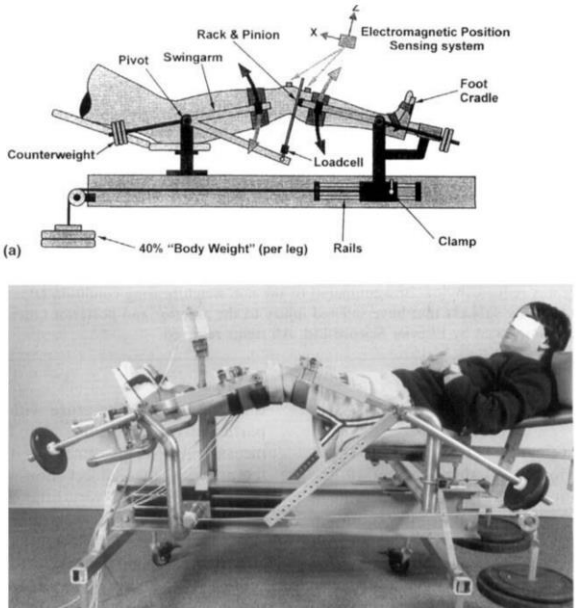

Figure 2-19 Vermont Knee Laxity Device for all DOF Laxity testing from Un et al. [55]

Other devices have used hydraulics as a means of applying a very localized pressure with ease of application, such as in Figure 2-20 below [60]. This hydraulic pressure load application has the advantage of a small form factor, and lack of metal or moving parts, allowing the displacement measures to be gathered very accurately in MRI.

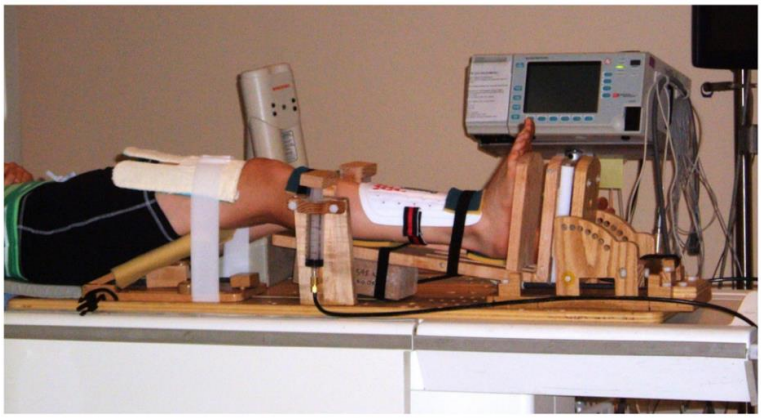

Figure 2-20 Knee Loading Apparatus (KLA) using hydraulics for Anterior Laxity Assessment from Kupper et al. [60]

While devices for rotational laxity have very similar designs for the applications of the loads. The overwhelming majority of Rotational Laxity devices consist of a boot rigidly clamped to the subject's shank, and a disk attached to the boot that causes a rotation to the disk and subsequently the boot from an applied torque, such as the example device in Figure 2-21 below [61,62].

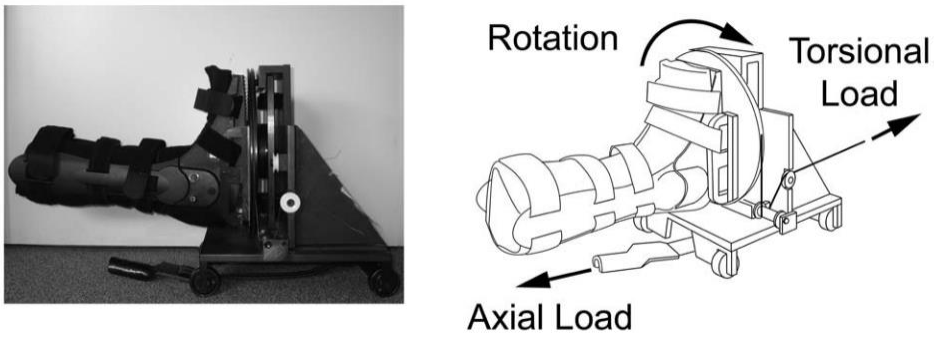

Figure 2-21 Example of in vivo rotational IE laxity device, from Carpenter et al. [61]

However, the overwhelming majority of these devices use surface-based measurements to calculate the underlying displacements. Previous work has demonstrated that marker-based surface measurements have significantly higher errors in measuring *in vivo* joint kinematics of the underlying bones compared to roentgenographic or bone pin-based methods [63,64]. Since 2002, recent work has attempted to design apparatuses capable of use in fluoroscopy and MRI as a means of gathering more accurate displacement measurements of the underlying bones, shown in Figure 2-22, Figure 2-23, and Figure 2-24 below [60–62,65–67].

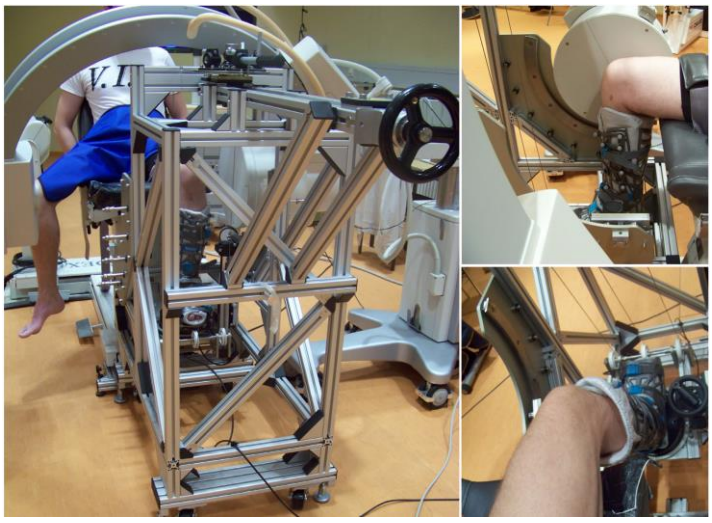

Figure 2-22 IE Laxity Device for use in Single Plane Fluoroscopy from Moewis et al. [67]

Figure 2-23 IE Laxity Device for use in MRI from Colombet et al. [62]

Figure 2-24 AP Laxity Device for use in MRI from Beukes et al. [65]

All of these devices are making significant improvements in the accuracy of data from *in* vivo laxity assessment. However, several problems still exist. All of these devices are only capable of measuring either AP or IE laxity, not both. The devices that use MRI, while incredibly accurate are limited by the time required to receive an MRI, and thus only capable of making a couple of measurements. MRI measurements, are also very space-constrained and thus make it difficult to assess other forms of *in* vivo data such as ROM, and basic ADL, that are of interest in many studies. Devices used in MRI, will not allow a lab to collect other useful data beyond just laxity assessments quickly, with the other data being another essential aspect in computational model calibration and validation. The devices intended for use in fluoroscopy were limited to single-plane fluoroscopy measurements. Single plane fluoroscopy use in laxity assessment has previously shown not to be adequate for laxity assessment [66].

Additionally, recent work has attempted to use the same robotic manipulators as *in* vitro testing, with minor modifications, to perform laxity assessment, shown in Figure 2-25 [48,68].

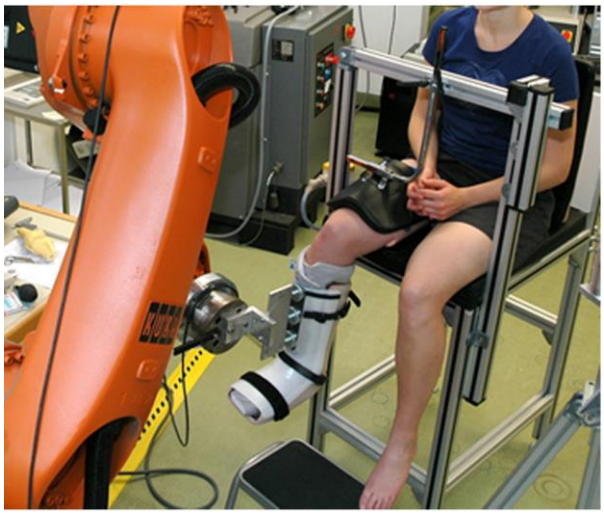

Figure 2-25 In vivo Knee Laxity Assessment using Robotic Manipulator from Lorenz et al. [68]

These have shown superior accuracy in measuring both loads and displacement, but suffer from several drawbacks. The biggest of which is the enormous cost associated with purchasing these robots, and modifying them for using *in vivo*, making their use limited to established research laboratories. Secondly, robotic devices rely on a control system to apply the chosen loads, and as such, have a more significant potential to be unsafe compared to other devices applied with known weight loads. If the robot is potentially allowed to overshoot, or move too rapidly, severe damage and injury could occur to the patient. As such, these devices, while accurate, will likely not be commonplace soon, and thus a means of safe, accurate, cheap, and versatile *in vivo* laxity measurement is still needed.

2.3. Computational Modeling from In Vivo Measurements

Computational modeling is a tool used extensively in biomechanics for a variety of reasons. Some computational models are built to asses and measure parameters such as joint contact force, which is difficult to measure *in vivo*. Other models are made to allow the integration of additional components to predict the performance of surgical interventions. Other models still, are used to estimate long term effects, that are impractical to perform experimentally. However, regardless of the purpose of the computational model, the validity of any model is based largely on the input data used to create the model [69]. As such, many different methods have been investigated and used as inputs for different aspects of the computational models. Historically many of these parameters have come from *in vitro* measurements, but future subject-specific modeling necessitates *in vivo* data to create accurate *in vivo* knee models. Several forms of *in vivo* data have previously been used in computational model calibration.

2.3.1. Kinematic and Dynamic Measurements for Calibration

Kinematics and/or dynamics are used in almost every computational model to drive the final motion of the model. Many computational models have used *in vivo* kinematics data from motion capture and HSSR. In 2019, Hume et al. used *in vivo* dynamic data consisting of force plate data, HSSR kinematics data for knee motion, and marker-based kinematics data for trunk and foot from a chair rise and gait motion as the input boundary conditions to the multi-scale finite element computational model [70]. The model uses the dynamics data as inputs to create the loads at various degrees of freedom, and to control the motion of the Flexion DOF for the knee, while optimizing the locations of the

joint for the other DOF. In 2020, Ali et al. used measured *in vivo* force plate data and HSSR data in a similar vain to determine underlying dynamics data such as joint torques and loads according to the flow diagram shown in Figure 2-26 [71].

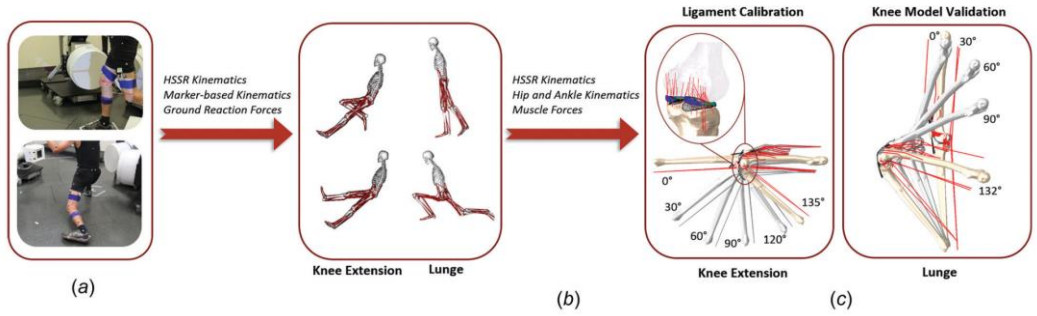

Figure 2-26 Computational Modeling Framework from In vivo Dynamics data from Ali et al. [71]

For example, the knee-flexion was controlled by PID controlled force input of the quadriceps muscle. Other studies have used similar *in vivo* measurements to act as the boundary condition inputs to drive the motion of the model [69,72].

2.3.2. EMG Measurements for Dynamics Calibration

Significant numbers of studies have used EMG data, which is inherently *in vivo* data, as part of the computational model to drive muscle force output, to measure the percent of muscle force output accurately, and then quantify the exact force in the muscle. In 2003, Lloyd et al. used filtered EMG data and kinematics data to drive a computational model to predict the inverse dynamic joint moments [73]. In general, studies use EMG data as a means of estimating the muscle activation at any given time. Then along with calibrated isometric MVC datasets, the muscle force at a given time can be estimated from the level of muscle activation. However, very few studies use EMG data to directly drive the force inputs of the muscles [74]. This non-direct drive is because, deep muscles

that are not easily measured using EMG, there is no obvious means of integration into the model. EMG is mostly used in models as a conversion from muscle activation relationships to an estimate of muscle force, after the fact.

2.3.3. In Vivo Cartilage and Meniscus Calibration from MRI

Some studies *have* used *in vivo* data captured from MRI to estimate the material properties of the cartilage and incorporate them into a subject-specific FE model. In 2012, Wei-Ching used a custom apparatus built into an MRI to create a simulated half bodyweight loading while an MRI was captured [75]. The observed cartilage deformation between the loaded and unloaded trials, as well as the change in T1ρ parameters, created a calibrated volume estimate of the modulus at each voxel. This data was then used in conjunction with an FE model representation to calibrate a subject-specific cartilage material to match the responses, which was then used to analyze joint mechanics of the subject with osteoarthritis. While the process was not novel, the author was unable to find any other studies that directly used loaded MRI scans of an individual to calibrate exact cartilage tissue parameters.

2.3.4. In Vivo Laxity Measurements

Very few computational models have been created using calibrated *in* vivo ligamentous data. In the few studies that have the majority of these models calibrate ligament properties by indirect calibration based on ROM or some other ADL motion trials [71]. In general, the only resource found that has calibrated ligament parameters, is a website of a graduate student from China. Wherein he used the anterior laxity

measurements taken from the KT1000, to calibrate the ligamentous properties of a subject-specific knee model, shown in Figure 2-27 below [76].

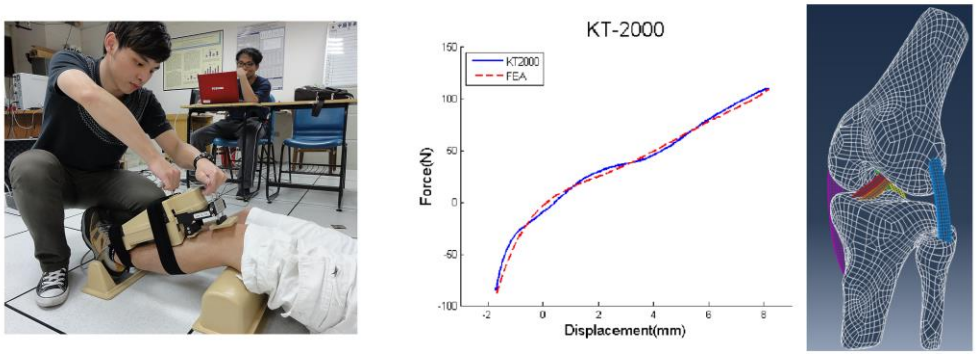

Figure 2-27 In vivo Computational Model Calibration from KT1000 laxity assessment from Lin [76]

As such, there is a need for an easy means of capturing laxity data on individual subjects *in vivo* that can then be used to calibrate the laxity parameters directly for the resulting subject-specific computational model.

Chapter 3: Leg Press Design

3.1. Design Overview

Aim 1 is to design a device capable of measuring the full passive and active ROM of an individual. ROM measurements are useful for in calibration and validation of computational models; however, these measurements have historically been limited by the total range that the subject was able to achieve. In fulfillment of this aim, a leg press was built to allow for full passive and active ROM kinematics to be gathered on individuals. The leg press centers around a commercially available leg press and a weight tower to apply a specific load to the track of the leg press, to allow for controlled load application throughout the ROM of the subject. The kinematics are tracked using HSSR and post-processed using custom scripts for analysis.

3.2. Intended Uses

The leg press is intended for *in vivo* capture of the full flexion ROM of the knee under variable loads applied to the lower limb of a subject to simulate weight-bearing and small weight nearly passive conditions.

3.3. Design Requirements

The design requirements of the leg press, in decreasing order of importance, are that the device is: safe, allows full range of motion, maintains the knee in view of the HSSR, adjustable height, allows controlled weight application, easy to set up/put away, and inexpensive.

3.3.1. Safety

The leg press shall be safe for use *in* vivo. The device should be stable and not tip during the use of the leg press since the subject will potentially be off the ground. The device is intended to be used for people with healthy and unhealthy knees and needs to be able to apply a small weight in a controlled manner. Lastly, while not critical to the safety of the subject, the leg press being as comfortable as possible is useful in ensuring the subject feels safe, and can perform the desired activity without apprehension.

3.3.2. Allow full ROM Measurement

The device shall gather full ROM for an individual. The device should be capable of allowing any person, regardless of height or weight, to perform the full range of motion of the knee.

3.3.3. Maintains the Knee in View of the HSSR

The device shall keep the knee in view of the HSSR during the full range of motion. This ensures that accurate tracking can be performed of the bones in HSSR, for the entire duration of the trial.

3.3.4. Adjustable Height

The device shall be able to adjust the height of the leg press. The device will be used with a range of individuals with individual anthropometrics. The device should be able to change the height to accommodate for individual anthropometrics. In addition, the HSSR requires re-calibration any time the system moves. In order to minimize the number of calibration routines necessary, the device should be able to adjust the height, such that no height change of the HSSR is necessary.

3.3.5. Allow Controlled Weight Application

The device shall be able to apply a controlled weight application to allow for controlled ROM testing. The device should be capable of applying a small weight for the majority of ROM trials, but should be capable of applying larger weights for simulated weight-bearing motion.

3.3.6. Ease of Setup

The device shall be easy to set up and put away. The ROM will be one of many trials taken in a giving testing session. As such, it must be set up and put away in as little time as possible to ensure smooth and seamless transitions between measurements.

3.3.7. Inexpensive

The device shall be as inexpensive as practical. While not critical to the design, the device should cost less than $2000.

3.4. Design

The design centers around a commercially available leg press. A leg press is a device used in gyms and rehab facilities for controlled weight application and simulated weight-bearing of the body to strengthen the quadriceps muscles. Leg presses usually consist of a means of load application, applied to the subject's torso, through the user's weight, or a system of weights. Then the user extends their leg against a plate and pushes their torso away from the board simulating a Ground Reaction force and a body force at the torso, and thus strengthening the knee extensor muscles.

The leg press used consists of a bar capable of changing the incline angle, a sled that the subject lies on, and a cable attached to the sled for resistance application. The leg

press sits on a custom hydraulic lift table capable of lifting the leg press – with a subject on it, to ensure the full ROM from deep flexion to full extension can be gathered. The kinematics are measured using validated HSSR techniques and motion capture. The loads are applied at a weight tower, which consists of a large wooden base, two vertical risers, and a cable pulley at the top. Discrete weights attached to a pulley cable are hung off the weight tower through its pulley and applied to a cable attached to the sled of the leg press using a system of pulleys. The leg press weights can be increased to create simulated controlled passive and active ROM trials, as well as simulated weight-bearing trials under known weights. The leg press, hydraulic lift table, and the weight application tower can be seen below in Figure 3-1, with the major subsystem components shown below in Figure 3-2.

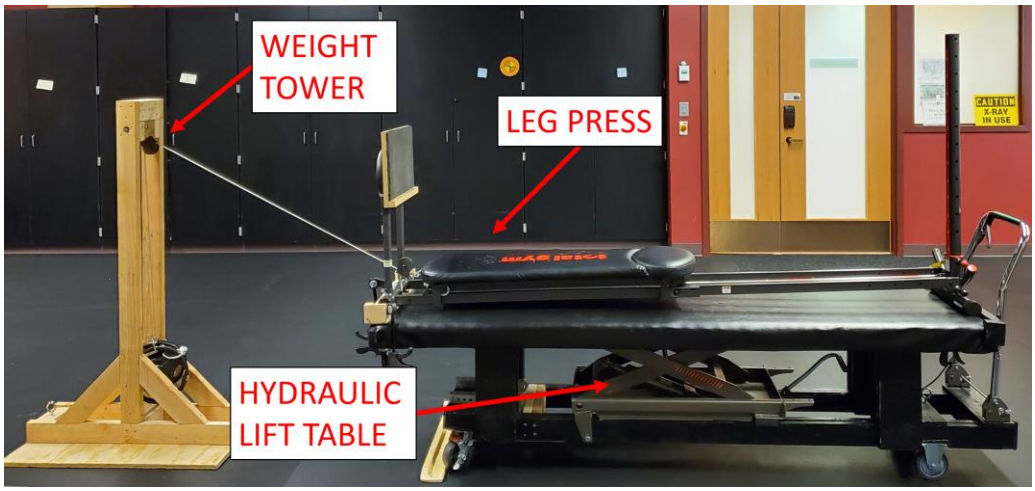

Figure 3-1 Image of Leg Press, weight application, and hydraulic lift table subsystems

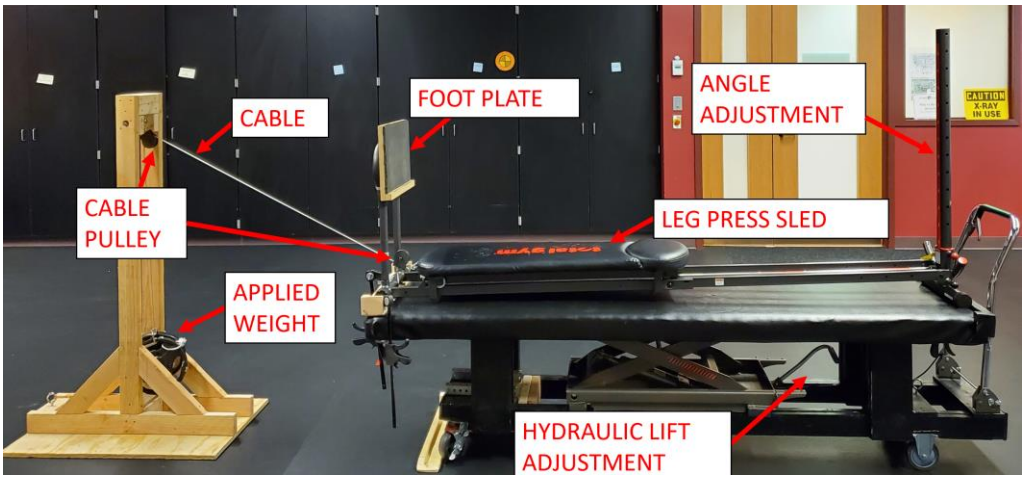

Figure 3-2 Image of Leg Press subsystem components

3.5. Satisfying Design Requirements

3.5.1. Safety

The device ensures safety by using a commercially available leg press. The leg press has a maximum subject weight capacity from the manufacturer of 300 lbf. However, since the design is used solely in the horizontal mode, this weight limit is likely significantly higher. The leg press comes pre-built with aluminum side rails and large cotter pins to ensure subject safety, under both static and dynamic loads. The device has no pinch points that can be touched by the subject for added safety. A considerable cushion pad on the runner aids with subject comfort, and additional pads can be added for additional comfort.

The hydraulic lift table is built around a commercially available stainless steel hydraulic lift. The hydraulic lift has a manufacturer rating of up to 1000 lbf; while the leg press weighs just shy of 100lbf, the top section of the hydraulic lift table is estimated to weigh around 100 lbf, and the leg press is rated to hold a 300 lbf person. As such, the designed Factor of Safety for the leg press system is 2. The hydraulic lift is designed to

support the full load at all levels of height adjustment. As an added safety measure, there are four leg brackets built into the four corners of the hydraulic table, with grade 8, 0.5 in steel bolts, placed that ensures that if the hydraulic lift were to fail, the largest distance the table with subject could drop is 4 in.

The weight tower is capable of applying a controlled weight to the sled of the leg press using a system of pulleys, and the weight can be as small as 2.5 lbf to apply as small a resistance as possible to the subject, ensuring subject safety. The weight platform, cables, and leg press are capable of handling loads upwards of 100 lbf, of allowing for simulated weight-bearing loads to be created. However, this requires additional weight to be added to the base of the tower to ensure that it does not tip over.

3.5.2. Allow full ROM Measurement

The leg press is designed for a subject to achieve a full ROM throughout the leg press motion. However, the HSSR used to measure the kinematic movement of the bones is unable to view the entire ROM because of the considerable vertical distance that the knee will move during the ROM trial. For this reason, motion of the knee is captured in two separate movements that requires changing the vertical position of the subject. As such, the hydraulic lift table is built to achieve around 18 in. of vertical travel. The travel is adjusted by using a leg press lever to lift the table into the air, and then a release valve lever to lower the table at a controlled speed slowly. The vertical travel allows for the full ROM of an individual, by capturing the leg press motion in 2 consecutive shots. The first biased toward the initial full flexion portion and then losing view of the leg towards mid flexion. Then the table can be raised – with the subject in the same position, and the trial

can be repeated with the leg initially out of view and then coming into view in the mid flexion area to the final full extension pose. These motions can then be tracked and combined in post-processing. The device also has no parts visible in the view of the HSSR system to ensure unobstructed views of the knee in both camera planes through the entire ROM.

3.5.3. Maintains the Knee in View of the HSSR

The leg press maintains the knee in view of the HSSR for the entire duration of the ROM. The length of the knee relative to the end plate is constant and thus the knee sweep out a circular arc, with a center at the end plate. As such, the only issue to keep the knee in place during the ROM is that the knee will drop below the Field of View (FOV) in the middle of a trial. Half of the ROM can be gathered between deep-flexion and mid-flexion by starting the knee in deep flexion. Then the hydraulic lift table can bias the knee higher, allowing the HSSR to capture mid-flexion to full-extension.

3.5.4. Adjustable Height

The leg press uses the hydraulic lift table to adjust the starting height for the individual, and the height needed for the full ROM measurement in two motion sets. This ensures that the leg press is capabale of viewing the full ROM for different subjects based on individual anthropometrics.

3.5.5. Allow Controlled Weight Application

The leg press has been adapted with a system of pulley cables attached to the sled and attached to a weight tower. A series of discrete weights can be added to the cable on the weight tower, thus applying the load to the sled of the leg press. The weights apply a

constant load to the subject for the duration of the trial, and any load upwards of 100 lbf can be applied.

3.5.6. Ease of Setup

The leg press is a commercial product designed for home gyms, and as such, can be folded and rolled in and out of the way quickly. The setup process consists of rolling the hydraulic lift table into place, unfolding the leg press, lifting the leg press onto the lift table, locking the leg press into place, having the subject lie on the leg press, rolling the table into the HSSR system, and lastly attaching the weight to the carabiner on the pulley sled cable. The disassembly process is the previous process performed in reverse. The setup process can be done with ease in approximately 5 minutes.

3.5.7. Inexpensive

By using a store-bought leg press and hydraulic lift, the only components that had to be built in-house were the surrounding table structure for the hydraulic lift and the weight tower, minimizing the cost and time required for custom fabrication of parts.

3.6. Design Use

The leg press setup is meant to be used during *in vivo* testing for full ROM measurements. To date, the knee motion of more than 50 subjects has been measured. An example of the full subject testing setup is shown below in Figure 3-3.

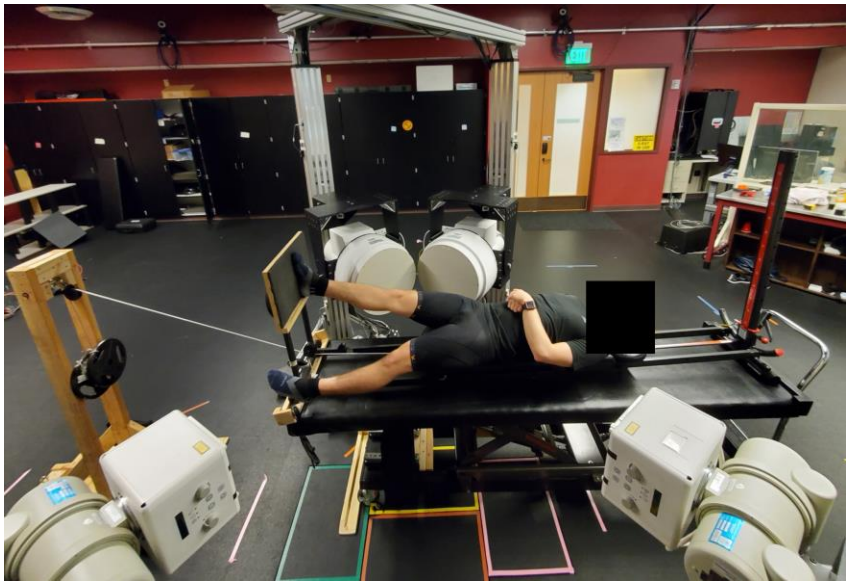

Figure 3-3 In vivo Leg Press Subject Testing Setup

The subject will first perform the full ROM starting at full-flexion through full extension and captures the full-flexion to mid-flexion region just before the knee falls out of the frame of view of the HSSR. The hydraulic lift table will then lift the subject up, and the subject will then perform the same motion, with the HSSR this time capturing the mid-flexion to full-extension portion of the ROM, as shown below in Figure 3-4.

Figure 3-4 In vivo Measurement using Leg Press. Full-Flexion to Mid-Flexion ROM Capture(Top). Mid-Flexion to Full-Extension ROM Capture (Bottom)

The HSSR data is captured in both planes and then tracked using 3D geometry from subject anatomy, via previously validated tracking methods, shown below in Figure 3-5.

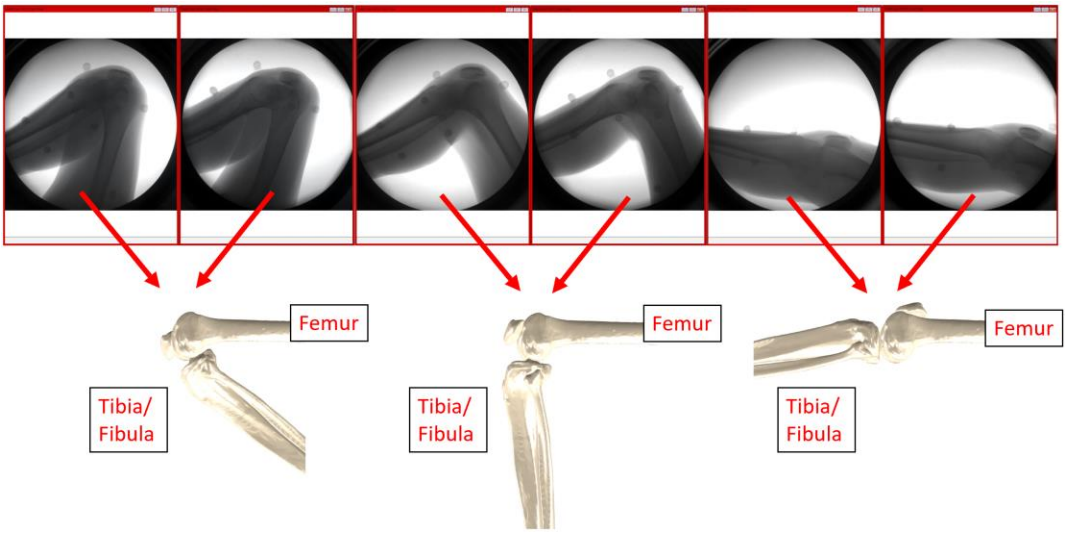

Figure 3-5 HSSR Images to Tracked Bone Positions for Leg Press Trial

The data can then be processed using created bone geometry coordinate systems according to Grood and Suntay, and calculate the resulting kinematic profiles as a function of the knee flexion angle [77]. The kinematics shown are an example dataset

compared to previous work from ROM kinematics, shown below in Figure 3-6 [78]. The leg press allows for the safe and accurate measurement of 6DOF knee kinematics, with values similar to those previously reported throughout the full knee ROM from deep flexion angles to full extension/hyperextension angles

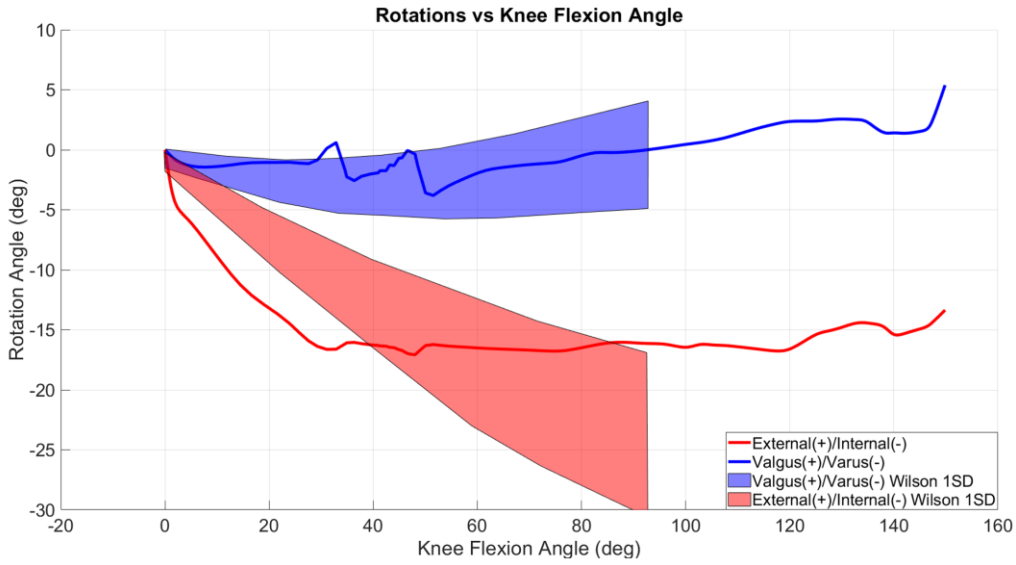

Figure 3-6 Sample in vivo Kinematics of the knee during the leg press activity as a Function of Knee Flexion Angle compared to Wilson et al. Standard Deviation [78]

3.7. Conclusion

ROM is an integral measurement for the ultimate goal of *in vivo* calibration/validation of computational models. However, ROM measurements have often been limited to a portion of the full ROM, and many devices to date are unable to capture both passive and active ROM. Aim 1 of this study was to create a device capable of applying a range of loads to a subject to create a simulated weight-bearing for full ROM measurement. A leg press was designed, in combination with a weight tower and a hydraulic lift table, to

allow for full ROM measurements in HSSR. The leg press capable of making full ROM measurements *in vivo* for use in calibration of subject-specific knee models.

However, pure ROM measurements are often not enough for calibration of computational models. For accurate model calibration of the ROM of the knee *in vivo*, these computational models require additional calibration data for the passive properties in the knee, particularly those from ligamentous properties. A device capable of making laxity measurements for ligament property calibration, is key to true *in vivo* subject-specific model creation.

Chapter 4: Knee Laxity Apparatus Design

4.1. Overview

Accurate computational models of subject-specific knees requires calibration of the underlying force-displacement relationship resulting from the ligamentous properties within the knee. While these measures have been easy to make *in vitro,* accurate measurements in *in vivo,* for both AP and IE, are challenging to come by. In fulfillment of Aim 2, a knee laxity device was built to allow for *in vivo* measurement of AP and IE laxity at various loads at 30 degrees and 90 degrees of knee flexion. The apparatus uses a system of pulleys and weights to apply distinct loads to the AP and IE DOF of the knee, and a series of straps to keep the body segments in place during testing. The loads are measured in real-time using a load cell, and the displacements are recorded using an HSSR system and previously validated tracking techniques. The resulting dynamic profiles are post-processed using custom scripts for analysis and creation of corresponding laxity curves.

4.2. Intended Uses

The knee laxity apparatus is intended for AP and IE laxity measurement of *in vivo* subjects for use in calibration of computational models.

4.3. Design Requirements

The design requirements for the knee laxity in decreasing order of importance are that the apparatus is: safe, comfortable, transparent in HSSR, allows for AP and IE measurements, allows for subject anthropometric variability, allows for multiple knee flexion angles, can be separated into separate pieces for ease of use, and can be cleaned disinfected.

4.3.1. Safety

The knee laxity apparatus shall be safe for *in vivo*. The apparatus is intended to be used on living subject testing, and as such, should be safe to use. The apparatus must not apply more than the prescribed load to ensure no potential injury to the subject. The apparatus must be able to release the load in the event of an emergency quickly. The apparatus must be stable and not yield or fracture under regular use. The apparatus must weight enough so as not to tip during use.

4.3.2. Comfortable

The knee laxity apparatus shall be as comfortable as possible. Comfort is a critical aspect of subjects feeling safe and relaxed. If the subject feels uncomfortable, it may affect their ability and willingness to perform more trials. In addition, accurate laxity measurements require the user to be as relaxed as possible to minimize the amount of muscle activation present, which has been shown to affect the AP laxity in particular by as much as 2 mm on average [19].

4.3.3. Transparent in HSSR

The knee laxity apparatus shall be made of materials that are radiolucent. The knee laxity apparatus is intended to be used in HSSR to improve the accuracy of the resulting measurements. It therefore needs to be made of as many radiolucent – XRay invisible materials as possible. Particularly the materials that will be in the view of one or both of the cameras.

4.3.4. Allow for AP and IE Laxity Assessment

The kee laxity apparatus shall be capable of making AP and IE laxity measurements. Part of the novelty of the apparatus is in its ability to measure both AP and IE laxity measurements and should, therefore, be designed around this as a critical design feature. The apparatus should thus be able to apply and measure the loads and resulting displacements in each of this DOF.

4.3.5. Allow for Subject Anthropometric Variability

The knee laxity apparatus shall allow for different joint anthropometrics of subjects from the height and weights of various segments. The apparatus is intended to be used to measure laxity on a wide range of subjects for the building of computational models. As such, the apparatus should be capable of height and length adjustment of each segment individually.

4.3.6. Allow for Multiple Knee Flexion Angles

The knee laxity apparatus shall allow for *in vivo* laxity assessment at several knee flexion angles. Laxity assessments are done at a range of flexion angles, with manual clinical measurements often done at 90°, while the majority of arthrometers are designed

for assessment at around 20-30° [16,20]. The apparatus should be able to measure AP and IE laxity at several flexion angles to allow for comparison to other reported values at different flexion angles. In addition, laxity measurements at multiple flexion angles are integral to the proper calibration of ligaments in computational models.

4.3.7. Allow for Apparatus Separation for Storage and Ease of Setup

The knee laxity apparatus shall be able to separate into smaller constituent components for ease of transport and setup. The apparatus will likely weigh a lot and therefore needs to be able to be separated into small pieces that can be moved individually and easy placed back together for testing.

4.3.8. Apparatus can be Cleaned and Disinfected

The knee laxity apparatus shall be able to be cleaned and disinfected between uses. Since the apparatus is intended for use in living subject testing, as well as occasional validation on cadaveric testing, the apparatus must be able to be cleaned and disinfected to ensure subject and tester safety.

4.4. Prototype

A mock-up and prototype of the apparatus was used to test design concepts and dimensions for human ergonomics, comfort, and use cases. The prototype version of the apparatus was made of wood and hand-cut, shown below in Figure 4-1.

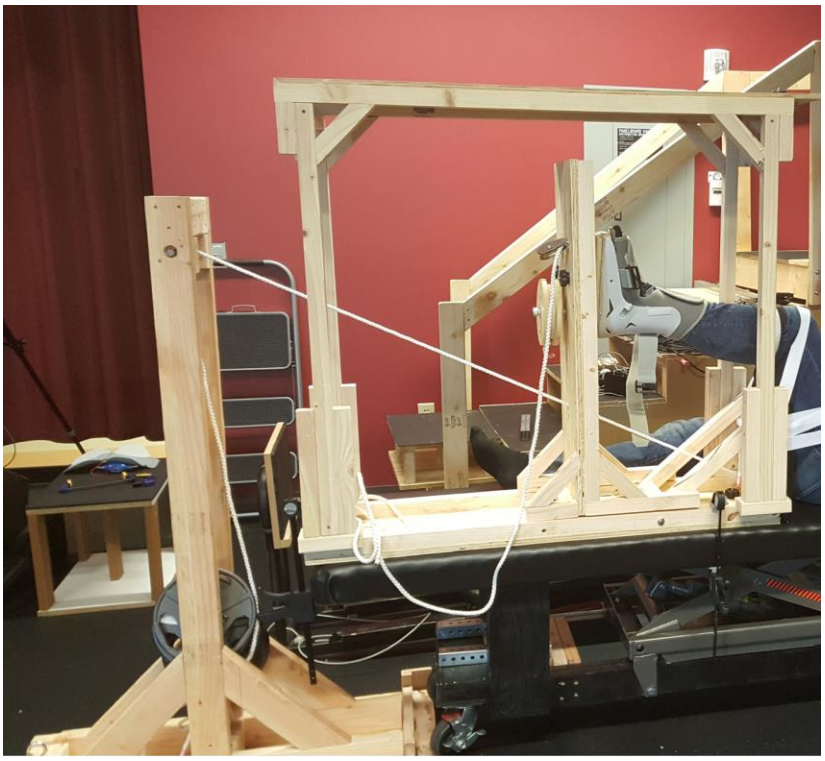

Figure 4-1 Image of Prototype Knee Laxity Apparatus

This iteration of the laxity apparatus demonstrated that the wood has the structural strength required for the final design and was radiolucent in Xray. However, because of its low machinability, many of the components were unable to achieve the desired tolerances. These low tolerances resulted in too much friction, and too much play in the majority of components, reducing the accuracy in resulting laxity measurements.

Plastic materials were used because of their machinability, ease of cleaning and radiolucency. Delrin was used for all components where friction was to be minimized to improve applied load efficiency and load application. In contrast, acrylic was used for all components where friction was to be maximized to maintain rigid contact. However, the vertical risers due to their size were unfeasible to make out of plastic because of the large size required to meet stiffness demands, and as such were made of hardwood.

4.5. Design

The knee laxity apparatus has primarily been designed by combining different aspects of prior implementations, specifically those in Figure 2-19, Figure 2-20, and Figure 2-21, while adding additional components and design changes for use in HSSR. The designed knee laxity apparatus was designed with all CAD in SolidWorks and consisted of two separable pieces: a base assembly, and a top assembly, shown below in Figure 4-2 and Figure 4-3. The apparatus has a knee flexion angle pad where the subject's thigh sits, allows for the knee flexion angle to be changed, and a series of thumbscrews and plates allow for height and length adjustment based on subject's anthropometric measurements. The apparatus contains a series of pulleys and cables to allow for attachment via cuffs to the subject's shank to apply AP loads, as well as a series of cables and pulleys attached to a boot to apply IE torques. A load cell is attached inline to the cables to measure the load in real-time, and the opposite ends of the cable are fed through the previously described weight tower used for the leg press to apply discrete loads using weights. The kinematics are measured using previously validated techniques in HSSR.

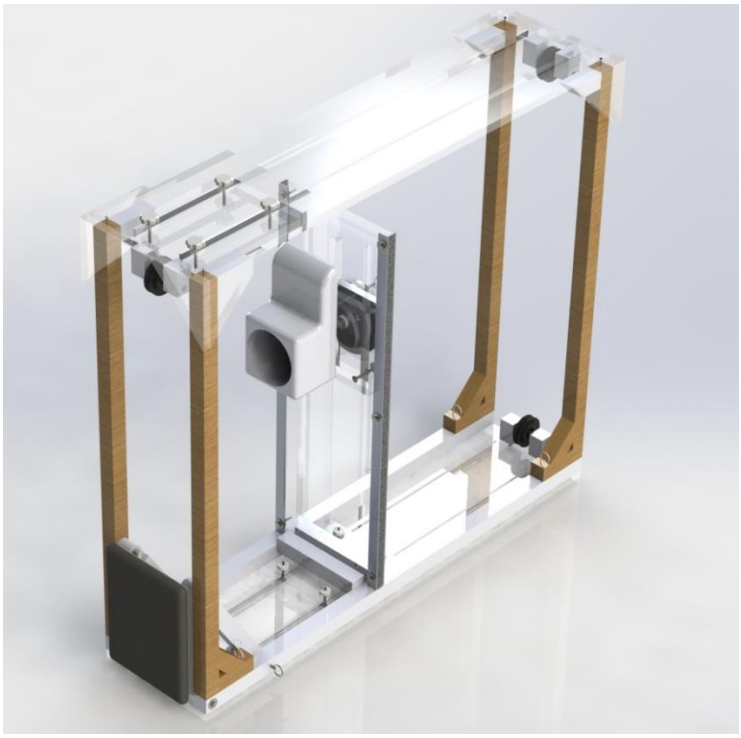

Figure 4-2 CAD Geometry of Total Knee Laxity Apparatus

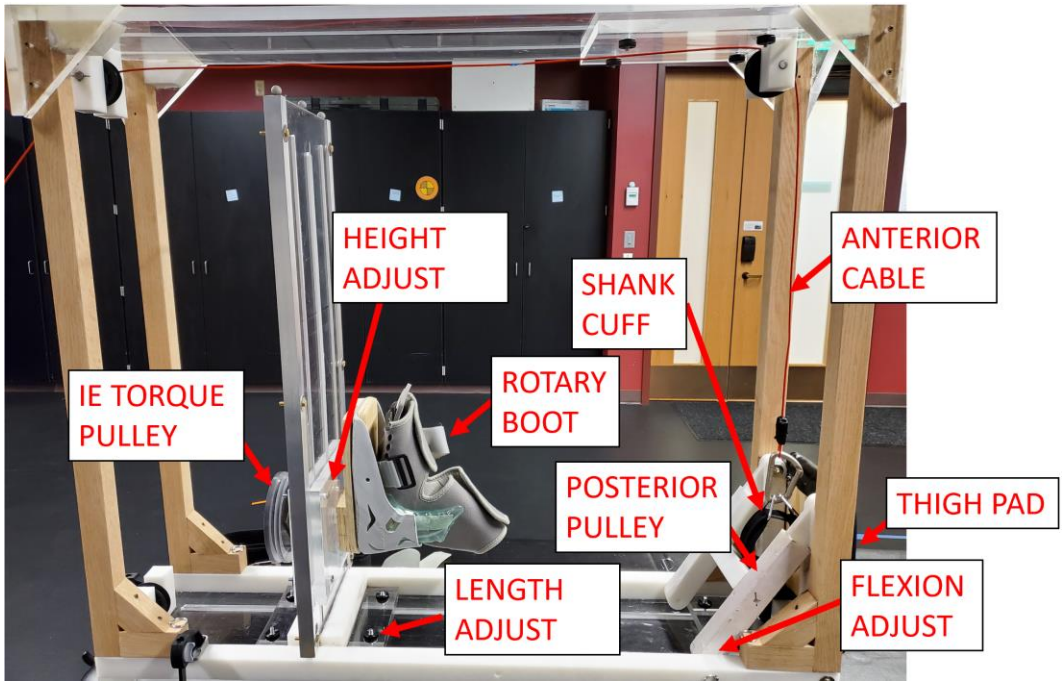

Figure 4-3 Image of Knee Laxity Apparatus with Labeled Major Components

4.5.1. Base Assembly

The majority of the components and bulk of the weight of the laxity apparatus is in the bottom base assembly shown below in Figure 4-4. The base assembly can be broken down into five components: an extended base plate, shown below in Figure 4-5, a knee flexion adjustment pad, shown below in Figure 4-6, a posterior load Pulley, shown below in Figure 4-7, a vertical platform, shown below in Figure 4-8, and a rotational boot, shown below in Figure 4-9.

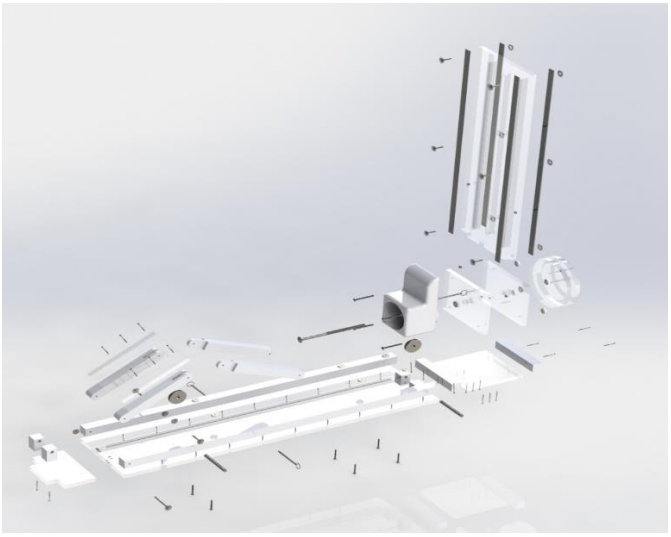

Figure 4-4 CAD Geometry of Exploded View of Bottom Base Assembly

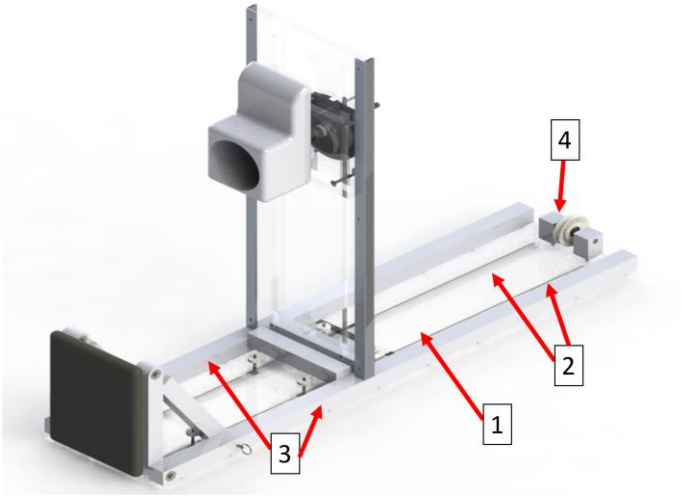

Figure 4-5 CAD Geometry of Long Base Plate Component in Bottom Base Assembly

The base assembly rests on the bottom plate (4 ft by 1ft by ¾ in cast acrylic, 1 in Figure 4-5) with 2 T-slots cut down the majority of the length of the material (2 in Figure 4-5). The T-slots allow for adjustment of the other components of the base assembly. Attached to the bottom plate are two side rails that run the length of the plate (Delrin, 3 in Figure 4-5). These side rails are bolted into the bottom plate, and have holes drilled to allow for attachment to the top assembly, as well as to the knee flexion pad. At the end of the plate are a pair of vertical Delrin rods, a steel rod, and a pulley with rolling element bearings (4 in Figure 4-5) to allow for redirection of pulley cables if necessary.

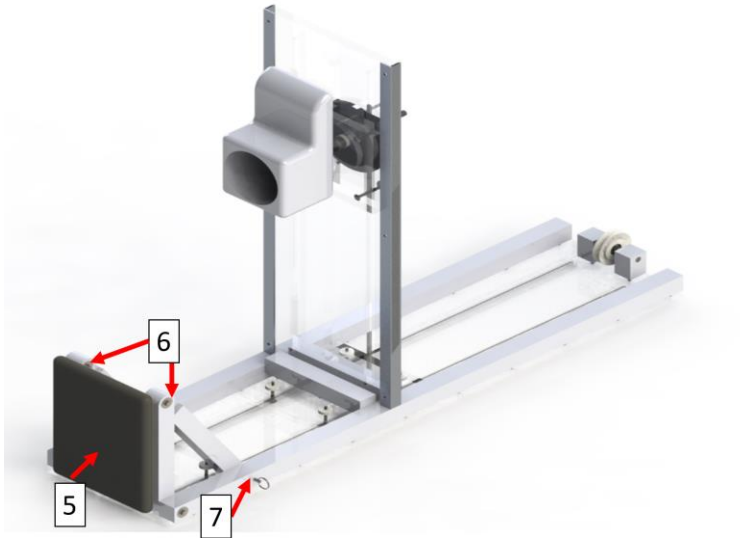

Figure 4-6 CAD Geometry of Knee Flexion Angle Pad Component in Bottom Base Assembly

The knee flexion pad (5 in Figure 4-6) adjustment consists of a wooden plate covered in a flexible rubber material, and a vinyl coating. This plate is then attached to 2 sets of Delrin rods with matching hinge joints (6 in Figure 4-6) cut to allow for connection and rotational motion about 1 DOF. The ends of the rods are bolted into the side of the Delrin rails of the bottom plate. The knee flexion angle can be adjusted by moving the rods and adjusting the hinge to specific holes drilled in the Delrin rails (7 in Figure 4-6) and inserting two cotter pins through the holes.

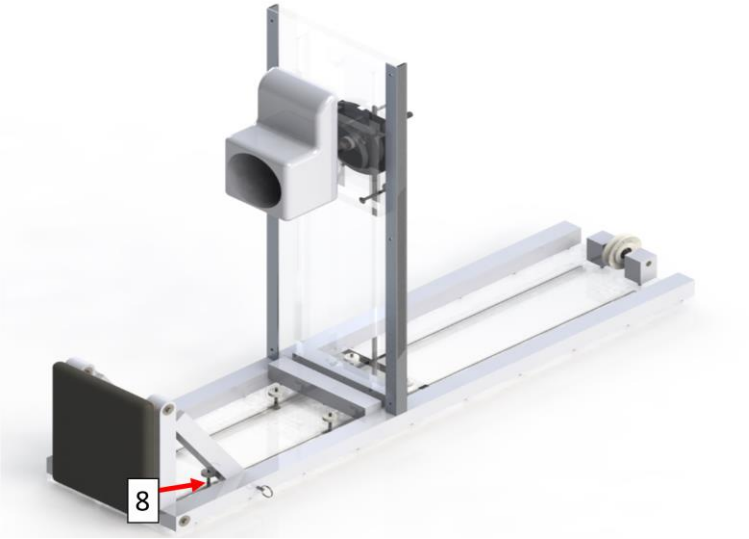

Figure 4-7 CAD Geometry of Posterior Pulley Plate Component in Bottom Base Assembly

The posterior load pulley consists of an acrylic plate, with two holes drilled at a distance to match the bottom plate T-Slots, as well as a set of vertical pieces and a steel rod to hold a pulley wheel in place, identical to the rear pulley (4 in Figure 4-5). The load pulley can be moved along the length of the bottom base, and can be fixed in place using a pair of bolts and thumbscrews using the T-Slots of the bottom plate (8 in Figure 4-7). The adjustment is performed to place the location of the posterior pulley so that the cable is directed perpendicular to the shank and below the knee joint line. Then a steel cable with a carabiner and a cuff is attached to the subject's shank, and the other end of the cable is redirected around the pulley to apply the posterior tibial load.

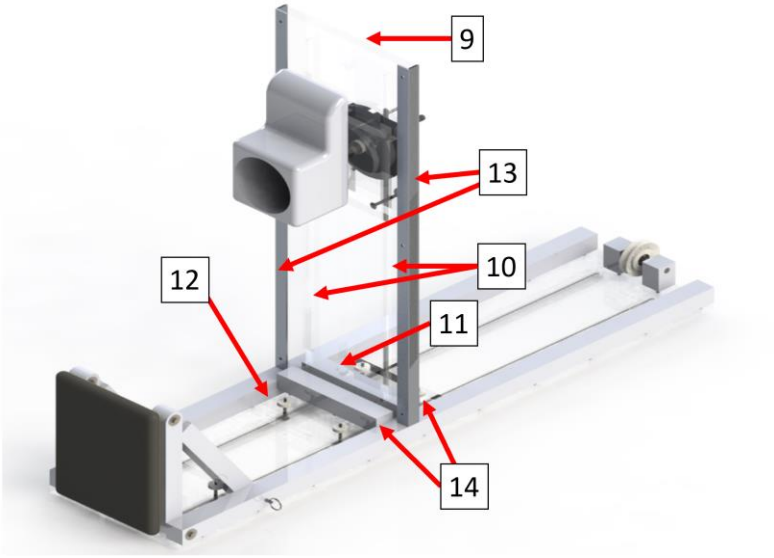

Figure 4-8 CAD Geometry of Vertical Plate Component in Bottom Base Assembly

The vertical platform (9 in Figure 4-8) is one of two critical components of the entire knee laxity apparatus. The vertical platform consists of a 3 ft by 12 in by ¾ in piece of acrylic with two ¼ in slots drilled along the edge (10 in Figure 4-8), and a larger 1 in slot along the centerline (11 in Figure 4-8). The piece is then rigidly butt jointed to another acrylic plate (12 in Figure 4-8) with four holes drilled in to allow thumb screws to attach this piece to the bottom plate. These thumbscrews allow for adjustment of the vertical riser to adjust for the knee flexion angle, and the length of the subject. The vertical riser is supported by two L-bracket pieces of aluminum (13 in Figure 4-8) and two Delrin blocks (14 in Figure 4-8) to increase bending stiffness.

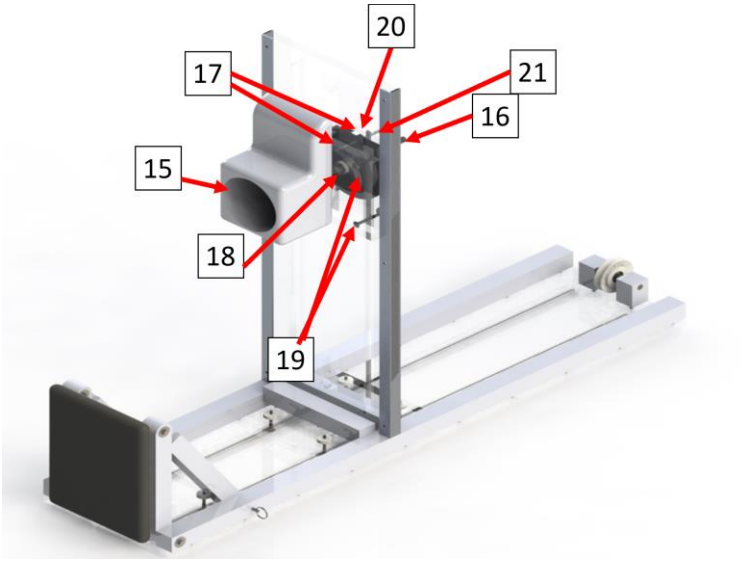

Figure 4-9 CAD Geometry of Rotational Boot Component in Bottom Base Assembly

The rotational boot component is one of two critical components in the knee laxity apparatus. The rotational boot consists of a boot and a steel plate that the subject's foot is placed into during testing (15 in Figure 4-9). The boot then has a ½ in steel bolt (16 in Figure 4-9) that is rigidly screwed onto the steel plate. The steel bolt goes through two acrylic plates (17 in Figure 4-9), with each acrylic plate having a ½ in bore rolling element bearing (18 in Figure 4-9), to allow for rotation of the bolt and thus the boot, about a fixed axis. A nut is placed on the steel bolt to prevent translation of the bolt, thus allowing only pure rotation about the bolt axis for the boot and the subject's foot. The acrylic plates (17 in Figure 4-9), have holes, to match the slots in the vertical platform. The smaller slots allow four sets of thumbscrews (19 in Figure 4-9) and carriage bolts to fix the plates to a vertical position along the vertical plate, and thus fix the foot at a fixed height. The center slot allows the bolt to pass through the vertical plate freely. An acrylic pulley (20 in Figure 4-9) is rigidly fixed to the steel bolt on the opposite side of the

vertical plate. A fixed load is applied to the edge of this pulley at the 5 in OD of the pulley, creating a known torque on the bolt, and thus the boot and foot of the subject. A cotter pin (21 Figure 4-9) can be placed through the acrylic plates into the steel plate on the boot to restrict rotation for AP laxity testing, and removed for IE laxity testing.

4.5.2. Top Assembly

The top assembly, shown in Figure 4-10, allows for Anterior Loading of the joint, as well as a means of converting the load applied with a discrete weight to the torque at the boot for IE loading. The top assembly can be broken down into three components: vertical support risers and top plate, fixed end pulley, movable track pulley.

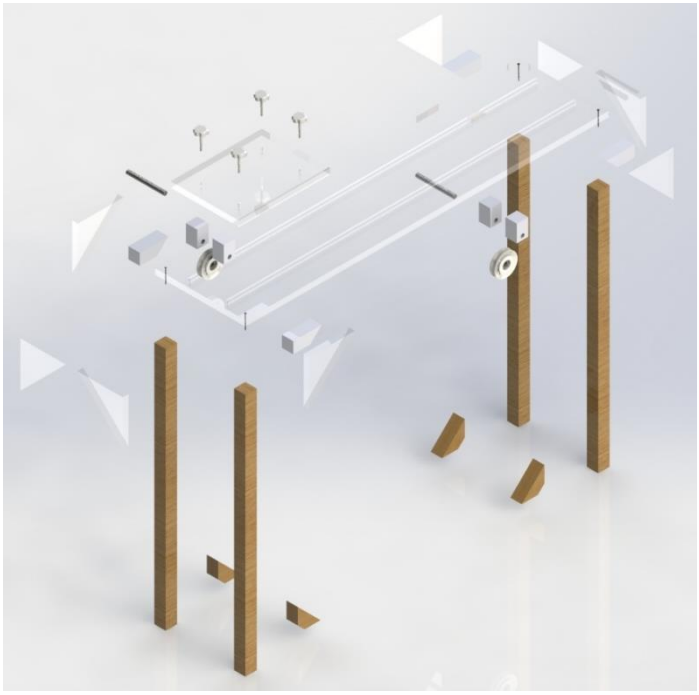

Figure 4-10 CAD Geometry of Exploded View of Top Assembly

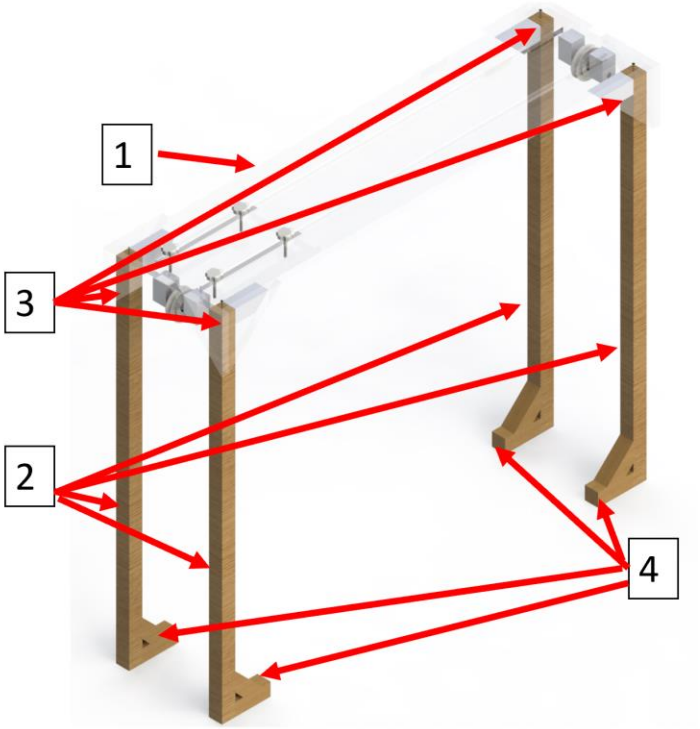

Figure 4-11 CAD Geometry of Top Support Plate and Vertical Risers Component of Top Assembly

The top support plate (1 in Figure 4-11) is a 4 ft by 12 in by ¾ in piece of acrylic with two slots cut along the length of it to allow for thumb screws and carriage bolts to be placed through it. The plate is rigidly attached to four vertical risers (2 in Figure 4-11) of oak that are 4 ft tall. These ensure a strong, rigid top without being too heavy or visible in Xray. The wooden risers are connected to the top plate using industrial grade adhesive and screws, as well as acrylic corner brackets (3 in Figure 4-11) to ensure a rigid connection. Four corner connectors are added at the feet of the vertical risers that allow for added stability. They have holes drilled through them to allow for a connection between the top assembly to the bottom base assembly using cotter pins.

Figure 4-12 CAD Geometry of Fixed Pulley Component of Top Assembly

The fixed pulley component consists of two vertical offsets made of Delrin and a steel rod that has a pulley with roller bearing elements in it (5 in Figure 4-12). This component allows for redirection of the cables around the rest of the structure.

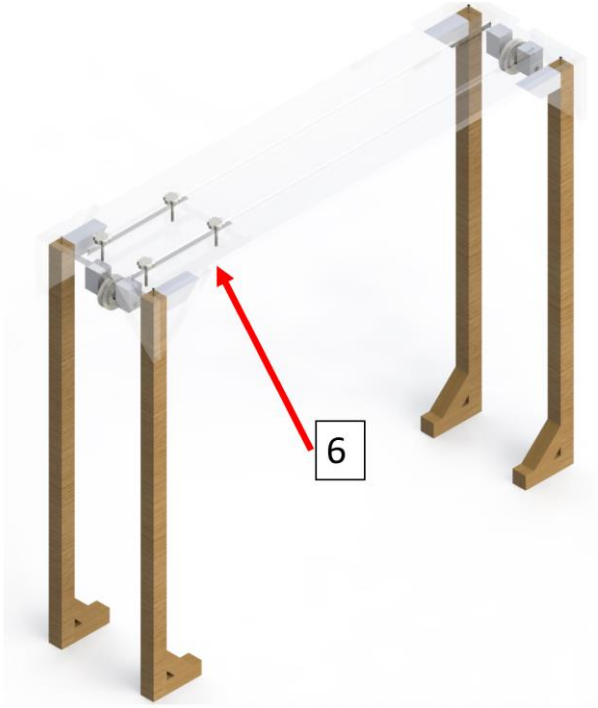

Figure 4-13 CAD Geometry of Movable Pulley Component in Top Assembly

The movable pulley component (6 in Figure 4-13), consists of an acrylic plate with four holes drilled in it to match the two slots running along the top plate. The pulley is attached to this plate in a similar manner as the fixed pulley (5 in Figure 4-12). The purpose of this movable pulley plate is to allow for a cable, carabiner, and cuff to be attached to the shank at the corresponding location around the joint line of the knee while accounting for subject anthropometric variability. The plate is secured using thumbscrews and carriage bolts to the top plate to keep it rigid at the desired location. The plate also moves back for the IE trial to allow for a redirection of the cable for IE torque application from the structure.

4.6. Satisfying Design Requirements

4.6.1. Safety

The apparatus ensures safety by applying loads to the individual using discrete weights. While other devices designed previously have relied mainly on control systems to apply the loads [60,65,68]. This method was deemed potentially unsafe, as any failure of the control system could potentially apply a large load to the joint, which could cause severe injury to the subject. The method of using discrete weights to apply the loads ensures that the load applied to the joint will at most reach the applied weight. For trials where a ramped load is desired, the discrete weights are gradually released by the operator, and load can be increased and decreased continuously to ensure that the maximum load does not exceed the current discrete weight applied.

The knee laxity apparatus applies the loads by use of the aforementioned weight tower and the use of cables. The loading cable is connected by a carabiner, and in the event of an emergency can be quickly snapped off to remove the load applied to the subject. This helps to ensure subject safety in the event of an emergency.

The previous design was determined to be too unstable from the low tolerance associated with cutting wood. In addition, the previous version flexed too much, and was known to splinter, potentially causing injury to the subject. The current knee laxity apparatus was primarily made out of stiffer and heavier materials: Delrin, Acrylic, and hardwood. These materials are CNC machinable, resulting in a higher tolerance fits between parts. As such, the stiffness and stability of the current version was vastly improved. The additional weight, along with improved tolerances has resulted in a safer,

more structurally sound device. In addition, the final knee laxity apparatus has been designed and analyzed to ensure that no fracturing, excessive bending, or yielding of the parts occurs and maintains a stiff structure. An example of the FEA models performed to ensure safety is shown below in Figure 4-14.

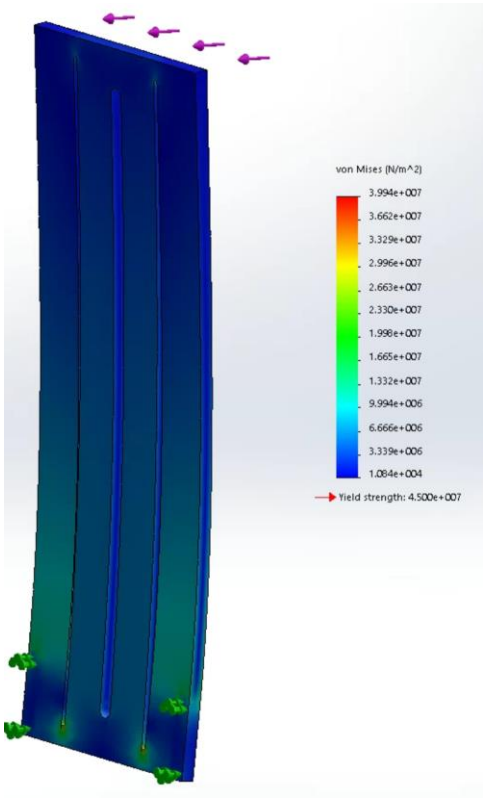

Figure 4-14 Von Mises Plot of Maximum Transverse Load Applied to Vertical Plate in SolidWorks

The apparatus was predicted to weight around 100 lbf, and the actual weight of the apparatus seems to weigh around 120 lbf, because of inaccurate prediction of the exact material properties of the wood components. In addition, ¾ of the weight is known to be in the bottom base assembly, resulting in a relatively lower Center of Gravity of approximately 19.3 in above the bottom plate. This means that to fall over, the apparatus

will need to tilt more than 17°, which does not take into account the additional weight of the subject's leg. Although it is unlikely that the apparatus will tip over under regular use, the device is clamped to the patient table prior to use.

4.6.2. Comfortable

The apparatus has a cushioned pad made of a soft rubber material on the knee flexion angle pad that the thigh rests on. In addition, the boot that contains the foot is an orthopedic boot. This orthopaedic boot, is a commercially available orthotic for the purpose of restraining the ankle post-injury and designed to hold the foot in place safely and comfortably after ankle injuries. In addition, the orthopaedic boot has air filled sacks on either side of the ankle, to help add additional constraint and comfort to the subject during testing. Any potentially sharp edges on the laxity apparatus have been buffed down, and towels and pads are placed to ensure no contact with the edges of the apparatus. These features help to ensure that the leg is placed as comfortably as possible in the apparatus during the duration of the testing.

4.6.3. Transparent in HSSR

With the exception of the carabiners, the L-brackets, the steel cables, and the metal connectors all of the components have been chosen because of their stiffness and weight as well as their radiolucent properties in Xray. All three of the materials, Delrin, acrylic, and hardwood, are known and have been validated to be amongst the most radiolucent materials available. These radiolucent materials ensure that there will be very few components in the field of view of the HSSR to interfere with the final image.

4.6.4. Allow for AP and IE Laxity Assessment

The apparatus has two pulleys on the top assembly that allow for a cable, carabiner, and cuff to be attached to the shank for anterior laxity measurement, while the bottom base assembly has two pulleys that can be set up similarly to apply for posterior measurement. The pulley attached to the boot, can be used with the cables to apply loads to this pulley and convert them to a pure torque applied to the knee in IE. These methods, along with the load cell, allows for accurate application and measurement of AP and IE loads. The cotter pin on the boot plate allows for AP laxity measurements to be made without allowing rotation of the bones, and can then be removed to apply IE rotations. In addition, all of the components that need to be able to move during measurement are made using low friction Delrin to minimize the effects of friction on the measurement. While the components that are not supposed to move during measurement are all made out of acrylic on acrylic contact, which has a relatively high frictional constant, ensuring that the components stay rigid during the trial. All of these features ensure that AP and IE laxity measurements can be made, and that the measurements are made accurately.

4.6.5. Allow for Subject Anthropometric Variability

The apparatus was designed in CAD using statistical values for anthropometrics of the lengths and sizes of the thigh and shank to ensure its viability for *in vivo* testing, shown below in Figure 4-15. The different setups analyzed are based on the 5^{th} percentile and 95^{th} percentiles of the length and size for individuals thighs and shanks from USAF testing [79]. The setups are shown for the 30°, and 90° knee flexion poses, and show that

the travel of the components is sufficient to allow these extremes of subject anthropometrics.

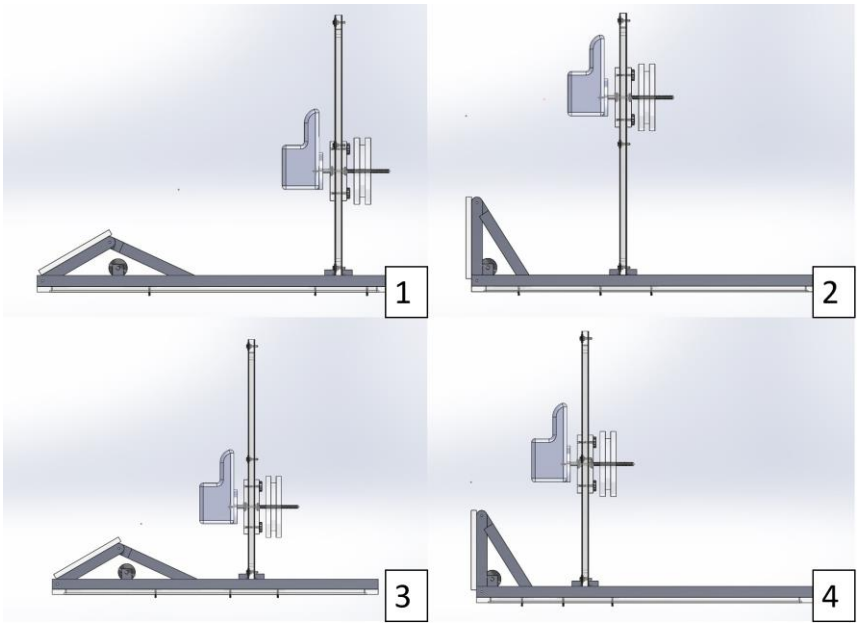

Figure 4-15 CAD Geometry of Different Setups for Subject Anthropometric Variability in SolidWorks. 95% Size Top, 5% Size Bot

4.6.6. Allow for Different Flexion Angles

As shown above in Figure 4-15, the apparatus is capable of measuring the laxity at different knee flexion angles. While the apparatus has currently only been tested at 30° and 90° of knee flexion, additional angles can be created simply by drilling additional holes at specific locations on the Delrin rails.

4.6.7. Allow for Apparatus Separation for Storage and Ease of Setup

The knee laxity apparatus is broken into a bottom base assembly and a top assembly that can be connected through the use of 4 cotter pins. This connection allows for the bottom and the top to be transported separately and connected during testing to improve

transportation and ease of setup, because of the decreased total weight of a single component.

4.6.8. Apparatus can be Cleaned and Disinfected

This apparatus is made up of all materials that can be cleaned using bleach wipes without side effects. In addition, all of the materials, other than the steel bolt connectors, are corrosion resistant. The connectors, if they ever corrode, can easily be replaced using components available in standard hardware stores. The materials chosen ensure that the entire knee laxity apparatus can be cleaned using bleach and other solvents without permanent damage to the look or structural integrity of the apparatus.

4.7. Design Use

The knee laxity apparatus applies loads to the knee in the AP and IE directions by applying loads to steel cables arranged in different means through a system of pulleys. Each of these loads are measured as the tension in the cable, and the resulting load applied to the knee, is either the same as the load to the knee, or in the case of IE, is determine as the load multiplied by the moment arm of the IE pulley. These applied loads can be seen below in Figure 4-16. The red arrows represent the load in the cable, and the green arrow represents the resulting load on the knee, or the resulting torque on the knee.

Figure 4-16 Images of Applied Cable Loads and Resulting Loads for Knee Laxity Apparatus. Top Left: Anterior. Bottom Left: Posterior. Right: Internal/External

The knee laxity apparatus is intended for use in *in vivo* knee laxity assessment using HSSR, such as the example test setup shown below in Figure 4-17.

Figure 4-17 Knee Laxity Apparatus in use during In Vivo measurement of right knee external rotation laxity in view of the HSSR

The subject is placed in the apparatus by adjusting the knee flexion angle to the desired angle, and using the cotter pins to lock the angle in place. The thigh of the subject is placed on the pad, and then the foot is placed in the boot. Everything is secured using straps. The AP cuff is attached to the shank, and then the carabiner and cables are setup to attach to the cuff. The load cell is placed inline with the cables, and various discrete loads are applied to the subject's knee at the current flexion angle. At each load, a recording of the HSSR image, the Vicon marker data, and the load cell data is recorded. The cable is then switched to apply the load in the opposite direction and repeated. Then the cables are moved to the IE load, and the cotter pin is removed from the boot to allow the boot to rotate freely. Discrete loads are applied to the cables, and the tension in the cables is measured, and then using the radius of the IE wheel, is converted to the appropriate torque measurement. If desired, the system is then adjusted for a different flexion angle and then the AP and IE measurements are repeated in the same manner as before, shown below in Figure 4-18.

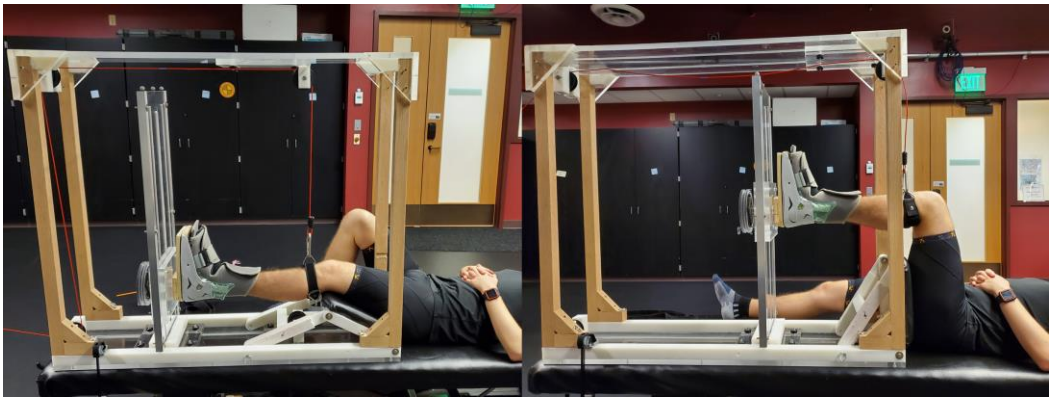

Figure 4-18 Knee Laxity Apparatus at 30 Degree and 90 Degree Knee Flexion

The data is tracked in the same manner as previously discussed in the leg press section in Figure 3-5. The plots are created as the kinematic of the specific degree of

freedom plotted against the load of the given trial. The displacement is reported as the Grood and Suntay (GS) kinematic value of the DOF at the current load relative to the GS value at the neutral unloaded position of the knee [77]. Loads can be applied statically through the use of a discrete weight or can be applied dynamically using the same weight being lifted up and down, resulting in a continuously changing force profile. In both cases, the maximum load applied is equivalent to the amount of the weight used. If the load is applied discretely, the measurement for a trial will be a single point on the laxity curve, while a continuous trial will create a series of continuous points. The applied loads were validated through the use of another load cell for AP, and a torque transducer for IE to verify accuracy of applied loads and quantify the frictional losses within the system, between the input and the output. In both cases, the input load and the resulting output force or torque was within 1% of the value predicted. An example AP laxity curve is shown below in Figure 4-19.

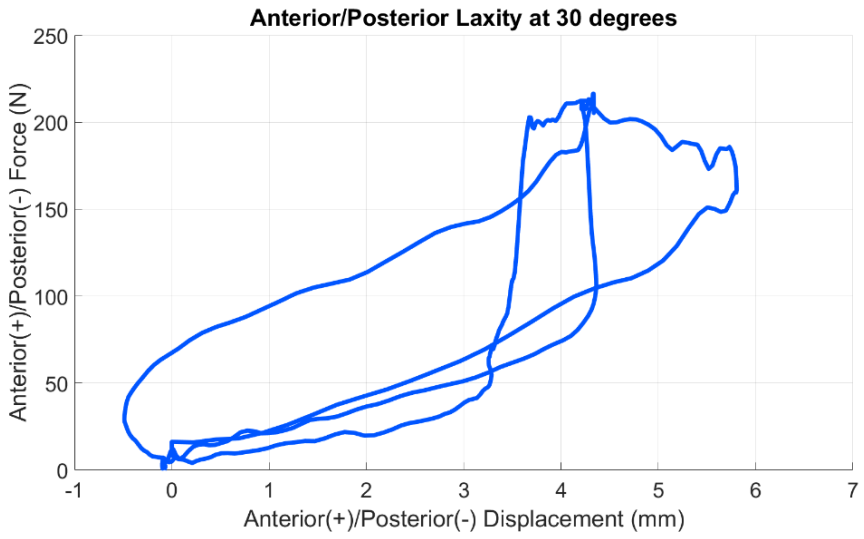

Figure 4-19 Example AP Laxity Curve from Knee Laxity Apparatus showing anterior displacement of the tibia relative to the femur in response to a ramped 200N anterior force.

Force-displacement characteristics from laxity measurements are an integral part of computational modeling calibration. However, the majority of computational models are based on *in vitro* measurements because of a lack of accurate and available *in vivo* data on individual subjects. Aim 2 of this study was to design and build a device capable of making accurate *in vivo* AP and IE laxity measurements on subjects. A device was built to allow for AP and IE laxity measurements to be made at various flexion angles on subjects *in vivo.* The next step is to determine the accuracy of the designed apparatus as part of Aim 3. Data collected from two cadavers and two subjects were used to evaluate the accuracy and validity of the knee laxity apparatus for use in *in vivo* laxity assessment.

Chapter 5: Validation of Knee Laxity Apparatus

This chapter is being prepared for eventual submission to the ASME Journal of Medical Devices.

5.1. Introduction

Personalized medicine has and will continue to grow in popularity in the future as the technology surrounding it becomes cheaper, faster, and more reliable. In orthopaedics, technological advancements have enabled personalized surgical plans, guides, and implants, with improved results compared to traditional surgical approaches [80–82]. This technology has created a surge in interest for advanced computational models, not only to aid in the design but to better understand the underlying phenomenological differences present within healthy and unhealthy populations. However, these models are highly dependent on the accuracy and amount of data used to calibrate their final properties.

In the knee, in particular, while many computational models derive kinematic data from *in* vivo testing, significant parts of most models are built using data taken from *in vitro* testing [22,42,69,70,83–86]. One such example is the passive properties of the knee. Often modeled from *in vitro* stiffness measurements because *in vivo* subject-specific measurements are unavailable, these stiffness measurements are used to adjust parameters of the knee model.

In particular, these measurements are used to calibrate the complex motion that occurs from the non-linear force-displacement relationship of the ligaments within the knee, known as laxity [14]. However, work has shown that these laxity assessments differ in values between sedated and non-sedated patients, and therefore bring in to question the viability of modeling *in vivo* kinematics using models built from *in vitro* measurements [19]. The next step is to make these models more subject-specific, and as such, there is a need for *in vivo* laxity assessments with an accuracy comparable to those *in vitro*.

While *in vitro* measurements can use load cells and markers rigidly attached to the bones to make accurate laxity assessments, *in vivo* measurements, have primarily been limited to force-displacement measurements made using surface-based probes; yielding higher uncertainty, and making them unpopular for use in modeling [19,20,52,83]. Recent work has attempted to use more accurate means of displacement measurement including MRI and Fluoroscopy as a means of accurately measuring the displacements [60–62,65–67]. However, none of these devices are capable of making both Anterior-Posterior (AP), and Internal-External (IE) laxity measurements over a range of knee flexion angles, which are both critical for accurate model calibration [83].

Our goal was to design a device capable of making *in vivo* AP and IE laxity measurements using previously validated methods, with an accuracy similar to existing *in vitro* methods. With the ultimate goal to accurately capture *in vivo* laxity measurements for use in subject-specific computational model calibration of the knee. We present a novel apparatus capable of making AP and IE laxity measurements using HSSR. To assess the accuracy and validity of the apparatus for *in vivo* testing, laxity measurements

were made on two cadavers and the results compared to a sophisticated in vitro measurement methods[37]. In addition, laxity measurements were obtained from two living subjects to demonstrate the use of the apparatus for *in vivo* soft tissue and compare to the in vitro measurements.

5.2. Methods

5.2.1. Design

The knee laxity apparatus, shown below in Figure 5-1, is made of radiolucent materials and holds the limb in place at a range of adjustable flexion angles during the duration of the AP or IE laxity tests.

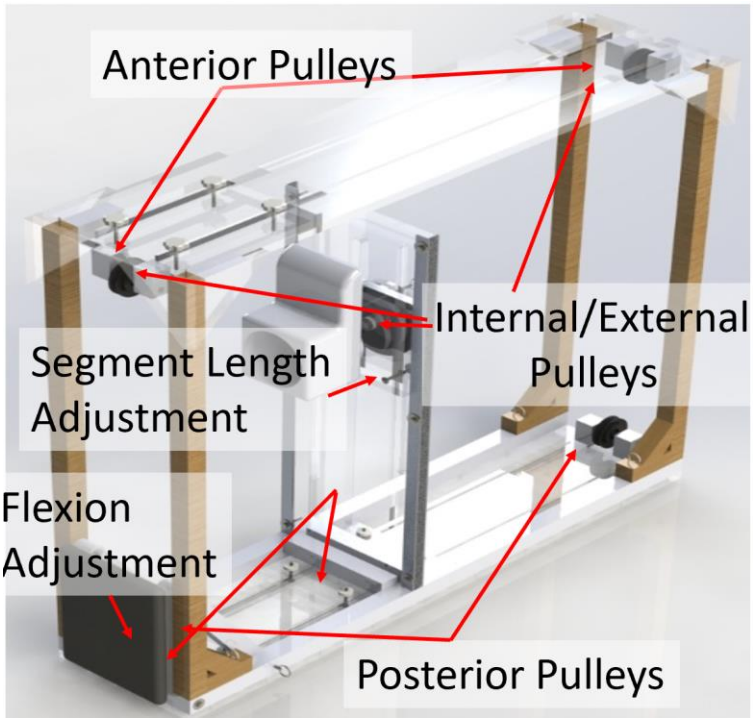

Figure 5-1 CAD Geometry of Knee Laxity Apparatus in SolidWorks

The subject lies supine on a table and has their hip flexed to allow their thigh to rest against a rubber pad, the knee then rests off the pad parallel to the ground, with the ankle

securely fastened into a plastic orthopaedic boot. The knee flexion angle is adjusted by tilting the rubbed pad and fixing it in place using a set of cotter pins and pre-drilled holes at specific locations. The boot is attached to a vertical stage with slots and thumbscrews to allow for a wide range of subject anthropometric differences.

Anterior-posterior loads are applied to the knee by a cuff attached to the shank through a system of cables and pulleys attached to the top and bottom frames of the laxity apparatus. The thigh is rigidly held in place using straps, and the foot is locked into place in the boot in the vertical position. By removing a cotter pin in the boot, internal-external torques can be applied through a cable applying a moment to a pulley rigidly attached to the boot where the subject's foot and shank are secured.

Loads are measured in real-time using a load cell, and can be applied through a series of discrete weights or via a continuous dynamic load, which have previously been shown to yield different results [24,87]. Kinematics are tracked by using previously validated bone tracking techniques combining high-speed stereo radiography (HSSR) with bone geometries from computed tomography (CT) or magnetic resonance imaging (MRI) [88,89].

5.2.2. Cadaveric Testing

To validate the use and accuracy of the knee laxity apparatus, the testing was separated into an "*in vivo"* testing setup using the knee laxity apparatus and a conventional *in* vitro setup using a robotic knee tester for each specimen.

5.2.2.1. Cadaveric Laxity Testing in Knee Laxity Apparatus

Two male pelvis-to-toes specimens (ages 64 and 29; BMI 17.8 and 32.1) were brought into view of the HSSR system and manually moved through a no-load joint flexion-extension range of motion (ROM). The specimens were then placed in the knee laxity apparatus in view of the HSSR, as shown in Figure 5-2 below, and AP and IE loads were applied at 30° and 90° knee flexion angles for both sides.

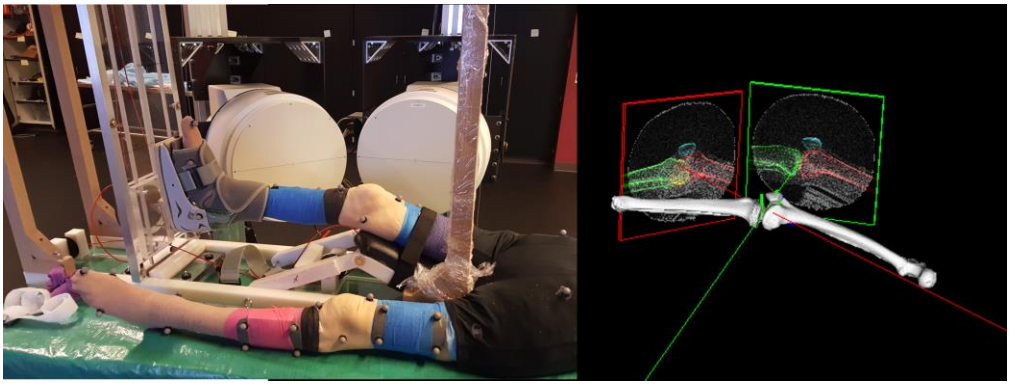

Figure 5-2 Knee Laxity Apparatus for Cadaveric Laxity Assessment and Tracked Bones in DSX

Per previous work, IE loads were applied in static, discrete amounts from 1.41 N*m up to 5.65 N*m, and then continuously ramped up to 6 N*m through a ramp and hold trapezoid wave profile [24,25]. Following this, AP loads were applied in discrete amounts from 44.5 N up to 178 N, followed by the same continuous ramp and hold profile as the IE loads up to 200 N [19,20,24]. To minimize the amount of time for tissue degradation, the specimens were tested in the following order: Left leg 90° flexion, left leg 30° flexion, right leg 30° flexion, right leg 90° flexion.

To obtain knee kinematics from the HSSR images, bone geometries were segmented from specimen CT scans using ScanIP software (Simpleware), and a Grood and Suntay

(GS) coordinate system was applied to the bones using the Transepicondylar Axis coordinate system [77,90]. Using Autoscoper (XROMM) and DSX (C-Motion), the bone geometries were used along with captured XRays from the HSSR system to track the bones in 3D space through the trials using previously validated techniques [63,88,89]. In brief, these techniques use calibrated positions of the camera system, and the bone geometries to manipulate the bone position in 3D space, until the resulting 2D projections of the bones onto each camera create the resulting captured image. Kinematics data was then processed using a custom script in MATLAB (MathWorks) to calculate the GS kinematics. For each trial, the displacement was recorded as the net difference between the trial GS position, and the GS passive position from the no-load motion, captured earlier. Force data captured from the load cell, was combined with this displacement data to create corresponding AP and IE laxity curves. The hysteresis in the loading and unloading portion of the continuous loading laxity curves was quantified by using the minimum and maximum displacements at a given load across 14 discrete loads, and then calculating the RMS difference (RMSD) between the max and mins at these loads.

5.2.2.2. Cadaveric Laxity Testing in Robotic Knee Tester

Following the knee laxity apparatus measurements, the specimens were taken and placed into a robotic knee tester, shown below in Figure 5-3, for comparison to the measurements made by the knee laxity apparatus.

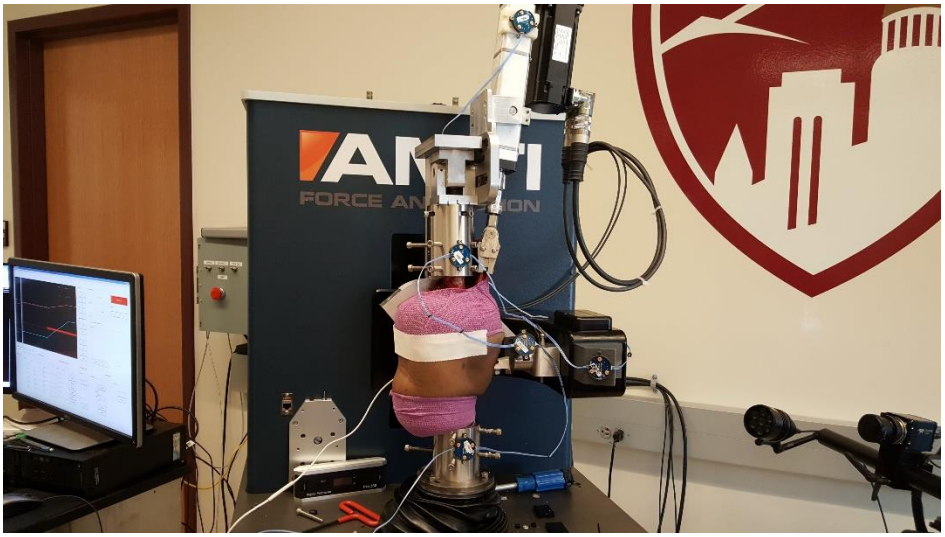

Figure 5-3 Robotic Knee Tester Setup for Cadaveric Laxity Testing

The specimens were dissected, leaving approximately 230 mm of the femur and 125 mm of the tibia, maintaining around 200 mm of soft tissue surrounding the knee intact. The knee was then potted using potting cement and custom fixturing in a VIVO (AMTI) Joint Simulator. A custom-designed apparatus was used to apply a 10 N load parallel to the femur to simulate the passive tension in the patellar tendon [91,92]. A passive ROM was similarly performed on the specimens as *in vivo* testing, to again act as a baseline GS position. AP and IE laxity measurements were made using similar continuous loading profiles to those in the knee laxity apparatus testing and performed at every flexion angle between 0-120° in 15° increments. The knee flexion angle was held constant during the trial, and then the DOF of interest was applied by following a ramping trapezoidal force profile. During the trials, all remaining DOF, were set to force control, and a force of zero-load, to allow for unconstrained movement. Kinematics were measured using the Optotrak (Northern Digital Inc.) motion capture system using markers rigidly affixed to the femur, tibia, and robotic system. A 6 DOF load cell built into the VIVO system was

used to measure the applied loads. The kinematics and loads were then combined using the same methods as previously described. Complete cadaveric datasets, including dynamics and laxity results, as well as CT, MRI, and Laserscan geometry, are available in Appendix A.

5.2.3. Subject Testing

To verify the use of the knee laxity apparatus for use in *in vivo*, laxity assessments were made on living subjects and compared to average values from literature. Two male subjects (ages 51 and 73; BMI 31.5 and 26.7) were collected as part of another study. Both subjects provided informed consent and were recruited after approval by the Institutional Review Board of the University of Denver. Reflective markers for use with a Vicon Motion Capture system (Vicon) were placed on anatomical landmarks, and electromyograms (EMG) sensors were placed on the quadriceps muscle groups, hamstrings, and the hip abductors. The subjects were brought into view of the HSSR system and performed a range of activities including gait, lunge, single and dual leg stance. After all primary motion trials were collected, subjects performed isometric maximal voluntary contractions (MVC) for both extension and flexion. We hypothesized that the fatiguing of the muscles from repeated MVC would reduce muscle activation, which has been shown to affect the accuracy of laxity measurements. In particular, it has been shown that increased muscle activation during a laxity assessment results in a lower total displacement being observed, compared to the same knee without muscle activation [19].

The subjects were then placed in the knee laxity apparatus at a 30° knee flexion angle, shown below in Figure 5-4.

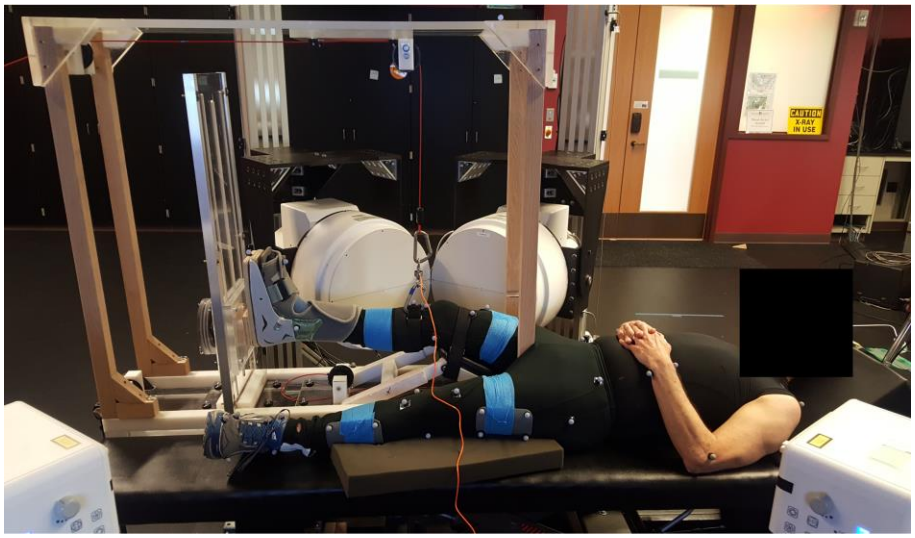

Figure 5-4 Knee Laxity Setup for In Vivo Anterior Laxity Assessment

Following previous work, anterior laxity loads were applied to the subject up to 40 lbf using discrete weights [20,24,43]. Loads increments were stopped if the subject expressed any discomfort. For time considerations, posterior loads were not performed as part of the larger study. The knee laxity apparatus was then reconfigured for IE laxity. Again, following previous work, loads were applied to the knees at loads up to 6 N*m, with the same safety measures in place as for the anterior testing [24,25,43]. Following Proprioceptive Neuromuscular Facilitation (PNF), subjects were instructed to first resist against the applied load, and then relax into it, as this has been shown to increase ROM of various joints [93]. After the subjects had wholly relaxed into the weight, the trial was captured. Data for the trials was tracked using the same process as previously stated, and laxity plots were made in the same format as before, by calculating the displacement at an applied load relative to the no-load joint GS position.

5.3. Cadaver Testing Results

The total AP displacement for both cadaveric specimens, shown in Figure 5-5 and Figure 5-6 below, was found to be within 1 mm of accuracy between the laxity apparatus measurement, and the robotic knee measurement, shown in Table 5-1 below. In addition, the total IE displacements, shown in Figure 5-7 and Figure 5-8 below, were found to be within 2.5° between the laxity apparatus measurement, and the robotic knee measurement, shown in Table 5-1 below. Additionally, the statistics of the differences between AP and IE displacements, between the knee laxity apparatus using the static measurements, vs. the corresponding values for the robotic knee tester are shown below in Table 5-2.

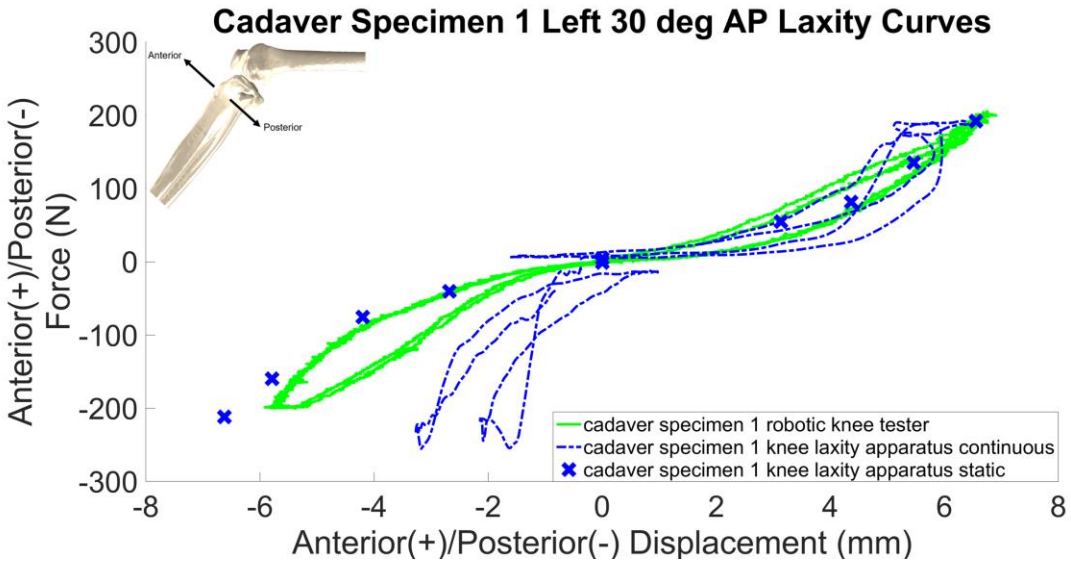

Figure 5-5 Knee Laxity Apparatus vs. Robotic Knee Tester AP Laxity for Specimen 1 Left at 30 degrees of Knee Flexion

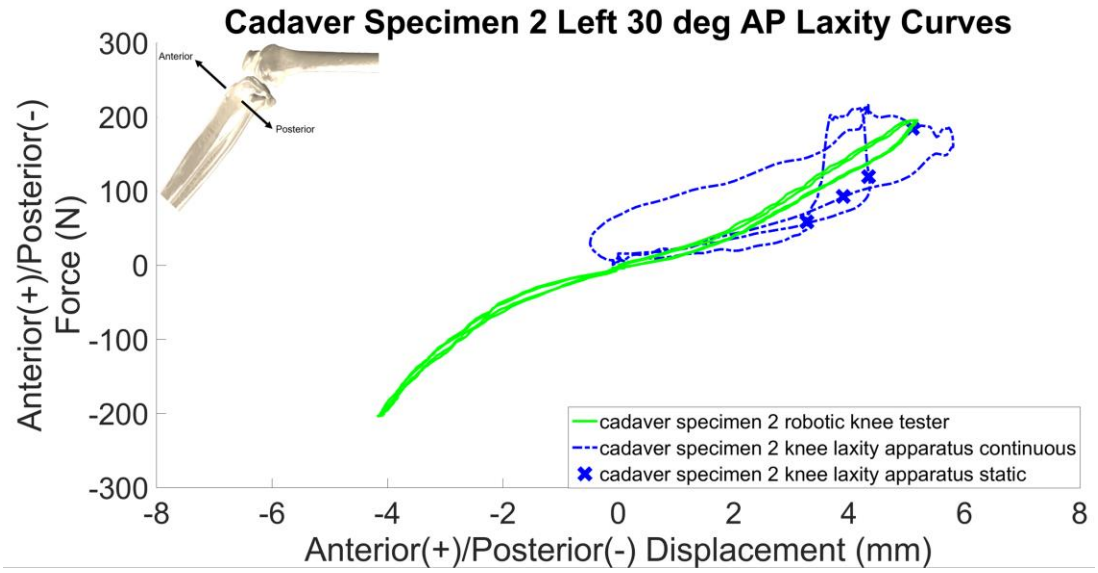

Figure 5-6 Knee Laxity Apparatus vs. Robotic Knee Tester AP Laxity for Specimen 2 Left at 30 degrees of Knee Flexion

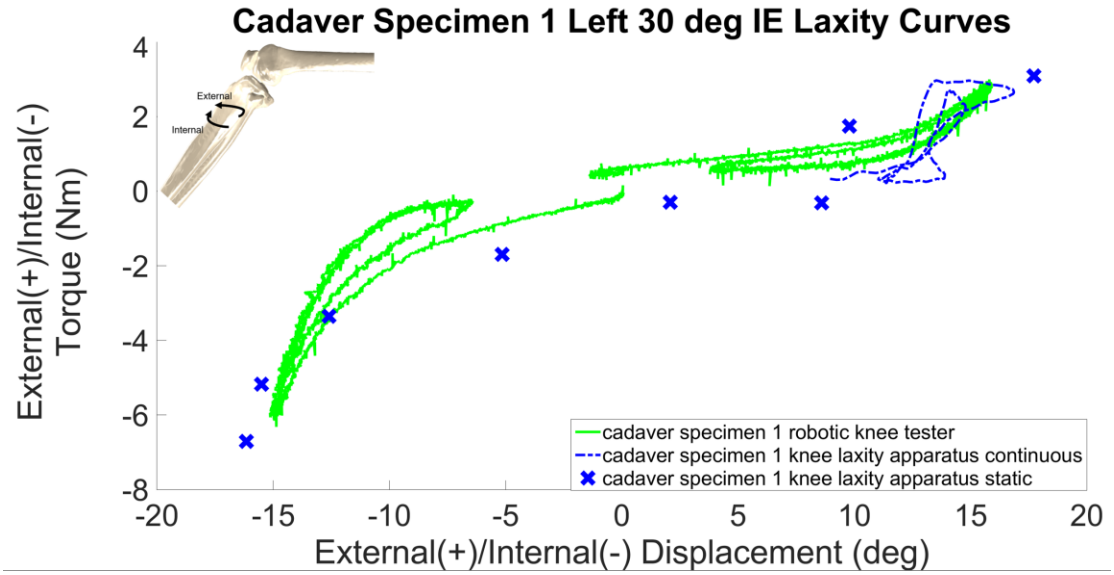

Figure 5-7 Knee Laxity Apparatus vs. Robotic Knee Tester IE Laxity for Specimen 1 Left at 30 degrees of Knee Flexion

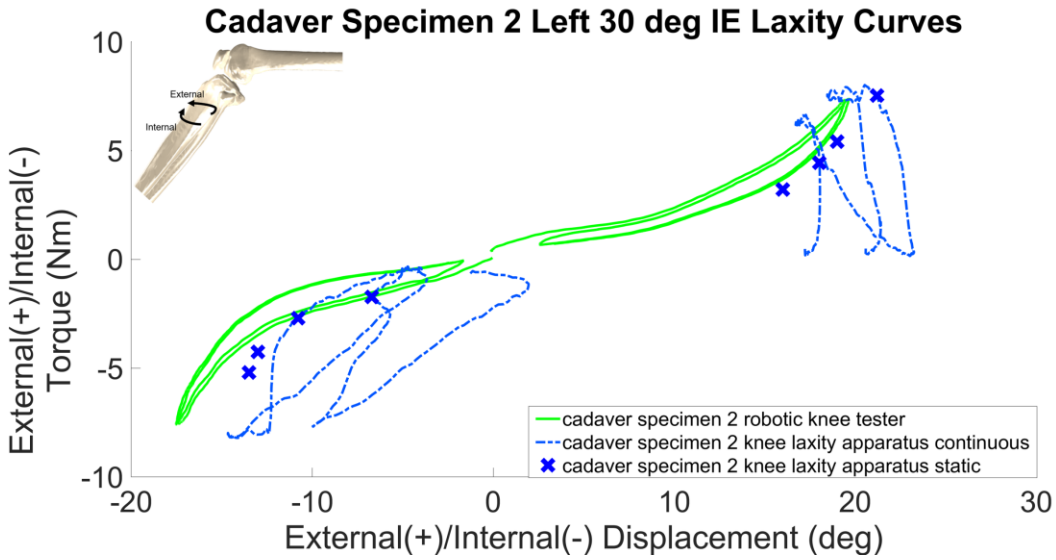

Figure 5-8 Knee Laxity Apparatus vs. Robotic Knee Tester IE Laxity for Specimen 2 Left at 30 degrees of Knee Flexion

Table 5-1 Total Laxity Displacement for Specimen Testing at 30 degrees

	Knee Laxity Apparatus Specimen #1	Robotic Knee Tester Specimen #1	Knee Laxity Apparatus Specimen #2	Robotic Knee Tester Specimen #2
Anterior (mm)	5.8	5.3	7.6	6.9
Posterior (mm)	N/A	-4.2	-6.6	-5.9
External (deg)	16.4	18.2	17.8	15.8
Internal (deg)	-17.4	-19.7	-17.3	-14.9

Table 5-2 AP and IE Laxity Errors for Cadaveric Specimen 1 and Cadaveric Specimen 2 for Static Knee Laxity Appartus vs. Robotic Knee Tester

	AP Laxity (mm)	IE Laxity (deg)
Maximum	0.7298	2.4967
RMS	0.4236	1.3361
Mean	0.3486	0.9443
Standard Dev	0.2573	1.0209

The continuous laxity measurements performed at 30° and 90° shown in Figure 5-9 below, show similar shifts in the laxity curves for knee laxity apparatus and robotic knee tester specimen testing between the two flexion angles.

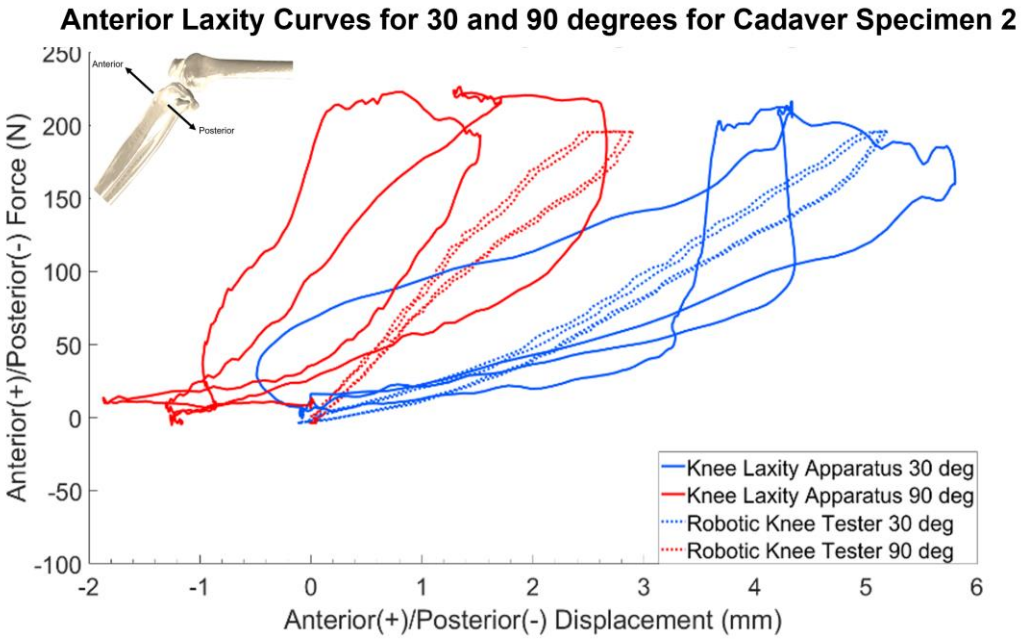

Figure 5-9 Graph of Specimen 2 Left Anterior Laxity at 30° and 90° of Knee Flexion

However, as shown in Figure 5-9, as well as below in Table 5-3 for both specimens, the hysteresis of the curves is significantly larger in the knee laxity apparatus, compared with the robotic tester.

Table 5-3 Measured RMS Difference of Laxity Hysteresis for Specimen Testing

	AP Root Mean Square Difference (mm)		IE Root Mean Square Difference (deg)	
	Specimen #1	Specimen #2	Specimen #1	Specimen #2
Knee Laxity Apparatus	2.77	1.6	6.39	2.95
Robotic Knee Tester	0.41	0.98	2.65	3.57

5.4. Subject Testing Results

Both the subject testing and the cadaveric testing show discrete laxity values within the range of values reported in the literature, shown in Figure 5-10 and Figure 5-11 below [24,43]. Values for both, are close to being within ±1 standard deviation, and are within ±2 standard deviations.

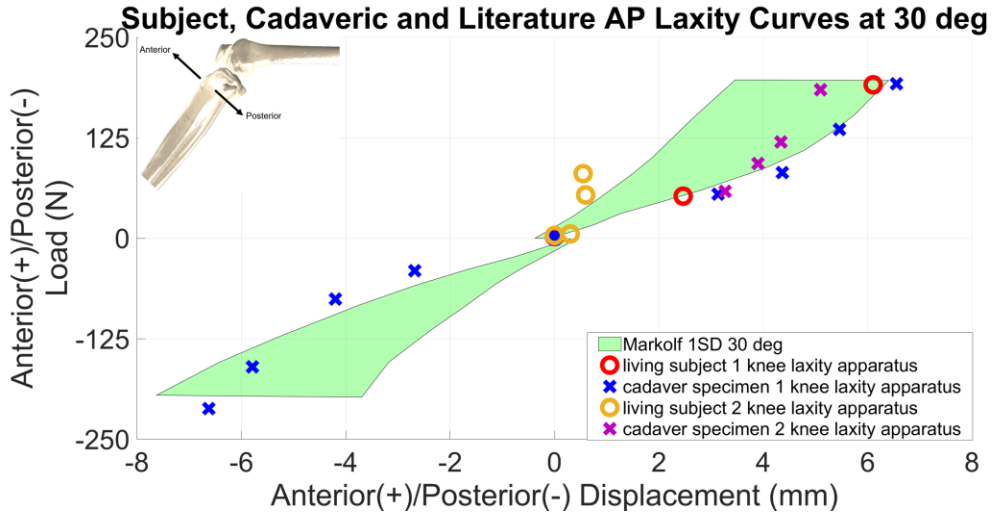

Figure 5-10 AP Laxity Curves for Knee Laxity Apparatus Compared to Markolf et al. Standard Deviation [43]

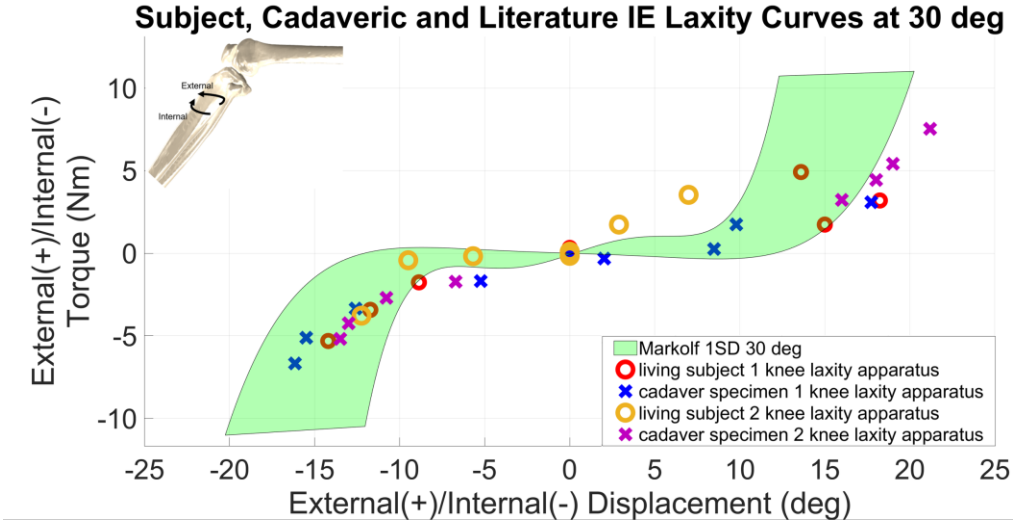

Figure 5-11 IE Laxity Curves for Knee Laxity Apparatus Compared to Markolf et al. Standard Deviation [24]

Additionally, displacement values for the cadaveric testing, for both the knee laxity apparatus and robotic knee tester; as well as, the subject testing was compared to other literature at 100N of Anterior load and 3 Nm of Internal load, shown in Figure 5-12 and Figure 5-13 below respectively [19,20,24,25,38,43,60,67,94].

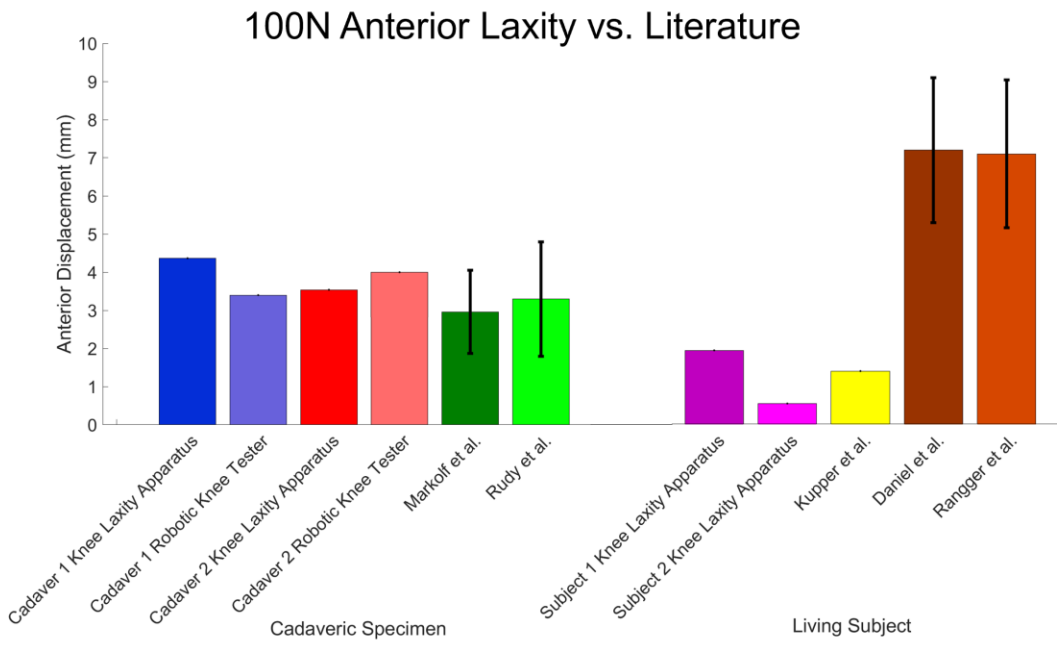

Figure 5-12 100N Anterior Displacements vs. Literature [19,20,24,38,43,60]

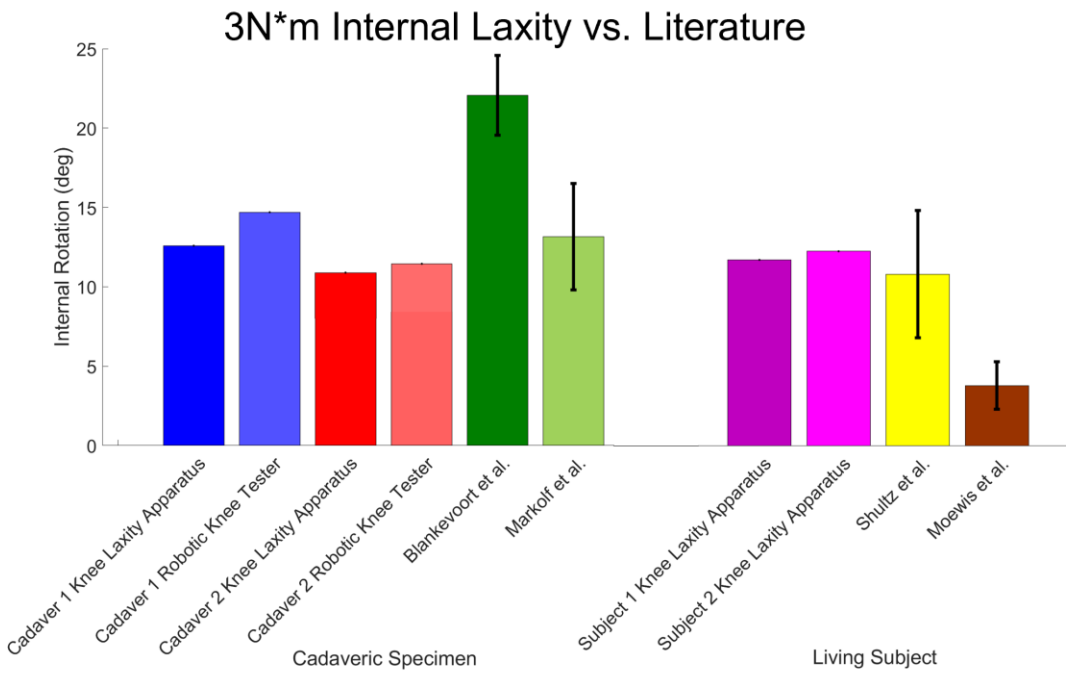

*Figure 5-13 3N*m Internal Displacements vs. Literature* [24,25,67,94]

5.5. Discussion

This study has introduced a novel apparatus for measuring *in vivo* knee laxity, that uses a system of pulleys and cables, as well as a rotational boot to apply AP and IE loads to the knee at a range of knee flexion angles. With the loads then being measured using a load cell, and the resulting displacements measured using HSSR techniques.

The validation of the apparatus was done by comparing the laxity measurements of two cadaveric specimens between the data obtained from the knee laxity apparatus, and the data collected from the robotic knee tester. The results in Table 5-1, showed that the proposed knee laxity apparatus has very similar total displacements to the *in* vitro testing at the maximum loads applied. The accuracy of the AP measurements was found to be within 1 mm of accuracy, while the IE measurements were found to be within 2.5° as shown the maximum errors listed in Table 5-2. The total displacements measured, were

similar to ranges reported previously in literature for knee laxity [19,24,25,43]. This shows that the knee laxity apparatus is capable of making accurate measurements for total displacements at maximum loads, with these measurements being the most clinically relevant [19,20]. In addition, the anterior displacement measurements of 5.3 mm and 6.9 mm made at these maximum loads are in agreement with previous work using the KT1000 arthrometer, wherein the anterior displacement was found to have a mean and standard deviation displacement of 7.2 mm and 1.9 mm respectively [19]. Additionally as shown in Figure 5-12 and Figure 5-13, the values recorded using the knee laxity apparatus were in agreement with the means and standard deviations reported in literature.

However, as noted in Table 5-3, the data also shows that the resulting laxity curves created for the knee laxity apparatus have larger hysteresis values than the robotic knee tester testing. This effect can most readily be seen in Figure 5-9, wherein the laxity curves for the robotic knee tester follow results made by previous work [60]. However, the knee laxity apparatus data has much larger hysteresis comparatively. In addition, while the robotic knee tester testing has both cycles effectively following the same laxity curves, the knee laxity apparatus testing shows curves with slightly different force-displacement profiles. This phenomena has previously been discussed in literature, resulting from slight changes in the exact loads and motion pathways of the remaining DOF not being tested [25]. The knee laxity apparatus, by its non-invasive nature, applies the loads to the surface of the segment without using rigid clamping, resulting in potentially higher load variability, which can cause the laxity not to follow the same path

during repeated loading and unloading cycles. In contrast, in the robotic knee tester the bonesare rigidly fixed to the robotic mechanism and the loads are directly applied to the bones through the use of a controller. This means that the robotic laxity test can apply loads purely in a single DOF, while leaving the others free.

In Figure 5-7, and Figure 5-9, it can be seen that the larger load variability results in the robotic knee tester laxity curves not lining up with the robotic knee tester. By contrast, the static, discrete loads have much higher accuracy relative to the robotic knee tester compared with the continuous loading. These errors are shown in Table 5-2, and emphasize that when using the static measurements, the knee laxity apparatus has a difference in measurement that is small, within 1mm for AP and 2.5° for AP. This is an appealing result since the static loads result in significantly lower radiation doses compared with continuous trials, making them preferred option for *in vivo* subject testing. The discrete loads used for testing on the two living subjects, were not only adequate, but as shown from these figures, was likely more accurate than if a continuous loading profile had been applied.

The *in vivo* subject testing performed validated the use of the knee laxity apparatus for its intended use on making laxity assessments of living people. Two subjects were subjected to Anterior and IE load sets, and the resulting measurements, shown in Figure 5-10 and Figure 5-11, were within the standard deviations previously reported by Markolf et al. [24,43]. This confirms that the knee laxity apparatus can make safe and accurate *in vivo* knee laxity measurements on subjects, and that the measurements are similar to previous work on laxity.

All of the measurement trials were further compared at the 100N Anterior and the 3N*m Internal loads against previous literature values, shown in Figure 5-12 and Figure 5-13. The bar graphs show the displacements, for each of the trials, and show similar agreement for both the Anterior and Internal testing, for the cadaveric specimens at these loads compared to other tests performed on cadaveric specimens.

Additionally, the values recorded for Anterior displacement on the living subjects are close to the values reported by Kupper et al. that used a dynamic MRI as the means of measuring the displacements [60]. However, the values for the Anterior displacement of the subject testing, and the cadaveric testing are all lower than the values reported in Daniel et al. and Rangger et al. [19,20]. Notably, these two studies are the only ones that used surface-based measurements with the KT1000, and emphasize the noted issue that the KT1000 and surface measurements, in general, tend to overestimate displacements of individuals [66]. These further cement that there is a need for accurate displacement measurements in laxity assessment, to not have the faults present in surface-based measurements, wherein displacements tend to be overestimated. Additionally, the values for the living subject testing, have significantly less Anterior laxity, than the cadaveric testing. This is likely a result of muscle guarding that has been discussed by Kupper et al., as well as other studies that mention that muscle activity of the individual has an effect on the resulting laxity measurement [19,60,95]. In particular, passive hamstring activation can act to “guard” the knee, and act to reduce the amount of displacement of the knee joint from an applied load, particularly in the Anterior direction.

For the Internal bars in Figure 5-13, the living subject internal rotations are in close agreement with the values from Shultz et al., which used a modified version of the Vermont Knee Laxity Device, to assess the laxity in living subjects [55,94]. These values are also close to the values for the cadaveric laxity measurements, which may suggest that the muscle guarding effects are more prominent in the AP laxity assessment, compared with the IE laxity assessments. Of note, is that the values reported in Moewis et al. are lower than the values reported for all of the subject testing, as well as all of the cadaveric testing, including from literature [67]. Notably, this study was the only one that used only continuous measurements, while the other ones included static measurements. This may confirm the observation made for the data in this study shown in Figure 5-5, Figure 5-6, Figure 5-7, Figure 5-8, Figure 5-9 and Table 5-3 above, that the continuous measurements tend to be less accurate compared with the discrete static measurements. This is theorized to be a result of the "envelope" of passive motion reported in Blankevoort et al., wherein they describe that the exact motion pathway of the knee, is highly dependent on the loads in the other DOF, as well as the specific loads in the actual DOF [25]. As such, continuous loads are likely being applied less accurately compared with the static, discrete loads – particularly in the other DOF, which likely causes the continuous loads to be less accurate compared with pure static measurements.

A limitation inherent to the study is the power of the study resulting from the small number of subjects: two cadavers, and two subjects. Future testing on a more significant number of specimens could provide more confidence in the reliability and accuracy of the knee laxity apparatus for *in vivo* testing. A basic one-sided t-test power analysis with a

power of 0.8 performed with the results - particularly standard deviations of errors from this study, suggests that three samples are needed for the reported AP accuracy of 1mm, and five samples are needed for the reported IE accuracy of 2.5°. Further testing, will aim to collect a few more samples of laxity data on cadaveric specimens, to meet the sample size suggested in the power analysis. Additionally, emphasis will be made to use healthier female specimens in the future since all testing, both cadaveric specimen and living subjects, was performed on males. These future female specimens will confirm that the device has similar accuracy on males and females, particularly with the known fact that women tend to have larger laxity values compared with males [45–49].

Another limitation of the study was the accuracy of the tracking of the bones in HSSR which is based on the clarity of the acquired images. While the tracking has been shown to have a sub-millimeter accuracy, the resulting accuracy in tracking of the bones is dependent on the final quality of the XRay images [88]. A grainy image can result from poor camera alignment, improper XRay capture parameters, and excess subject soft tissue, which can affect the final accuracy of the tracking. This study showed that the accuracy was adequate to within 1mm for AP and 2.5° for IE; however, additional accuracy may be achieved by improving the ultimate clarity of the capture images.

In summary, this study described and validated a knee laxity apparatus for use in *in vivo* AP and IE laxity assessment, with accuracies similar to *in vitro* testing methods. This was accomplished by improving the displacement measurements for the resulting laxity assessments by utilizing HSSR techniques for tracking. Validation was done by comparing measurements made from the knee laxity apparatus to a robotic knee tester.

Additional testing on living subjects demonstrated the knee laxity apparatus' use for *in vivo* testing. The knee laxity apparatus will be utilized in future studies as a means of collecting *in vivo* laxity data for calibration of subject-specific computational knee models. The apparatus and underlying data capture principles may enable future technology and studies with improved clinical measurements of knee laxity for diagnosis and assessment of the underlying pathologies present.

Chapter 6: Discussion and Concluding Remarks

6.1. Discussion

6.1.1. Introduction

Personalized medicine has created a demand for computational models to more accurately understand underlying human pathologies. However, as is the case with any computer model, the model's accuracy is limited by the data used to calibrate its parameters. In the past, data has limited many models to measurements taken from large sets of *in vitro* testing, because of a lack of accurate and available *in vivo* datasets. The next milestone in computational modeling is to create subject-specific models that are calibrated to an individual's anatomy and characteristics. To this aim, a method of more accurately collecting *in vivo* subject data is required. The ultimate goal of this work was to create and evaluate a means of accurately collecting *in vivo* data using HSSR for use in calibration of subject-specific computational models.

The work performed in this thesis, centered around evaluating and answering three aims: 1) to create a leg press for measurement of the full knee ROM of an individual, with particular emphasis on the deep knee flexion portion, 2) to create a device capable of AP and IE laxity measurements, and 3) to evaluate the efficacy of the created laxity device and measurement methodology.

6.1.2. Range of Motion

ROM of the knee can largely be broken down into passive and active ROM [1]. Passive ROM is defined as the total ROM without any external load applied to the joint, while active ROM is often more significant, particularly in individuals with muscle output discrepancies. In the knee joint, in particular, ROM is used in computational models as a means of calibrating and validating the passive properties of the knee, with emphasis on the ligamentous parameters [3]. Many means of data capture have been used to gather ROM, including motion capture, MRI, and Fluoroscopy [7–9]. Passive ROM motion is easily captured, but active ROM is more complicated. To get the active ROM, most work involved having the subject perform a lunge, but the results have shown that the motion is not very repeatable and difficult to achieve the full ROM[11–13]. As such, a leg press was designed as a proposed means of getting the full active ROM during a controlled, repeatable activity.

The leg press, shown in Figure 3-1, was designed to allow for a range of loads to be applied to the subject using a set of discrete weights. With the loads being applied uniformly during the duration of motion to the track of the sled. The leg press was built to accommodate a range of subject size variations. HSSR was used to capture the full knee flexion range using previously validated techniques [88]. However, because of the large vertical travel of the knee during this range, a hydraulic table was built to allow for the full flexion range to be gathered.

To date, knee kinematics during leg press has been collected on many subjects, and as shown in the dataset in Figure 3-6, the leg press is capable of applying a 20 lbf weight to

the subject, while allowing knee flexion angles from hyperextension all the way to >140° knee flexion to be observed. The leg press shows a great ability to capture active ROM through the entire flexion range. The dataset as shown in Figure 3-6, shows agreement with literature that the tibia naturally rotates internally with increased knee flexion angle [24,25,78]. The leg press shows promise for future use in capturing full ROM trials on individuals, particularly for active ROM measurements.

Currently, the leg press is limited to observing ROM in two trial sets because of the large vertical movement of the knee. This has been solved through the use of a hydraulic lift table to bias the knee during the 2nd trial. However, improvements to the HSSR system as a whole could enable dynamic movement of the HSSR system during the trial. As such the camera could track the motion of the knee as opposed to forcing the knee motion to fit within the limits of the HSSR capture volume. This could improve accuracy since it wouldn't require two separate trials, which may have slight differences between the two trials. In addition, the current leg press is only capable of making measurements at a specific knee rotation. Work has shown the particular usefulness of observing the ROM under constant IE torque loads, which the current device is not capable of [22,25]. Future work may involve the creation of a means of applying a consant IE torque during the ROM to the knee, similar to the IE loads of the laxity rig, to observe the change in kinematics under constant torque loads.

6.1.3. Knee Laxity

Laxity is a term that, in general, describes the complex non-linear force-displacement that results from the passive properties within a joint [14]. In the knee, in particular,

laxity is used as a means of calibrating the passive ligamentous properties in models of the joint. However, the majority of studies have used *in vitro* knee laxity values, because accurate *in vivo* measurements are challenging to acquire [22,42,69,70,83–86]. The majority of knee laxity measurements performed *in vivo* have used surface-based probes as a means of determining the displacements of the bones relative to one another, while recent work has attempted to use MRI and fluoroscopy as a means of more accurately determining the displacements [52,59–61,65]. However, none of the devices can measure both AP and IE laxity at multiple knee angles. As such, there is a need for a more accurate means of capturing *in vivo* knee laxity data for both the AP and IE directions.

The designed knee laxity apparatus, shown in Figure 4-2, uses radiolucent materials, and a series of cables and pulleys, along with a boot rigidly attached to the tibia to allow for measurement of the *in* vivo AP and IE knee laxity at a range of knee flexion angles. A set of cuffs, and straps are used to apply the loads, as well as restrict the motion of the femur relative to the tibia. The knee laxity apparatus uses discrete weights, and a load cell to apply and measure the loads to the joint, as well as using previously validated HSSR techniques to measure the resulting displacement of the joint [88].

Two specimens were placed in the knee laxity apparatus at 30° and 90° of knee flexion, and then a series of AP and IE loads were applied to the specimens. The loads were applied to the knee using static loads, as well as continuous load profiles, with the loads applied having similar magnitudes as previous work [19,24,25,43]. The specimens were then dissected to leave as much of the knee intact as possible, and then potted and placed in a robotic knee tester to perform the standard *in vitro* laxity assessments in 15°

increments between 0° and 120°. Loads were measured in real-time using a load cell, and displacements were recorded as the difference in GS kinematics between the trial and the no-load reference position. The loads and displacements were combined to create the resulting laxity curves.

The laxity curves in Figure 5-5, and Figure 5-7, show that the knee laxity apparatus has very similar total displacements to the *in vitro* data from the robotic knee tester, with an accuracy of 1 mm for AP translations, and 2.5° for IE rotations. The data also shows similarities between the overall profiles for static loads. However, for the continuous dynamic data, the knee laxity apparatus shows significantly more hysteresis than the corresponding robotic knee tester. In addition, the data paths follow different force-displacement paths, whereas the force-displacement data for the *in vitro* testing is much more consistent between the cycles. This is likely a result of increased load variability in the knee laxity apparatus compared to the robotic knee tester. The knee can have slightly different loads for the other DOF as a result, and can drastically change the exact path taken by the knee [25]. This shows that the static loads are more repeatable and accurate compared to the exact dynamics involved with the continuous loading. This is a good result, as it shows that static trials are adequate to measure the laxity of an individual, and any many cases, more accurate than a continuous trial, which has the added advantage of lower collection times, and as such, a lower radiation exposure time.

The testing was also performed on two living subjects at discrete anterior and IE loads. These values, and the specimen values were then compared against reported values from the literature, shown in Figure 5-10, and Figure 5-11, which show agreement with

published data on the averages and standard deviations of AP and IE laxity measurements [24,43]. This agreement confirms that the laxity apparatus can make safe and accurate laxity measurements that have similar values as previously reported data from *in vitro* and *in vivo* testing. These measurements show promise for future data collections on *in vivo* knee laxity.

The knee laxity apparatus is however, currently limited to AP and IE laxity measurements. In particular because work has shown that the total displacement in varus-valgus (VV) amongst healthy individuals is very small, at only a a few degrees for a 10 N*m applied torque [24]. However, colateral ligament stability, as well as, VV laxity are key aspects of orthopaedic evaluation of Total Knee Arthroplasty (TKA) [96]. In addition, work has suggested that increased total displacement during VV laxity assessments, has correlation to increased pain in osteoarthritic knees [97]. As such, the ability to measure VV laxity, particularly on studies involving subjects with Osteoarthritis, and/or TKA is desirable. Future work on the knee laxity apparatus, may involve adding additional functionality, or a new device entirely for evaluation of VV laxity *in vivo* using HSSR with a similar accuracy to the current AP and IE means available with the current device.

6.2. Concluding Remarks

The work in this thesis has discussed the design and validation of two devices, a leg press, and a knee laxity apparatus for use in accurate *in vivo* data collection. These methods were individually validated for accuracy and viability. Both devices were validated for accuracy, and show promise for use in *in vivo* testing using HSSR. Future

data collections should capture full ROM data, as well as knee laxity data on subjects. These measurements, in combination with subject anatomy, should be used in the future to create computational models, and ultimately validate their usefulness for subject-specific model calibration.

References

[1] Miner, A. L., Lingard, E. A., Wright, E. A., Sledge, C. B., and Katz, J. N., 2003, "Knee Range of Motion after Total Knee Arthroplasty: How Important Is This as an Outcome Measure?," J. Arthroplasty, **18**(3), pp. 286–294.

[2] Shah, N., 2008, "Increasing Knee Range of Motion Using a Unique Sustained Method.," N. Am. J. Sports Phys. Ther., **3**(2), pp. 110–3.

[3] Nardini, F., Belvedere, C., Sancisi, N., Conconi, M., Leardini, A., Durante, S., and Parenti-Castelli, V., 2020, "An Anatomical-Based Subject-Specific Model of in-Vivo Knee Joint 3D Kinematics from Medical Imaging," Appl. Sci., **10**(6), pp. 8–12.

[4] Roaas, A., and Andersson, G. B. J., 1982, "Normal Range of Motion of the Hip, Knee and Ankle Joints in Male Subjects, 30-40 Years of Age," Acta Orthop., **53**(2), pp. 205–208.

[5] Hancock, G. E., Hepworth, T., and Wembridge, K., 2018, "Accuracy and Reliability of Knee Goniometry Methods," J. Exp. Orthop., **5**(1).

[6] Naylor, J. M., Ko, V., Adie, S., Gaskin, C., Walker, R., Harris, I. A., and Mittal, R., 2011, "Validity and Reliability of Using Photography for Measuring Knee Range of Motion: A Methodological Study," BMC Musculoskelet. Disord., **12**, pp. 1–10.

[7] Johal, P., Williams, A., Wragg, P., Hunt, D., and Gedroyc, W., 2005, "Tibio-Femoral Movement in the Living Knee. A Study of Weight Bearing and Non-Weight Bearing Knee Kinematics Using 'interventional' MRI," J. Biomech.,

38(2), pp. 269–276.

[8] Feng, Y., Tsai, T.-Y., Li, J.-S., Rubash, H. E., Li, G., and Freiberg, A., 2016, "In-Vivo Analysis of Flexion Axes of the Knee: Femoral Condylar Motion during Dynamic Knee Flexion," Clin. Biomech., **32**(1), pp. 102–107.

[9] Hamai, S., Moro-Oka, T. A., Dunbar, N. J., Miura, H., Iwamoto, Y., and Banks, S. A., 2013, "In Vivo Healthy Knee Kinematics during Dynamic Full Flexion," Biomed Res. Int., **2013**.

[10] D'Isidoro, F., Eschle, P., Zumbrunn, T., Sommer, C., Scheidegger, S., and Ferguson, S. J., 2017, "Determining 3D Kinematics of the Hip Using Video Fluoroscopy: Guidelines for Balancing Radiation Dose and Registration Accuracy," J. Arthroplasty, **32**(10), pp. 3213–3218.

[11] Jalali, M., Farahmand, F., Mousavi, S. M. E., Golestanha, S. A., Rezaeian, T., Broujeni, S. S., Rahgozar, M., and Esfandiarpour, F., 2015, "Fluoroscopic Analysis of Tibial Translation in Anterior Cruciate Ligament Injured Knees with and without Bracing during Forward Lunge," Iran. J. Radiol., **12**(3).

[12] Van De Velde, S. K., Gill, T. J., and Li, G., 2009, "Dual Fluoroscopic Analysis of the Posterior Cruciate Ligament-Deficient Patellofemoral Joint during Lunge," Med. Sci. Sport. Exerc., **41**(6), pp. 1198–1205.

[13] Stiehl, J. B., Komistek, R. D., Dennis, D. A., Paxson, R. D., and Hoff, W. A., 1995, "Fluoroscopic Analysis of Kinematics After Posterior-Cruciate-Retaining Knee Arthroplasty," J. Bone Jt. Surg., **77**(B), pp. 884–889.

[14] Emery, M., Moffroid, M., Boerman, J., Fleming, B., Howe, J., and Pope, M., 1989,

"Reliability of Force/Displacement Measures in a Clinical Device Designed to Measure Ligamentous Laxity at the Knee," J. Orthop. Sports Phys. Ther., **10**(11), pp. 441–447.

[15] Tofts, L. J., Elliott, E. J., Munns, C., Pacey, V., and Sillence, D. O., 2009, "The Differential Diagnosis of Children with Joint Hypermobility: A Review of the Literature," Pediatr. Rheumatol., **7**, pp. 1–10.

[16] Jensen, K., 1990, "Manual Laxity Tests for Anterior Cruciate Ligament Injuries," J. Orthop. Sports Phys. Ther., **11**(10), pp. 474–481.

[17] Kim, S. J., and Kim, H. K., 1995, "Reliability of the Anterior Drawer Test, the Pivot Shift Test, and the Lachman Test," Clin. Orthop. Relat. Res., (317), p. 237—242.

[18] Makhmalbaf; et al., 2013, "Accuracy of Lachman and Anterior Drawer Tests," Arch Bone Jt. Surg., **94**(2), pp. 94–97.

[19] Daniel, D. M., Stone, M. Lou, Sachs, R., and Malcom, L., 1985, "Instrumented Measurement of Anterior Knee Laxity in Patients with Acute Anterior Cruciate Ligament Disruption," Am. J. Sports Med., **13**(6), pp. 401–407.

[20] Rangger, C., Daniel, D. M., Stone, M. L., and Kaufman, K., 1993, "Diagnosis of an ACL Disruption with KT-1000 Arthrometer Measurements," Knee Surg. Sport. Traumatol. Arthrosc., **1**(1), pp. 60–66.

[21] Cimino, F., Volk, B. S., and Setter, D., 2010, "Anterior Cruciate Ligament Injury: Diagnosis, Management, and Prevention," Am. Fam. Physician, **82**(8), pp. 917–922.

[22] Blankevoort, L., and Huiskes, R., 1996, “Validation of a Three-Dimentional Model of the Knee,” J. Biomech., **29**(7), pp. 955–961.

[23] Ali, A. A., Harris, M. D., Shalhoub, S., Maletsky, L. P., Rullkoetter, P. J., and Shelburne, K. B., 2017, “Combined Measurement and Modeling of Specimen-Specific Knee Mechanics for Healthy and ACL-Deficient Conditions,” J. Biomech., **57**, pp. 117–124.

[24] Markolf, K. L., Mensch, J. S., and Amstutz, H. C., 1976, “Stiffness and Laxity of the Knee - The Contributions of the Supporting Structures,” J. Bone Jt. Surg., **58-A**(5), pp. 583–594.

[25] Blankevoort, L., Huiskes, R., and de Lange, A., 1988, “The Envelope of Passive Knee Joint Motion,” J. Biomech., **21**(9), pp. 705–720.

[26] Malcom, L. L., Daniel, D. M., Jamison, C. M., and Landesman, R. E., 1986, “Knee Ligament Testing System.”

[27] Paine, R., and Lowe, W., 2012, “Comparison of Kneelax and KT-1000 Knee Ligament Arthrometers.,” J. Knee Surg., **25**(2), pp. 151–154.

[28] Lee, J. C. Y., Yung, P. S. H., Lam, M. H., Hung, A. S. L., Fong, D. T. P., Chan, W. Y., and Chan, K. M., 2019, “A Non-Invasive Biomechanical Device to Quantify Knee Rotational Laxity: Verification of the Device in Human Cadaveric Specimens,” Asia-Pacific J. Sport. Med. Arthrosc. Rehabil. Technol., **16**, pp. 19–23.

[29] Harris, M. D., Cyr, A. J., Ali, A. A., Fitzpatrick, C. K., Rullkoetter, P. J., Maletsky, L. P., and Shelburne, K. B., 2016, “A Combined Experimental and Computational

Approach to Subject-Specific Analysis of Knee Joint Laxity," J. Biomech. Eng., **138**(8), pp. 1–8.

[30] Salvadore, G., Meere, P. A., Verstraete, M. A., Victor, J., and Walker, P. S., 2018, "Laxity and Contact Forces of Total Knee Designed for Anatomic Motion: A Cadaveric Study," Knee, **25**(4), pp. 650–656.

[31] Siston, R. A., Maack, T. L., Hutter, E. E., Beal, M. D., and Chaudhari, A. M. W., 2012, "Design and Cadaveric Validation of a Novel Device to Quantify Knee Stability during Total Knee Arthroplasty," J. Biomech. Eng., **134**(11), pp. 1–7.

[32] Thompson, M. ., Conditt, M. ., Ismaily, S. ., Agarwal, A., and Noble, P. ., 2004, "Brief Report: Validation of a System for Automated Measurement of Knee Laxity," Clin. Biomech., **19**(3), pp. 308–312.

[33] Nohmi, S., Ishibashi, Y., Tsuda, E., Yamamoto, Y., Tsukada, H., and Toh, S., 2012, "Biomechanical Comparison between Single-Bundle and Double-Bundle Anterior Cruciate Ligament Reconstruction with Hamstring Tendon under Cyclic Loading Condition," Sport. Med. Arthrosc. Rehabil. Ther. Technol., **4**(1), pp. 2–9.

[34] Nielsen, E. T., Stentz-Olesen, K., de Raedt, S., Jørgensen, P. B., Sørensen, O. G., Kaptein, B., Andersen, M. S., and Stilling, M., 2018, "Influence of the Anterolateral Ligament on Knee Laxity: A Biomechanical Cadaveric Study Measuring Knee Kinematics in 6 Degrees of Freedom Using Dynamic Radiostereometric Analysis," Orthop. J. Sport. Med., **6**(8), pp. 1–13.

[35] Maletsky, L. P., and Hillberry, B. M., 2005, "Simulating Dynamic Activities Using a Five-Axis Knee Simulator," J. Biomech. Eng., **127**(1), pp. 123–133.

[36] Markolf, K. L., Boguszewski, D. V., Yamaguchi, K. T., Lama, C. J., and McAllister, D. R., 2018, "Prediction of Anterior Cruciate Ligament Force Produced by Tibiofemoral Compression during Controlled Knee Flexion: A New Robotic Testing Methodology," J. Biomech. Eng., **140**(12), pp. 1–6.

[37] Fitzpatrick, C. K., Maag, C., Clary, C. W., Metcalfe, A., Langhorn, J., and Rullkoetter, P. J., 2016, "Validation of a New Computational 6-DOF Knee Simulator during Dynamic Activities," J. Biomech., **49**(14), pp. 3177–3184.

[38] Rudy, T. W., Livesay, G. A., Woo, S. L. Y., and Fu, F. H., 1996, "A Combined Robotic/Universal Force Sensor Approach to Determine In Situ Forces of Knee Ligaments," J. Biomech., **29**(10), pp. 1357–1360.

[39] Mueller, J. K. P., Wentorf, F. A., and Moore, R. E., 2014, "Femoral and Tibial Insert Downsizing Increases the Laxity Envelope in TKA," Knee Surgery, Sport. Traumatol. Arthrosc., **22**(12), pp. 3003–3011.

[40] Baldwin, M. A., Clary, C. W., Fitzpatrick, C. K., Deacy, J. S., Maletsky, L. P., and Rullkoetter, P. J., 2012, "Dynamic Finite Element Knee Simulation for Evaluation of Knee Replacement Mechanics," J. Biomech., **45**(3), pp. 474–483.

[41] Halloran, J. P., Clary, C. W., Maletsky, L. P., Taylor, M., Petrella, A. J., and Rullkoetter, P. J., 2010, "Verification of Predicted Knee Replacement Kinematics during Simulated Gait in the Kansas Knee Simulator," J. Biomech. Eng., **132**(8), pp. 1–6.

[42] Baldwin, M. A., Clary, C., Maletsky, L. P., and Rullkoetter, P. J., 2009, "Verification of Predicted Specimen-Specific Natural and Implanted

Patellofemoral Kinematics during Simulated Deep Knee Bend," J. Biomech., **42**(14), pp. 2341–2348.

[43] Markolf, K. L., Kochan, A., and Amstutz, H. C., 1984, "Measurement of Knee Stiffness and Laxity in Patients with Documented Absence of the Anterior Cruciate Ligament," J. Bone Jt. Surg., **66**(2), pp. 242–253.

[44] Anderson, A. F., Snyder, R. B., Federspiel, C. F., and Lipscomb, A. B., 1992, "Instrumented Evaluation of Knee Laxity: A Comparison of Five Arthrometers," Am. J. Sports Med., **20**(2), pp. 135–140.

[45] Pollard, C. D., Braun, B., and Hamill, J., 2006, "Influence of Gender, Estrogen and Exercise on Anterior Knee Laxity," Clin. Biomech., **21**(10), pp. 1060–1066.

[46] Rozzi, S. L., Lephart, S. M., Gear, W. S., and Fu, F. H., 1999, "Knee Joint Laxity and Neuromuscular Characteristics of Male and Female Soccer and Basketball Players," Am. J. Sports Med., **27**(3), pp. 312–319.

[47] Harmon, K. G., and Ireland, M. L., 2000, "Gender Differences in Noncontact Anterior Cruciate Ligament Injuries.," Clin. Sports Med., **19**(2), pp. 287–302.

[48] Park, H. S., Wilson, N. A., and Zhang, L. Q., 2008, "Gender Differences in Passive Knee Biomechanical Properties in Tibial Rotation," J. Orthop. Res., **26**(7), pp. 937–944.

[49] Park, S. K., Stefanyshyn, D. J., Loitz-Ramage, B., Hart, D. A., and Ronsky, J. L., 2009, "Changing Hormone Levels during the Menstrual Cycle Affect Knee Laxity and Stiffness in Healthy Female Subjects," Am. J. Sports Med., **37**(3), pp. 588–598.

[50] Barcellona, M. G., Morrissey, M. C., Milligan, P., Clinton, M., and Amis, A. A., 2015, "The Effect of Knee Extensor Open Kinetic Chain Resistance Training in the ACL-Injured Knee," Knee Surgery, Sport. Traumatol. Arthrosc., **23**(11), pp. 3168–3177.

[51] Shultz, S. J., Carcia, C. R., and Perrin, D. H., 2004, "Knee Joint Laxity Affects Muscle Activation Patterns in the Healthy Knee," J. Electromyogr. Kinesiol., **14**(4), pp. 475–483.

[52] Collette, M., Courville, J., Forton, M., and Gagnière, B., 2012, "Objective Evaluation of Anterior Knee Laxity; Comparison of the KT-1000 and GNRB® Arthrometers," Knee Surgery, Sport. Traumatol. Arthrosc., **20**(11), pp. 2233–2238.

[53] Fiebert, I., Gresley, J., Hoffman, S., and Kunkel, K., 1994, "Comparative Measurements of Anterior Tibial Rans Slat Ion Using the KT-1 000 Knee Arthrometer With the Leg in Neutral, Internal Rotation, and External Rotation," J. Orthop. Sports Phys. Ther., **19**(6), pp. 331–334.

[54] Freisinger, G. M., Hutter, E. E., Lewis, J., Granger, J. F., Glassman, A. H., Beal, M. D., Pan, X., Schmitt, L. C., Siston, R. A., and Chaudhari, A. M. W., 2017, "Relationships Between Varus–Valgus Laxity of the Severely Osteoarthritic Knee and Gait, Instability, Clinical Performance, and Function," J. Orthop. Res., **35**(8), pp. 1644–1652.

[55] Un, B. S., Beynnon, B. D., Churchill, D. L., Haugh, L. D., Risberg, M. A., and Fleming, B. C., 2001, "A New Device to Measure Knee Laxity during Weightbearing and Non-Weightbearing Conditions," J. Orthop. Res., **19**(6), pp.

1185–1191.

[56] Heesterbeek, P. J. C., Verdonschot, N., and Wymenga, A. B., 2008, “In Vivo Knee Laxity in Flexion and Extension: A Radiographic Study in 30 Older Healthy Subjects,” Knee, **15**(1), pp. 45–49.

[57] Starkel, C., Hawkins, D., and Ashuckian, E., 2014, “Investigation of the Temporal Response of Anterior Knee Laxity Following Strenuous Exercise,” Med. Sci. Sport. Exerc., **46**(1), pp. 410–411.

[58] Deep, K., 2014, “Collateral Ligament Laxity in Knees: What Is Normal?,” Clin. Orthop. Relat. Res., **472**(11), pp. 3426–3431.

[59] Moewis, P., Boeth, H., Heller, M. O., Yntema, C., Jung, T., Doyscher, R., Ehrig, R. M., Zhong, Y., and Taylor, W. R., 2014, “Towards Understanding Knee Joint Laxity: Errors in Non-Invasive Assessment of Joint Rotation Can Be Corrected,” Med. Eng. Phys.

[60] Kupper, J. C., Westover, L., Frayne, R., and Ronsky, J. L., 2016, “Application of a Novel Measure of in Vivo Knee Joint Laxity,” J. Biomech. Eng., **138**(10), pp. 1–7.

[61] Carpenter, R. D., Shefelbine, S. J., Lozano, J., Carballido-Gamio, J., Majumdar, S., and Ma, C. B., 2008, “A New Device for Measuring Knee Rotational Kinematics Using Magnetic Resonance Imaging,” J. Med. Devices, Trans. ASME, **2**(4), pp. 1–5.

[62] Colombet, P., Jenny, J. Y., Menetrey, J., Plaweski, S., and Zaffagnini, S., 2012, “Current Concept in Rotational Laxity Control and Evaluation in ACL Reconstruction,” Orthop. Traumatol. Surg. Res., **98**(8 SUPPL), pp. S201–S210.

[63] Hume, D. R., Kefala, V., Harris, M. D., and Shelburne, K. B., 2018, “Comparison of Marker-Based and Stereo Radiography Knee Kinematics in Activities of Daily Living,” Ann. Biomed. Eng., **46**(11), pp. 1806–1815.

[64] Benoit, D. L., Ramsey, D. K., Lamontagne, M., Xu, L., Wretenberg, P., and Renström, P., 2006, “Effect of Skin Movement Artifact on Knee Kinematics during Gait and Cutting Motions Measured in Vivo,” Gait Posture, **24**(2), pp. 152–164.

[65] Beukes, G. L., Patnaik, S., and Sivarasu, S., 2018, “In Vitro Functional Verification of a Novel Laxity Measurement Stress Radiography Device,” *2018 Design of Medical Devices Conference,* American Society of Mechanical Engineers, pp. 6–9.

[66] Fleming, B. C., Brattbakk, B., Peura, G. D., Badger, G. J., and Beynnon, B. D., 2002, “Measurement of Anterior-Posterior Knee Laxity: A Comparison of Three Techniques,” J. Orthop. Res., **20**(3), pp. 421–426.

[67] Moewis, P., Duda, G. N., Jung, T., Heller, M. O., Boeth, H., Kaptein, B., and Taylor, W. R., 2016, “The Restoration of Passive Rotational Tibio-Femoral Laxity after Anterior Cruciate Ligament Reconstruction,” PLoS One, **11**(7), pp. 1–14.

[68] Lorenz, A., Krickl, V., Ipach, I., Arlt, E. M., Wülker, N., and Leichtle, U. G., 2015, “Practicability for Robot-Aided Measurement of Knee Stability in-Vivo Orthopedics and Biomechanics,” BMC Musculoskelet. Disord., **16**(1), pp. 1–9.

[69] Beillas, P., Papaioannou, G., Tashman, S., and Yang, K. H., 2004, “A New Method to Investigate in Vivo Knee Behavior Using a Finite Element Model of the

Lower Limb," J. Biomech., **37**(7), pp. 1019–1030.

[70] Hume, D. R., Navacchia, A., Rullkoetter, P. J., and Shelburne, K. B., 2019, "A Lower Extremity Model for Muscle-Driven Simulation of Activity Using Explicit Finite Element Modeling," J. Biomech., **84**(xxxx), pp. 153–160.

[71] Ali, A. A., Mannen, E. M., Rullkoetter, P. J., and Shelburne, K. B., 2020, "Validated Computational Framework for Evaluation of In Vivo Knee Mechanics," J. Biomech. Eng., **142**(8).

[72] Fregly, B. J., Banks, S. A., D'Lima, D. D., and Colwell, C. W., 2008, "Sensitivity of Knee Replacement Contact Calculations to Kinematic Measurement Errors," J. Orthop. Res., **26**(9), pp. 1173–1179.

[73] Lloyd, D. G., and Besier, T. F., 2003, "An EMG-Driven Musculoskeletal Model to Estimate Muscle Forces and Knee Joint Moments in Vivo," J. Biomech., **36**, pp. 765–776.

[74] Fregly, B. J., Besier, T. F., Lloyd, D. G., Delp, S. L., Banks, S. A., Pandy, M. G., and D'Lima, D. D., 2012, "Grand Challenge Competition to Predict in Vivo Knee Loads," J. Orthop. Res., **30**(4), pp. 503–513.

[75] Wei-Ching, L., 2012, "UCSF UC San Francisco Electronic Theses and Dissertations."

[76] Lin, T.-C., 2018, "Tsung-Chi Lin Three-Dimensional Finite Element Analysis of the Knee Ligaments During Cycling in Normal Young Subjects Goemetric Model of the Knee and Ligaments Constitutive Modeling of Ligaments Constitutive Modeling of Ligaments," pp. 1–6 [Online]. Available:

https://www.lintsungchi.com/fea-of-knee-ligaments-during-cyclin.

[77] Grood, E. S., and Suntay, W. J., 1983, “A Joint Coordinate System for the Clinical Description of Three-Dimensional Motions: Application to the Knee,” J. Biomech. Eng., **105**(2), pp. 136–144.

[78] Wilson, D. R., Feikes, J. D., Zavatsky, A. B., and O’Connor, J. J., 2000, “The Components of Passive Knee Movement Are Coupled to Flexion Angle,” J. Biomech., **33**(4), pp. 465–473.

[79] Churchill, E., and McConville, J. T., 1976, “Sampling and Data Gathering Strategies for Future USAF Anthropometry,” AMRL-TR, **74**(102), pp. 1–133.

[80] Ng, V. Y., DeClaire, J. H., Berend, K. R., Gulick, B. C., and Lombardi, A. V., 2012, “Improved Accuracy of Alignment with Patient-Specific Positioning Guides Compared with Manual Instrumentation in TKA,” Clin. Orthop. Relat. Res., **470**(1), pp. 99–107.

[81] Haglin, J. M., Eltorai, A. E. M., Gil, J. A., Marcaccio, S. E., Botero-Hincapie, J., and Daniels, A. H., 2016, “Patient-Specific Orthopaedic Implants,” Orthop. Surg., **8**(4), pp. 417–424.

[82] Patil, S., Bunn, A., Bugbee, W. D., Colwell, C. W., and D’Lima, D. D., 2015, “Patient-Specific Implants with Custom Cutting Blocks Better Approximate Natural Knee Kinematics than Standard TKA without Custom Cutting Blocks,” Knee, **22**(6), pp. 624–629.

[83] Harris, M. D., Cyr, A. J., Ali, A. A., Fitzpatrick, C. K., Rullkoetter, P. J., Maletsky, L. P., and Shelburne, K. B., 2016, “A Combined Experimental and Computational

Approach to Subject-Specific Analysis of Knee Joint Laxity," J. Biomech. Eng., **138**(8), pp. 1–8.

[84] Mootanah, R., Imhauser, C. W., Reisse, F., Carpanen, D., Walker, R. W., Koff, M. F., Lenhoff, M. W., Rozbruch, S. R., Fragomen, A. T., Dewan, Z., Kirane, Y. M., Cheah, K., Dowell, J. K., and Hillstrom, H. J., 2014, "Development and Validation of a Computational Model of the Knee Joint for the Evaluation of Surgical Treatments for Osteoarthritis," Comput. Methods Biomech. Biomed. Engin., **17**(13), pp. 1502–1517.

[85] Ali, A. A., Shalhoub, S. S., Cyr, A. J., Fitzpatrick, C. K., Maletsky, L. P., Rullkoetter, P. J., and Shelburne, K. B., 2016, "Validation of Predicted Patellofemoral Mechanics in a Finite Element Model of the Healthy and Cruciate-Deficient Knee," J. Biomech., **49**(2), pp. 302–309.

[86] Li, G., Lopez, O., and Rubash, H., 2001, "Variability of a Three-Dimensional Finite Element Model Constructed Using Magnetic Resonance Images of a Knee for Joint Contact Stress Analysis," J. Biomech. Eng., **123**(4), pp. 341–346.

[87] Weiss, J. A., Gardiner, J. C., and Bonifasi-Lista, C., 2002, "Ligament Material Behavior Is Nonlinear, Viscoelastic and Rate-Independent under Shear Loading," J. Biomech., **35**(7), pp. 943–950.

[88] Kefala, V., Cyr, A. J., Harris, M. D., Hume, D. R., Davidson, B. S., Kim, R. H., and Shelburne, K. B., 2017, "Assessment of Knee Kinematics in Older Adults Using High-Speed Stereo Radiography," Med. Sci. Sports Exerc., **49**(11), pp. 2260–2267.

[89] Ivester, J. C., Cyr, A. J., Harris, M. D., Kulis, M. J., Rullkoetter, P. J., and Shelburne, K. B., 2015, "A Reconfigurable High-Speed Stereo-Radiography System for Sub-Millimeter Measurement of in Vivo Joint Kinematics," J. Med. Devices, Trans. ASME, **9**(4), pp. 1–7.

[90] Kozanek, M., Hosseini, A., Liu, F., Van de Velde, S. K., Gill, T. J., Rubash, H. E., and Li, G., 2009, "Tibiofemoral Kinematics and Condylar Motion during the Stance Phase of Gait," J. Biomech., **42**(12), pp. 1877–1884.

[91] Behnam, Y. A., Krishnan, A. A., and Clary, C. W., 2020, "Experimental Method and Computational Model for Evaluation of Knee Joint Mechanics," *ORS 2020 Annual Meeting Paper No.1058*, p. 2017.

[92] McKay, W. P., Chilibeck, P. D., Daku, B. L. F., and Lett, B., 2010, "Quantifying the Mechanical Work of Resting Quadriceps Muscle Tone," Eur. J. Appl. Physiol., **108**(4), pp. 641–648.

[93] Hindle, K., Whitcomb, T., Briggs, W., and Hong, J., 2012, "Proprioceptive Neuromuscular Facilitation (PNF): Its Mechanisms and Effects on Range of Motion and Muscular Function," J. Hum. Kinet., **31**(1), pp. 105–113.

[94] Shultz, S. J., Shimokochi, Y., Nguyen, A.-D., Schmitz, R. J., Beynnon, B. D., and Perrin, D. H., 2007, "Measurement of Varus–Valgus and Internal–External Rotational Knee Laxities in Vivo—Part i: Assessment of Measurement Reliability and Bilateral Asymmetry," J. Orthop. Res., **25**(8), pp. 981–988.

[95] Kupper, J. C., 2008, "A Novel Measure of In-Vivo Knee Joint Laxity," University of Calgary.

[96] Hino, K., Ishimaru, M., Iseki, Y., Watanabe, S., Onishi, Y., and Miura, H., 2013, "Mid-Flexion Laxity Is Greater after Posteriorstabilised Total Knee Replacement than with Cruciate-Retaining Procedures: A Computer Navigation Study," Bone Jt. J., **95 B**(4), pp. 493–497.

[97] Miura, H., Takasugi, S. ichiro, Kawano, T., Manabe, T., and Iwamoto, Y., 2009, "Varus-Valgus Laxity Correlates with Pain in Osteoarthritis of the Knee," Knee, **16**(1), pp. 30–32.

Appendices

Appendix A

Experimental Biomechanics Cadaver Laxity Data

This section contains the laxity measurements taken for the cadaveric specimens during the robotic knee tester measurements.

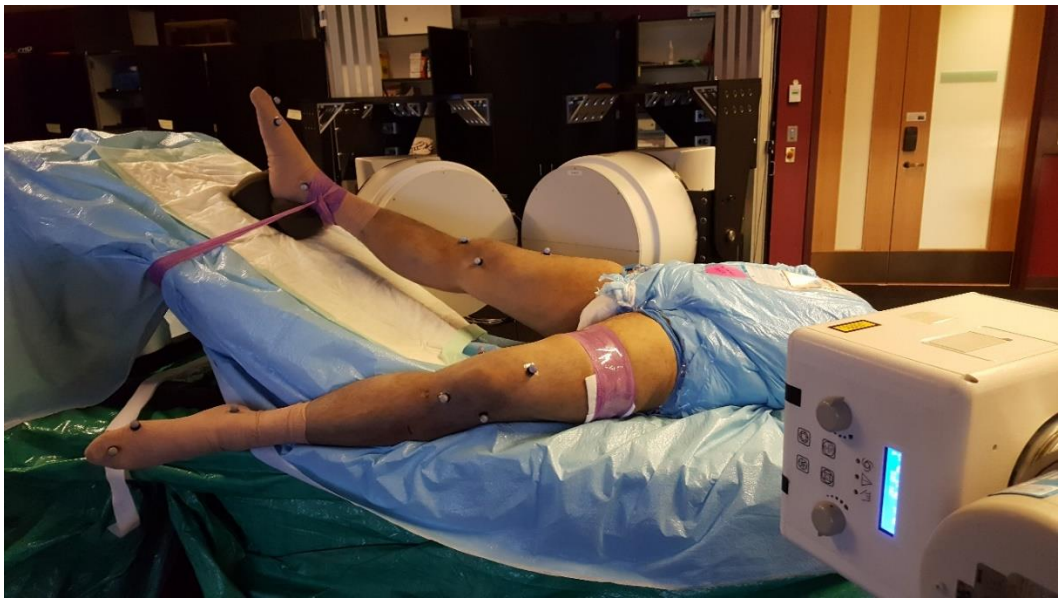

Figure A 1 Specimen S192803

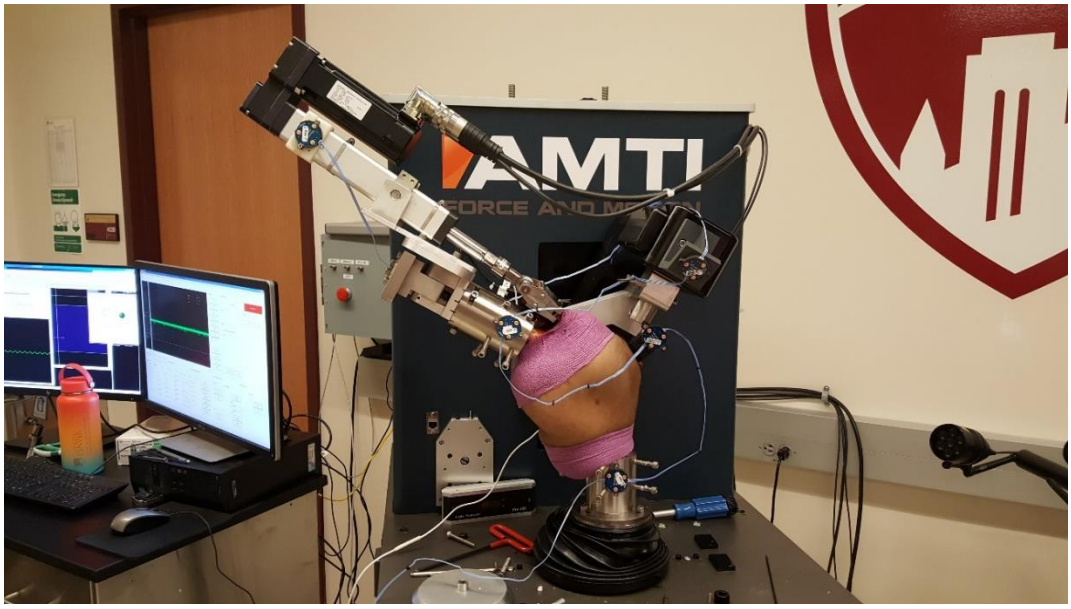

Figure A 2 Image of Specimen S192803 Left Testing

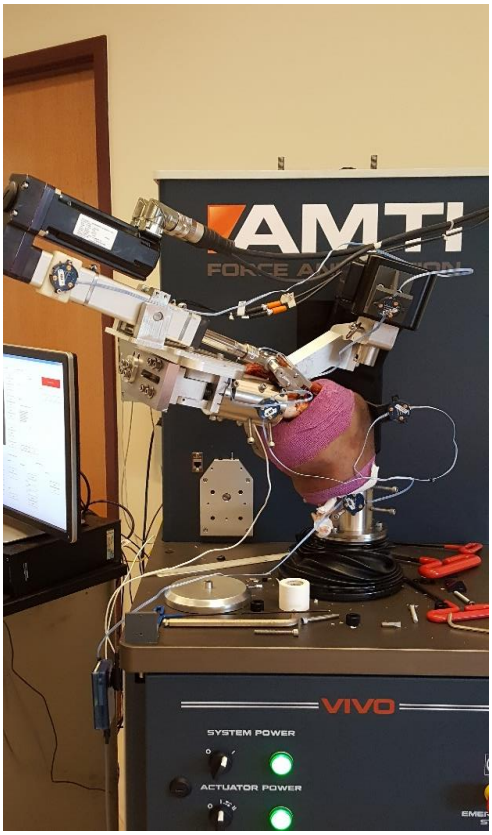

Figure A 3 Image of Specimen S192803 Right Testing

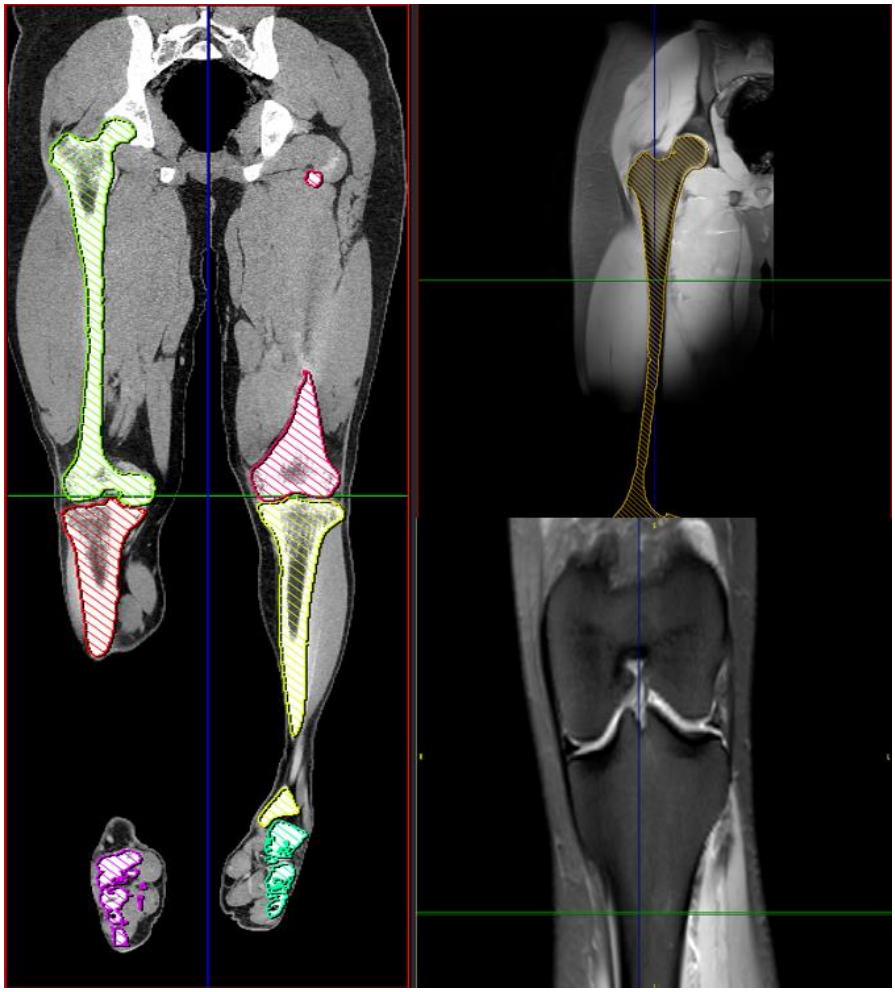

Figure A 4 Specimen S192803 CT and MRI Scans

Figure A 5 Specimen S192803 Left Laser Scans

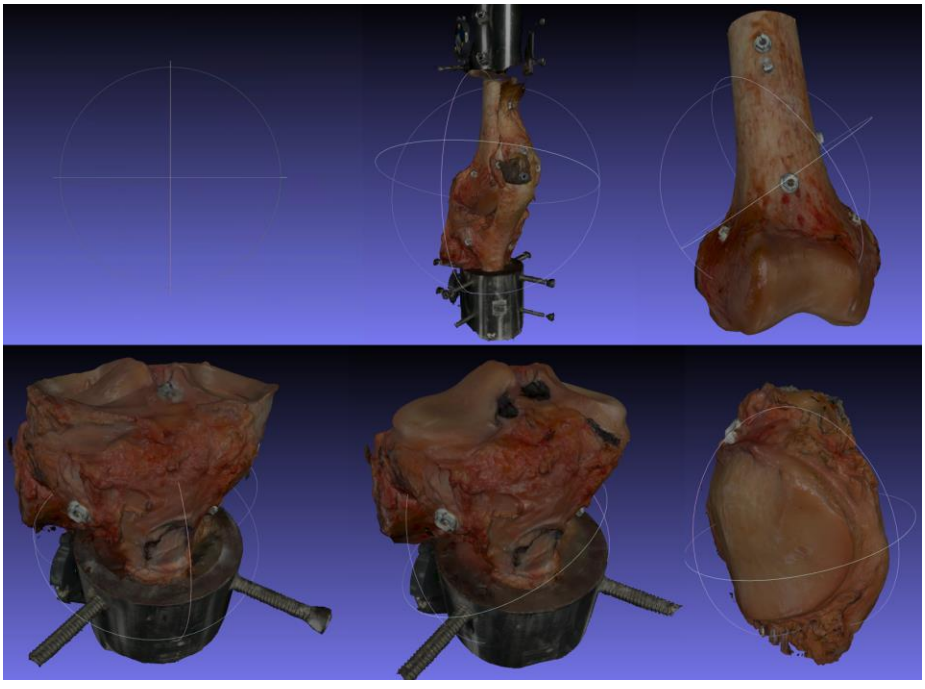

Figure A 6 Specimen S192803 Right Laser Scans

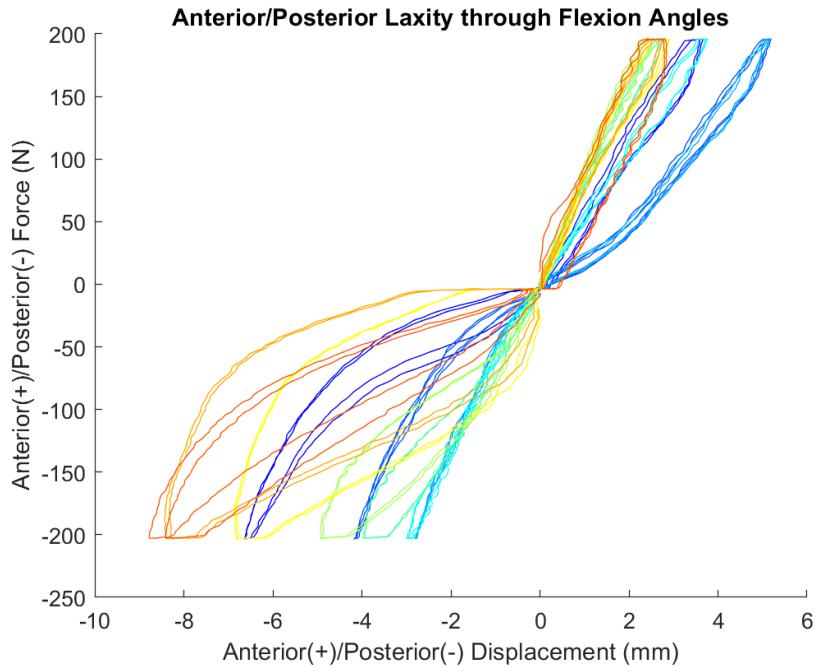

Figure A 7 Specimen S192803 Left AP Laxity Curves

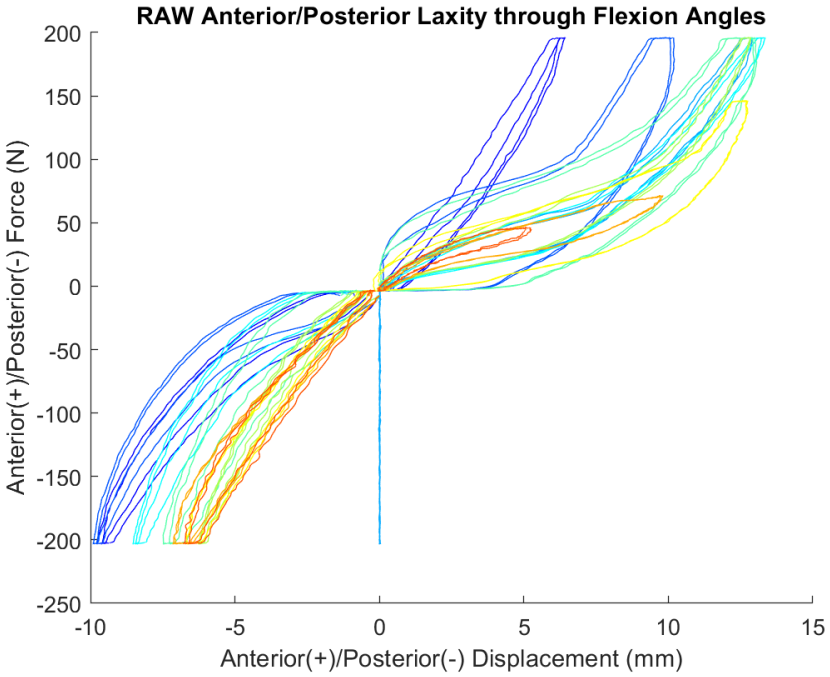

Figure A 8 Specimen S192803 Left No ACL AP Laxity Curves

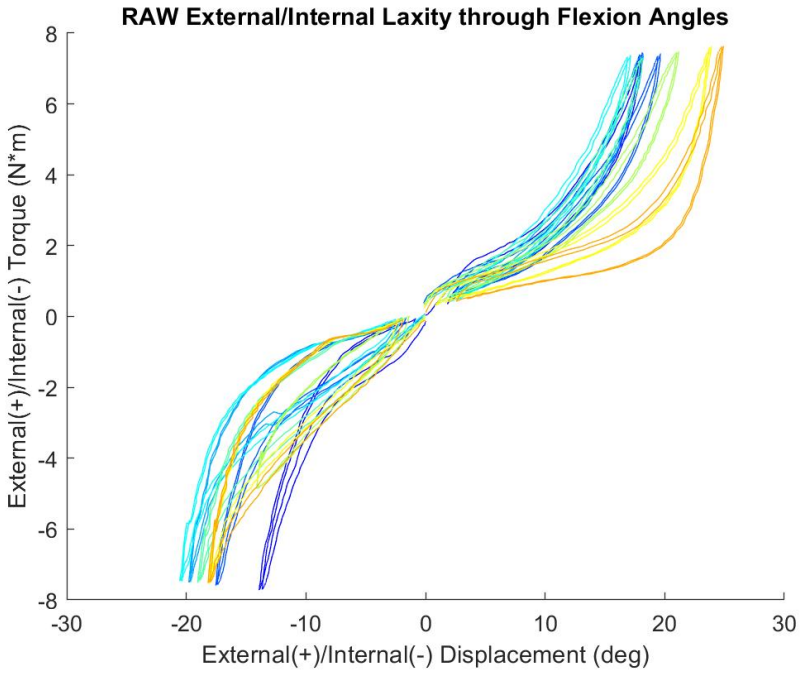

Figure A 9 Specimen S192803 Left IE Laxity Curves

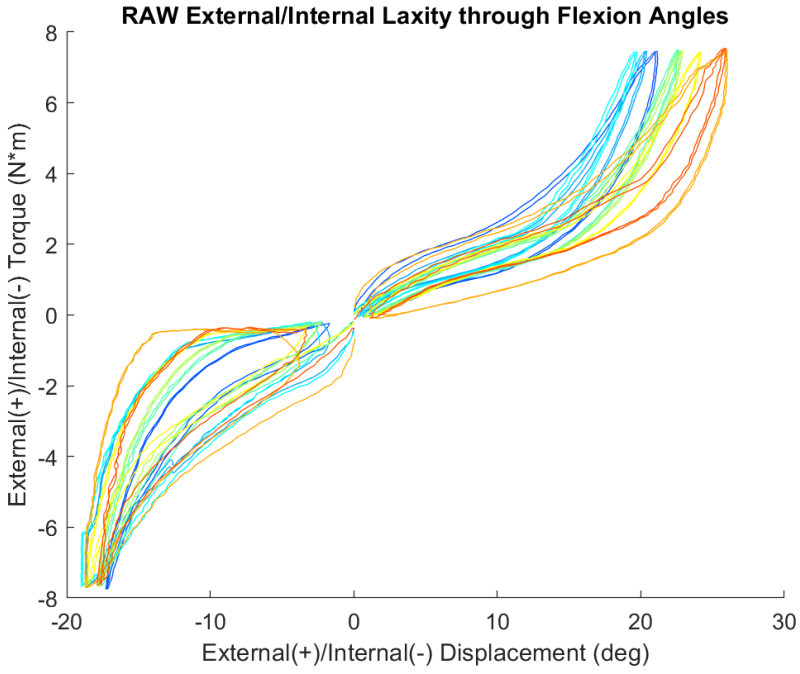

Figure A 10 Specimen S192803 Left No ACL IE Laxity Curves

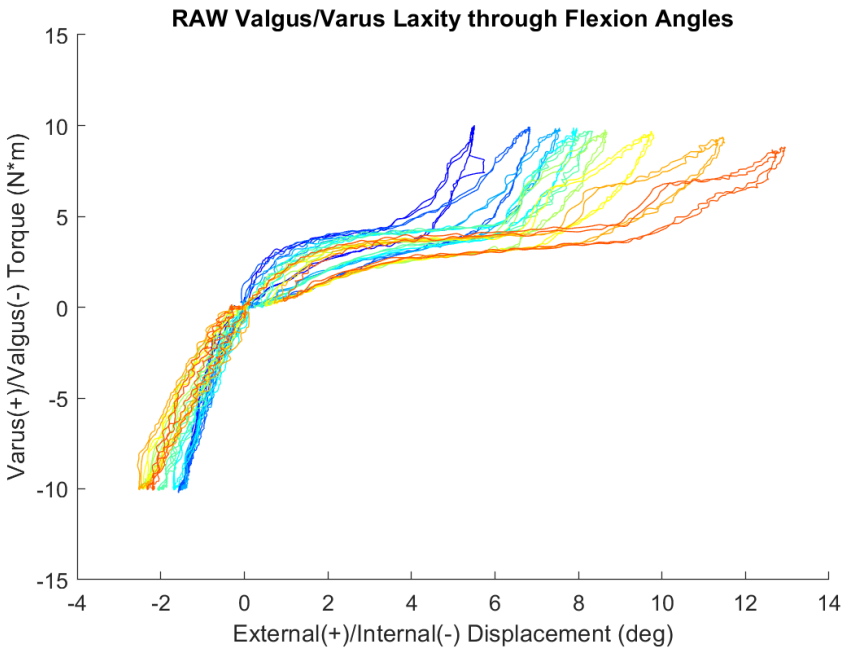

Figure A 11 Specimen S192803 Left VV Laxity Curves

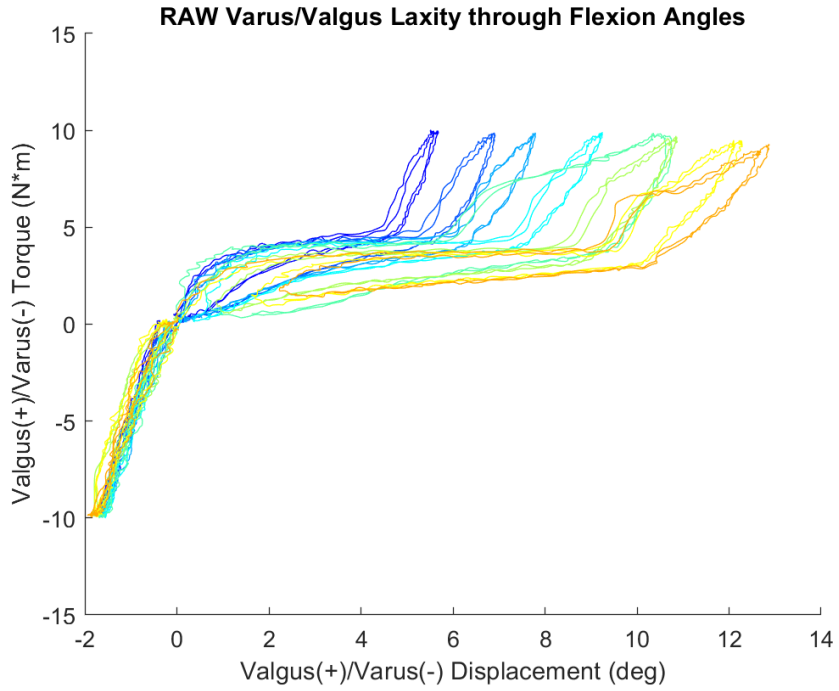

Figure A 12 Specimen S192803 Left No ACL VV Laxity Curves

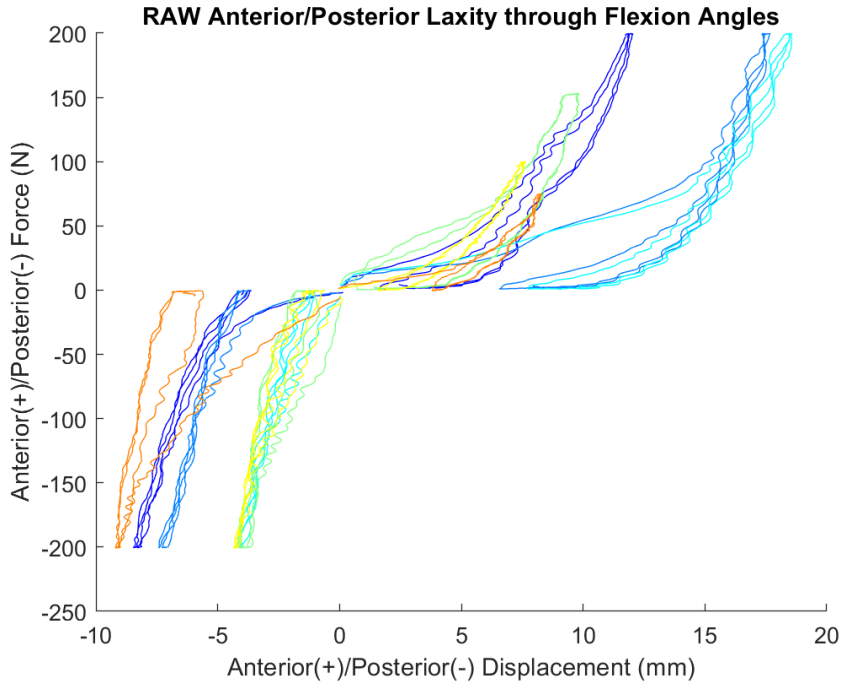

Figure A 13 Specimen S192803 Right AP Laxity Curves

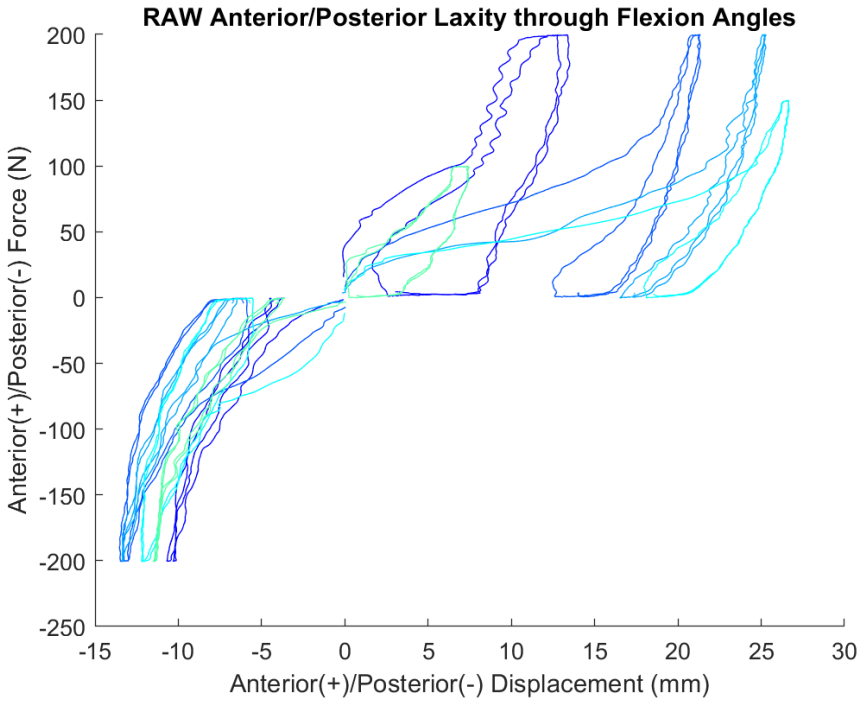

Figure A 14 Specimen S192803 Right No ACL AP Laxity Curves

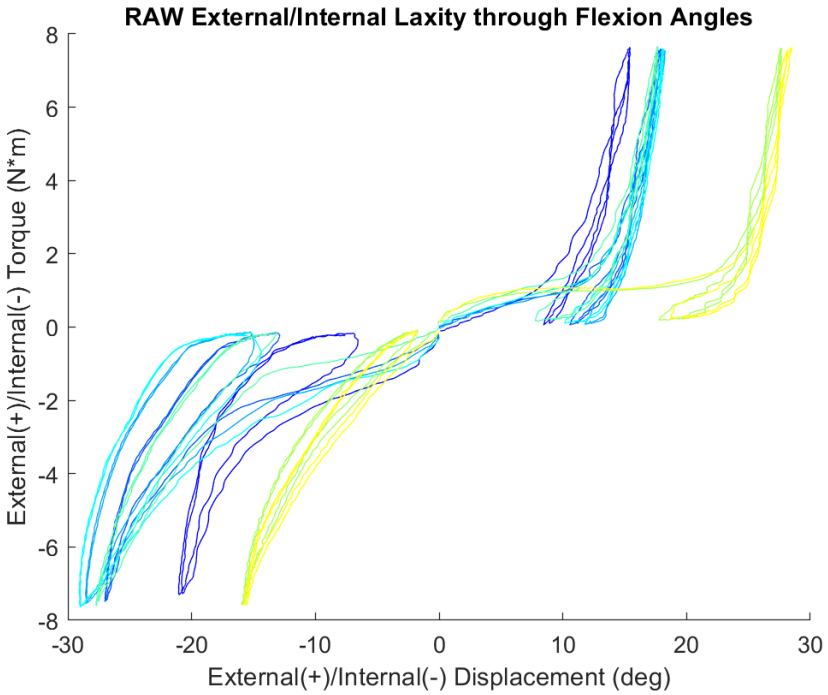

Figure A 15 Specimen S192803 Right IE Laxity Curves

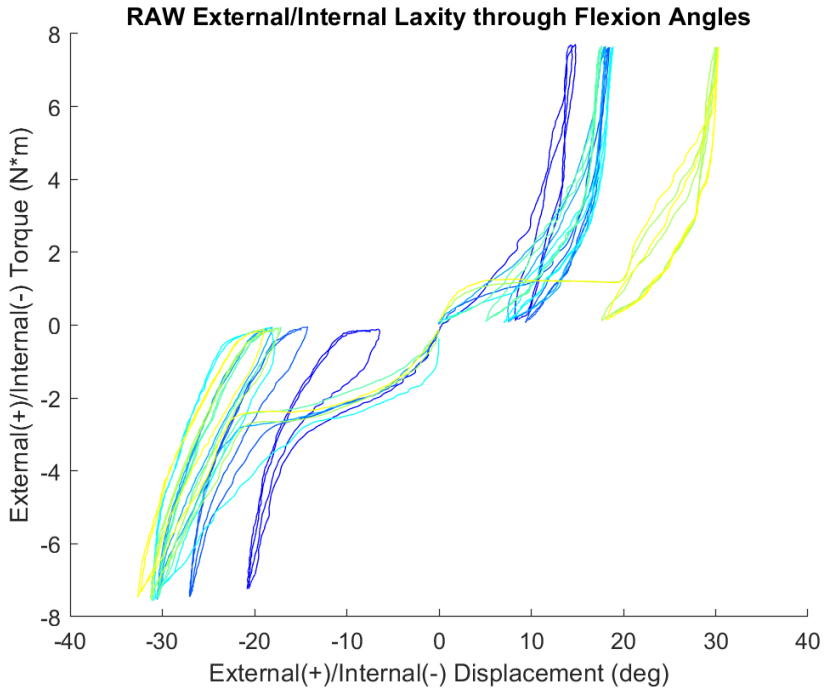

Figure A 16 Specimen S192803 Right No ACL IE Laxity Curves

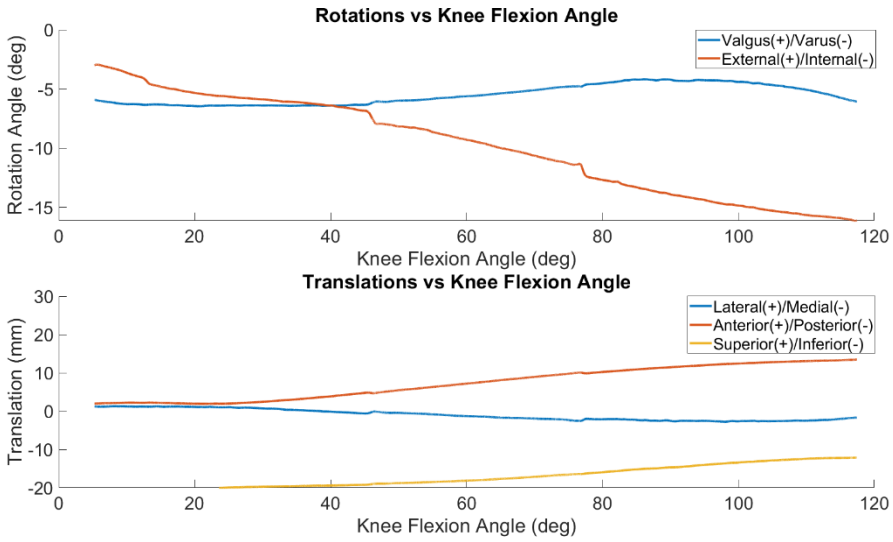

Figure A 17 Specimen S192803 Left Passive ROM Kinematics

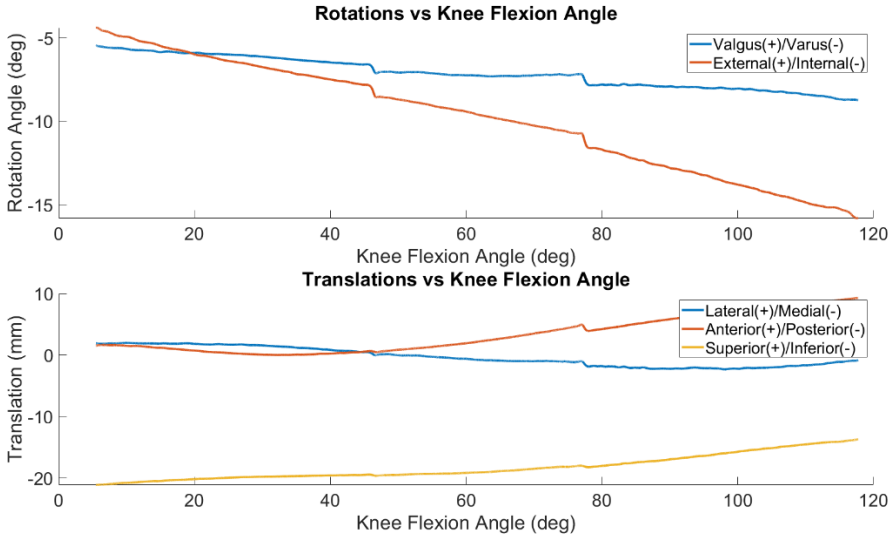

Figure A 18 Specimen S192803 Left Passive ROM Kinematics

Figure A 19 Specimen S193761

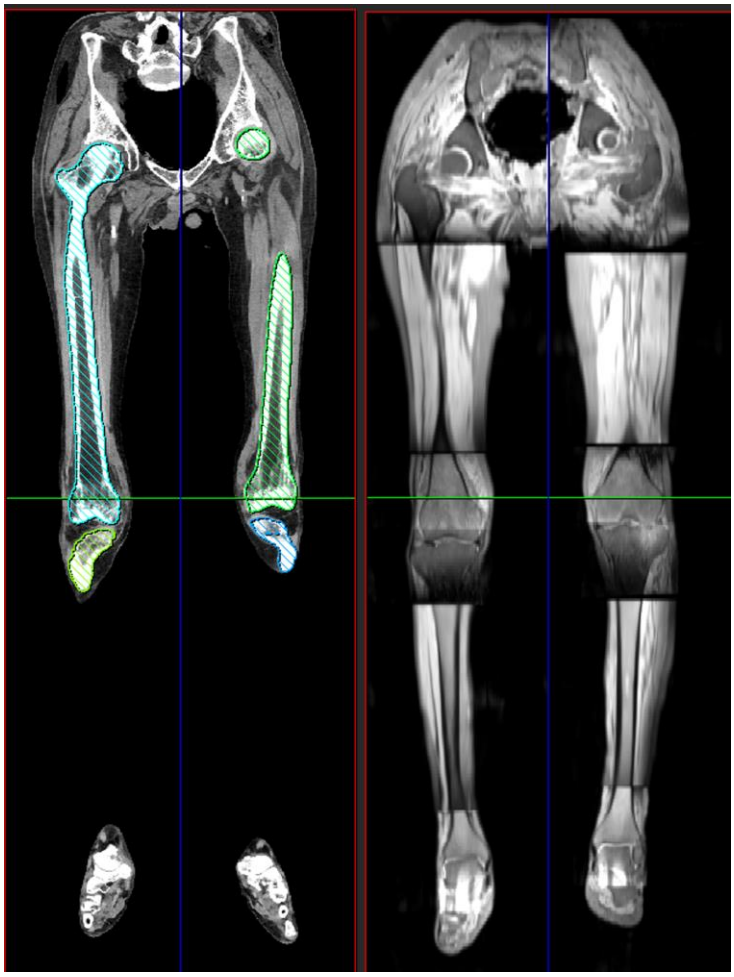

Figure A 20 Specimen S193761 CT and MRI Scans

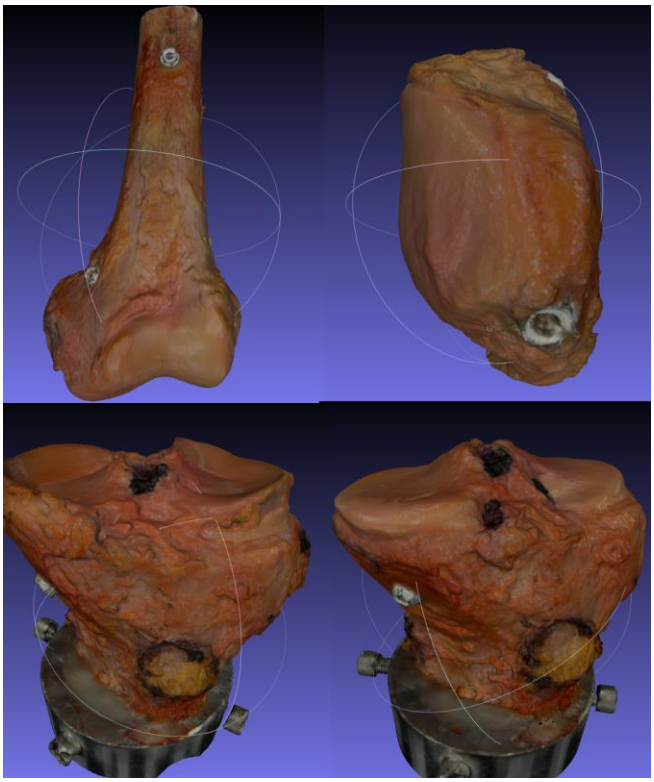

Figure A 21 Specimen S193761 Left Laser Scans

Figure A 22 Specimen S193761 Left ACL Cut Image

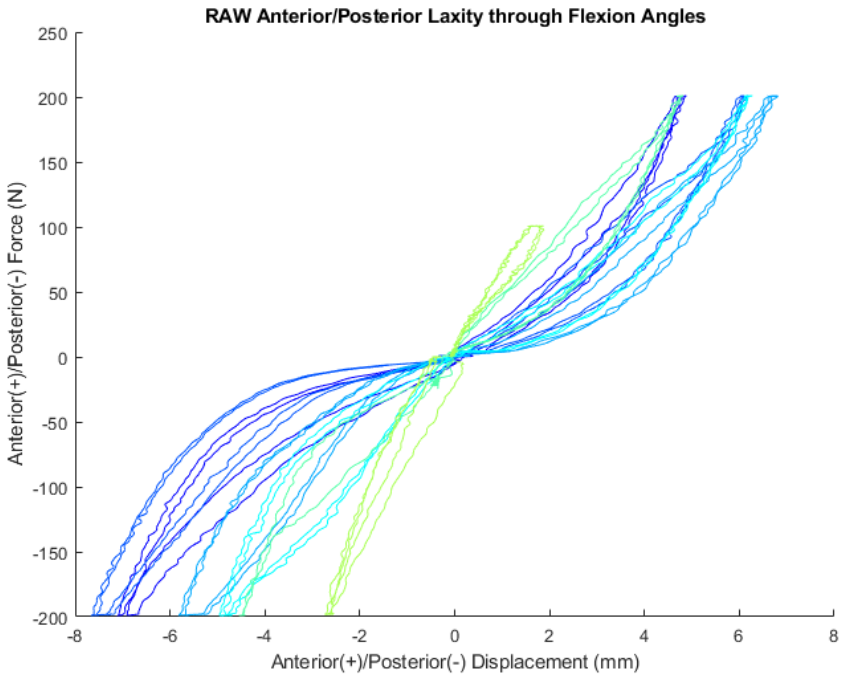

Figure A 23 Specimen S193761 Left AP Laxity Curves

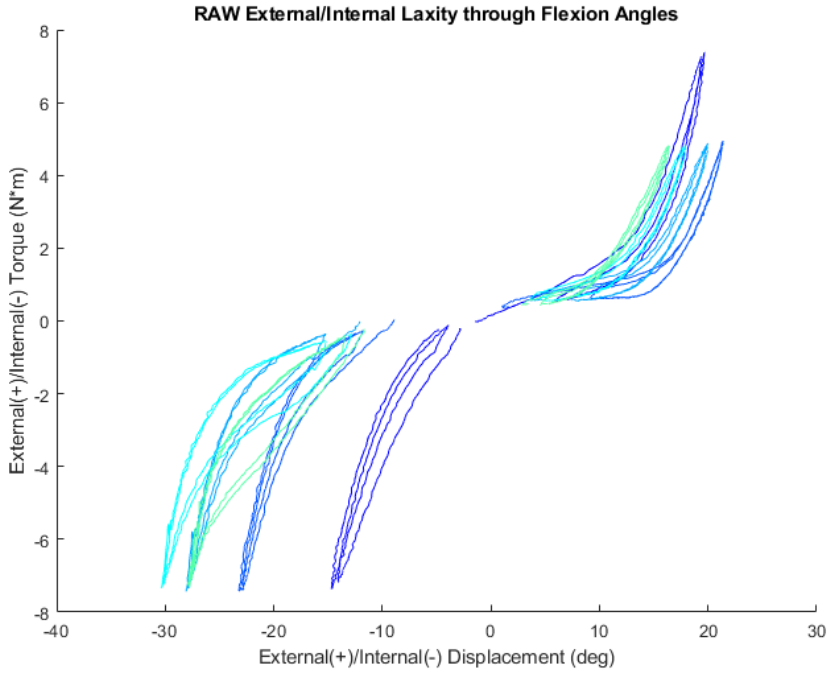

Figure A 24 Specimen S193761 Left IE Laxity Curves

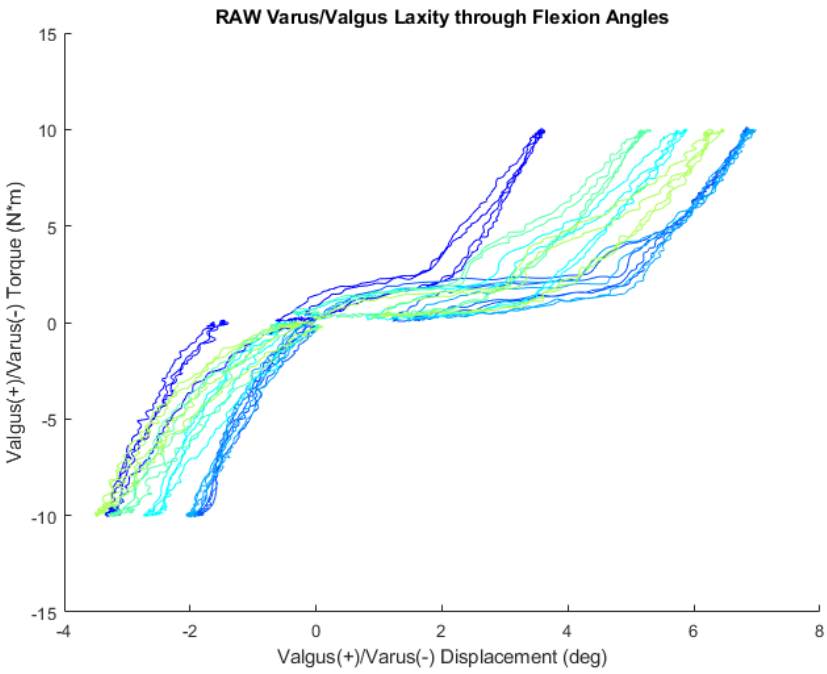

Figure A 25 Specimen S193761 Left VV Laxity Curves

Appendix B

6.2.1. Process for Re-Alignment of Bones to Probe Points, if Faulty Probe Points were made

This section contains information, on the process performed during this work, to use sphere fitting trilateration to re-determine the location of the actual probe points, based on a faulty probe for alignment of the bone correctly in 3D space. In addition, it runs through the process performed on the patella to use the initial probe points as an initial value, and the flexed knee kinematics of the other bones, to optimize the otherwise faulty position, of the patella from insufficient probe points.

Background:

Tracking of the bones in the EBL is performed by attaching rigid body markers (set of 3 rigid IR LEDs) to a fixed site on each of the bones. The Optotrak then records the location of the IR LEDs and using previously created rigid body definitions, can track the Cardan rotations and translations of the Rigid Bodies through space, relative to the Global Coordinate System (GCS). The key step in order to track the bones in the GCS is to probe the location of the bones relative to each of the rigid body definitions, so that motion of the rigid body can be correlated to the appropriate motion and location of the attached bone.

Previously, a provided probe was used to probe points on the articular surfaces of a bone in the corresponding Rigid Body Coordinate System (RBCS) of the rigid body that was fixed to that bone. Then a software such as Hypermesh would be used to manually align the bone geometry to the measured probe points and the corresponding

transformation required to move the bone to its location within the rigid body coordinate system (based on the probe points) would be recorded and used. However, the major issue that occurred was the need for manual alignment by a person, leading to potential error and variability in final alignment of the bone in the RBCS.

The current method used to determine the location is an attempt to remove human error by removing the manual alignment of bone geometry to probe points. This is done by use of fiducial screws with sphere cutouts drilled into them (matching the probe tip sphere). The screws are then screwed into the bones at various locations (while the rigid bodies are still attached to the bones), with at least 3 being used. The probe is then used to measure the locations of these fiducial screw points in the RBCS of the current rigid body. The bone is then laser scanned, and special care is taken to ensure proper scanning of all of the fiducial screws. Then points are created in the geometry of the fiducial screws and SVD is used to auto align the points of the screws in the laserscan, to their corresponding location in the RBCS based on the probe points. As such, no manual alignment of the bone is necessary, helping to reduce the uncertainty associated with manual alignment. This drastically increases the accuracy of alignment and increases the speed at which the registration alignment can be performed.

Problem:

The issue that occurred is that the probe used to measure the reference fiducial points in the rigid body space was messed up. While the ultimate issue has not been proven, it is suspected that the calibration file for the probe was chosen as a previous iteration of the

probe. The previous probe was shorter than the actual probe used and resulted in a distance offset between the measured position and the actual position of the probe tip.

As a result, each coordinate is offset by the same distance (unknown), but in a completely random direction based on the orientation of the probe handle when the measurement was made. This results in a sphere shell of possibilities of where the real coordinate could be, based on the point that was measured. This error occurs at each fiducial probe point with the same distance, but each measurement is oriented in a random direction. This creates an infinite number of possibilities of the actual position of the fiducial marker, at each of the fiducial marker measurements.

Solution:

For the Femur and the Tibia, the bones were aligned using the process of trilateration similar to satellite GPS tracking. At each satellite, a sphere creates the possible directions to the corresponding GPS receiver. Multiple satellites, are used to progressively narrow down the list of possibilities to the transceiver, as shown in Figure A 1.

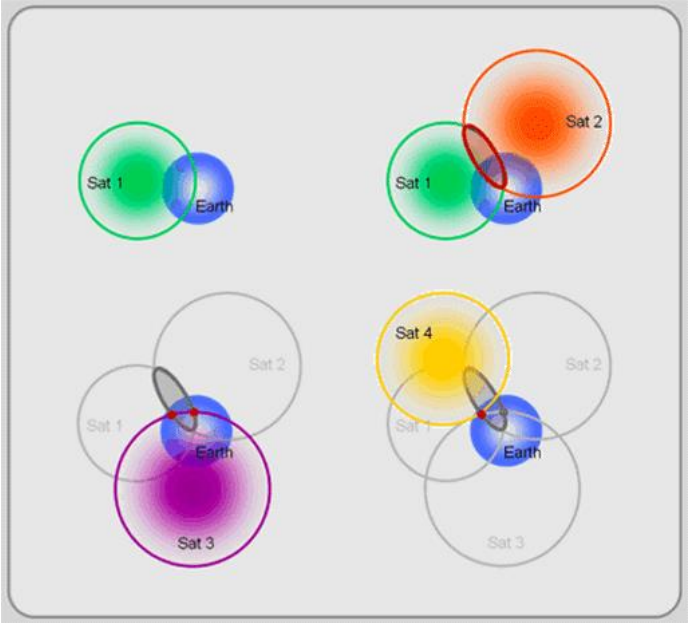

Figure A 26 Trilateration Spheres and Resulting Locations [*https://giscommons.org/chapter-2-input/*](https://giscommons.org/chapter-2-input/)

For satellites, the combination of 4 satellites will resolve the final object to a single (X,Y,Z) coordinate in 3D space.

The correction of the probe points was done in a similar manner. At each of the measured probe points in the Optotrak space, there is an infinite sphere of possibilities of where the actual probe point could be. At each of these fiducial points in Optotrak space, a sphere was created, by first approximating the distance to each point from the Optotrak space to the approximate laser scan point. This sphere contains a single point, that contains the location of the original probe point. That was offset from the original scan. Points were created in SolidWorks with the corresponding spheres, using the coordinates of the fiducial marker locations in the Optotrak, as shown in Figure A 27

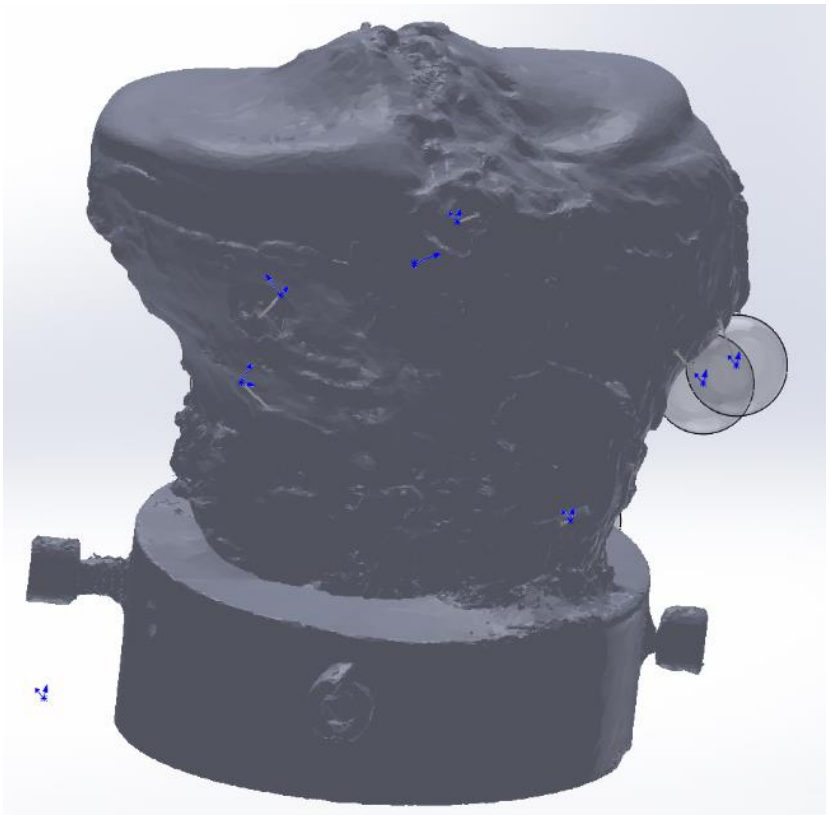

Figure A 27 Sphere and Fiducial Points

Corresponding points for the fiducial locations were chosen on the laser scan, and created as corresponding points in 3D and then rigidly fixed relative to one another. Then using the mate feature in SolidWorks, the points on the 3D laser scan geometry were aligned in 3D, to match the corresponding sphere surface, as shown in Figure A 28. This was repeated for each of the spheres, and thus aligned the bone. NOTE: While satellites use 4 spheres, to determine the location of the GPS receiver, this can only resolve a 3D location, but not the orientation. Mathematically, we can prove that 2 more Spheres are needed to resolve the 3 rotational DOF, and as such 6 spheres were needed to align the bones.

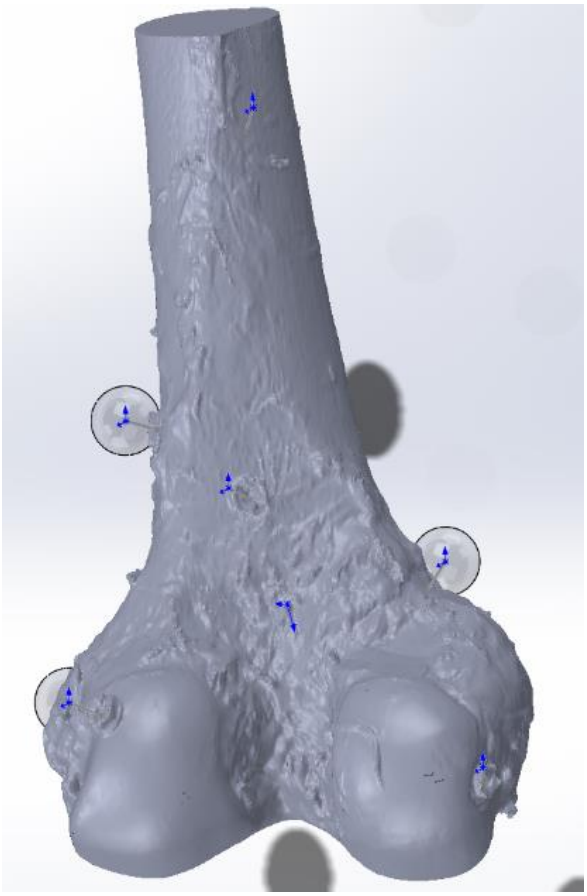

Figure A 28 Femur with Final Sphere Alignments and Predicted Probe Direction

The resulting errors for the distance of the bones, as shown below in Figure A 29, was determined to be 0mm between the location of the fiducial points onto the spheres. This was done by iteratively changing the offset distance of the probe, by changing the radius of the spheres until the distance between each point and its corresponding sphere was able to be “mated”, resulting in no error. This ensures that the locations of all the fiducial markers is in the optimal location based on the original probe error. Of note, is that if the chosen location of a fiducial point on the original laser scan is slightly off, there may be a slight non-zero distance between one or two of the points and their corresponding spheres; however, this tends to be a very small distance.

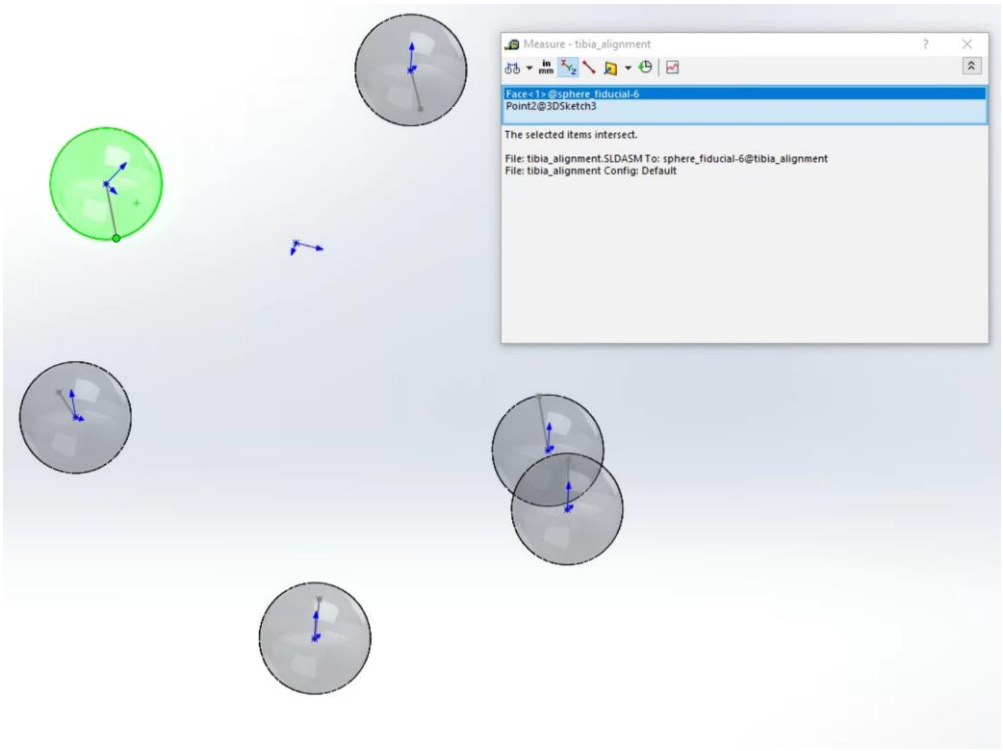

Figure A 29 Final Sphere Alignment Accuracy

While the Femur, and Tibia benefitted from having 6 fiducial marker locations between combinations of the screws and corresponding tantalum bead inserts. However, the Patella only had 4 marker locations total, and as such could not be resolved entirely. What was performed thereafter, was first the Patella was aligned approximately using the alignment described previously in SolidWorks, as shown below in Figure A 30. Notably, since the patella only had 4 spheres to align, the patella can manually be moved in SolidWorks, since its exact position/orientation is not completely constrained, whereas the femur and tibia are not able to be moved in SolidWorks because all of their DOF are completely restrained.

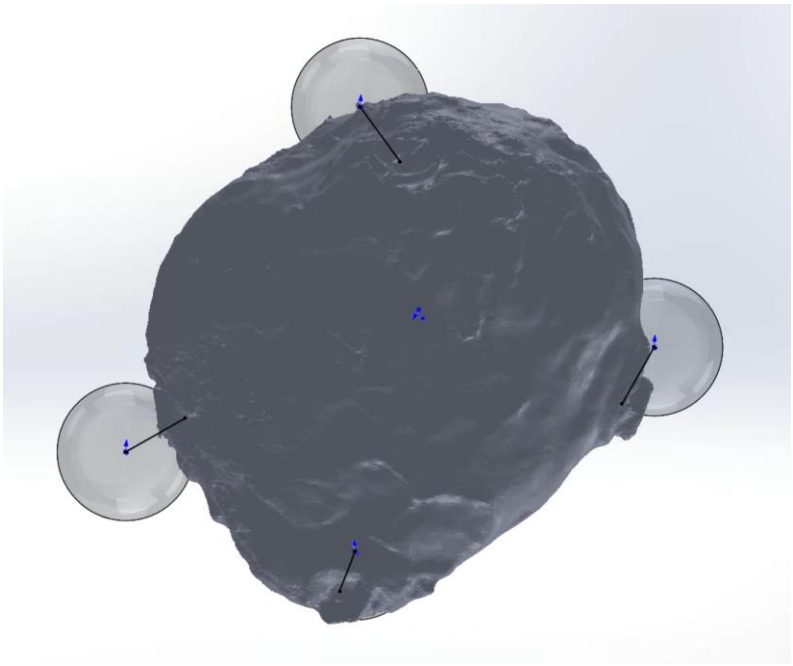

Figure A 30 Initial Manual Patella Alignment using Sphere Method in SolidWorks

Then the bones were loaded using a custom MATLAB script, and a trial at near 90 degrees of knee flexion, was used to determine the position of the bones relative to one another. In particular, the femur and tibia, in the correct final positions at 90 degrees, but with the patella in an approximate position. Then the position of the patellar articular surface, relative to the femoral articular surface was determined initially from the manual alignment as shown below in Figure A 31.

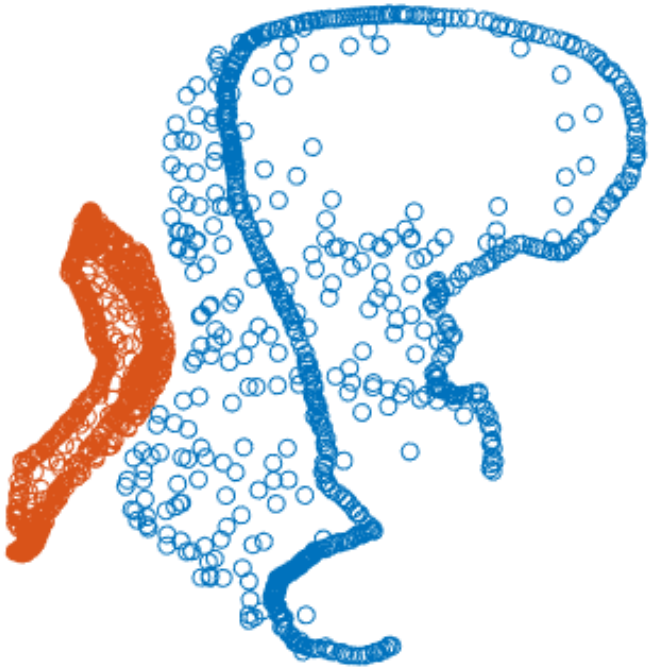

Figure A 31 Initial Patella and Femoral Articular Surface Alignment

Then a custom MATLAB script was created to optimize the patellar position in 3D space, to sit in the groove of the Femur. During the trial, it was known that at this 90 degree of flexion, because of the applied quadriceps load, the patella should sit in line of the groove of the femur. As shown in the previous image, it was approximately correct, but left a gap.

The custom MATLAB script, created constraint functions for each of the spheres, an the corresponding points in 3D space of the corresponding fiducial screws. These constraints were held as equality constraints to ensure the proper location of the screws points relative to the measured “spheres” in the Optotrak space. The objective function to minimize was determined, by using a custom script to determine the minimum distance between a node and a corresponding face triangular set. Of note, this code returns a

negative number when the distance is measured with a negative dot product. The code then attempts to minimize the average distance between a node on the patellar articular surface, and the femoral articular surface. Additionally, an External Penalty Method, was used to determine if any point had over closed between the femoral and patellar articular surfaces, done by looking for a negative value. If any of the values were negative, this was determined as an overclosure and used to steer the optimization solution away from a solution that would cause an overclosure between the bones. An example of what would happen without this, is shown below in Figure A 32.

Figure A 32 Overclosed Patella and Femoral Articular Surface Alignment

This in combination with minimizing the distance between the bones, allowed for a reasonable solution to the Translational and Euler rotations, required to move the patella from the original laser scan space, to the correct space in the Optotrak, and then determine the corresponding location. The optimization was performed using the built-in MATLAB function fmincon, and was able to perform the optimization in around 300 iterations, in about 15 minutes. The final location of the patellar articular surface relative the femoral surface is shown below in Figure A 33.

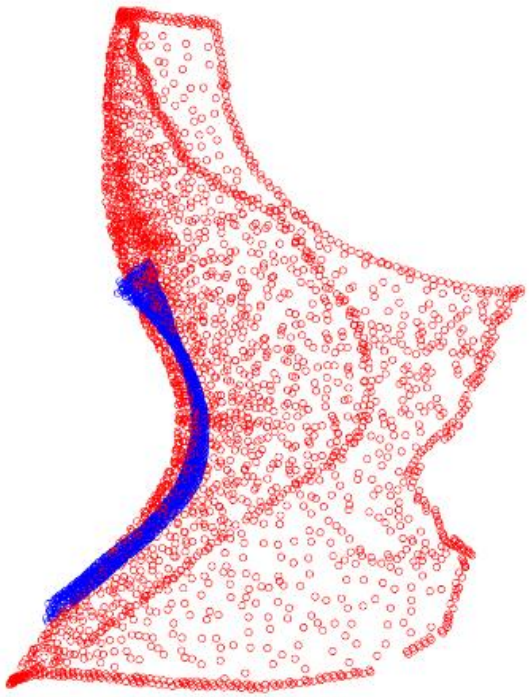

Figure A 33 Final Patella and Femoral Articular Surface Alignment

Code:

```
%% Optotrak Patella Realignment Optimization
% Created by Thor Andreassen
% 3/10/20

%% Clearing
clear
```

```
close all
clc

%% Load transformations
pat_path=['R:\Research Common\HDL\Projects\HSSR\Data\U01\Aim 2\S193761\EBL
    Testing\Left\Segmentation\Segmented STLs\Patella\Solidworks Sphere Alignment\'];
pat_transmat_filepath=[pat_path,'patella_optimization_alignmnet_transmat.mat'];

load(pat_transmat_filepath);

%% LOAD Articular Geometry

[patella_geom.nodes,patella_geom.elements]=stlread_ascii_binary('patella_laser_art_surface_4.stl');
[patella_geom.elements_reduce,patella_geom.nodes_reduce]=reducepatch(patella_geom.elements,patella_
    geom.nodes,5000);

[femur_geom.nodes,femur_geom.elements]=stlread_ascii_binary('femur_laser_art_surface_6.stl');
[femur_geom.elements_reduce,femur_geom.nodes_reduce]=reducepatch(femur_geom.elements,femur_geo
    m.nodes,5000);

%% Load Fiducial Points
pat_fid_filepath=['R:\Research Common\HDL\Projects\HSSR\Data\U01\Aim 2\S193761\EBL
    Testing\Left\Optotrak DATA\Probe Points\patella_fiducial.txt']
pat_fiducial_fid = fopen(pat_fid_filepath,'r');
pat_fiducial_nodes = [];
while ~feof(pat_fiducial_fid)
   temp_scan = textscan(pat_fiducial_fid,'%f %f %f %f'); temp = fgetl(pat_fiducial_fid);
   pat_fiducial_nodes = [pat_fiducial_nodes(1:end,1:end); temp_scan{1} temp_scan{2} temp_scan{3}
      temp_scan{4}];
end
fclose(pat_fiducial_fid);
pat_fiducial_coords=pat_fiducial_nodes(:,2:4);

%% Load Laserscan Points
pat_laser_coords=csvread('patella_laser_screw_pts.txt');


%% Create Sphere constraint equations
% Determine circle offset probe distance in mm
R=6.8;
syms x1 y1 z1 x2 y2 z2 x3 y3 z3 x4 y4 z4
xs=[x1,x2,x3,x4];
ys=[y1,y2,y3,y4];
zs=[z1,z2,z3,z4];
for counti=1:size(pat_fiducial_coords,1)
   eq(counti)=(xs(counti)-pat_fiducial_coords(counti,1)).^2+(ys(counti)-
      pat_fiducial_coords(counti,2)).^2+(zs(counti)-pat_fiducial_coords(counti,3)).^2-R.^2;
end

sphere_constraints_eqs=matlabFunction(eq);

%% MAIN CODE
```

```
%% Initial Rotation and Translations
X0=[0,0,0,0,0,0];

%% Define optimization constraint equation
functionConstraints=@(X) sphereConstraints(X,pat_laser_coords,sphere_constraints_eqs);


%% define test nodes
pat_art_coords=patella_geom.nodes_reduce;
fem_art_coords=femur_geom.nodes_reduce;

%% move femur to patella rigid body space
Femur_Laser_to_PATRB_TransMat=Patella_Laser_to_Patella_RigidBody_TransMat*inv(Patella_Laser_t
    o_GCS_TransMat(:,:,1))*Femur_Laser_to_GCS_TransMat(:,:,1);
fem_art_coords_PATRB=Femur_Laser_to_PATRB_TransMat*[ones(length(fem_art_coords),1),fem_art_c
    oords]';
fem_art_coords_PATRB=fem_art_coords_PATRB(2:4,:)';

%% move patella to patella rigid body space for initial alignment
pat_art_coords_PATRB=Patella_Laser_to_Patella_RigidBody_TransMat*[ones(length(pat_art_coords),1),
    pat_art_coords]';
pat_art_coords_PATRB=pat_art_coords_PATRB(2:4,:)';

%% Plot Starting Alignment
figure()
hold on
plot3(fem_art_coords_PATRB(:,1),fem_art_coords_PATRB(:,2),fem_art_coords_PATRB(:,3),'ro')
plot3(pat_art_coords_PATRB(:,1),pat_art_coords_PATRB(:,2),pat_art_coords_PATRB(:,3),'bo')

%% Initialize the Transformation Matrix, based on Previous Values
[X0(3),X0(2),X0(1)]=dcm2angle(Patella_Laser_to_Patella_RigidBody_TransMat(2:4,2:4));
X0(4:6)=Patella_Laser_to_Patella_RigidBody_TransMat(2:4,1);

%% Define Optimization equation
optimfunc=@(X) costFunc(X,pat_art_coords,fem_art_coords_PATRB,femur_geom.elements_reduce);

%% MAIN Optimization Function
Aeq=[];
beq=[];
lb=[-2*pi,-2*pi,-2*pi,-100,-100,-100];
ub=[2*pi,2*pi,2*pi,125,125,125];
A=[];
b=[];
options = optimset('PlotFcns','optimplotfval','TolX',1e-7,'TolFun',1e-7);
X_optim=fmincon(optimfunc,X0,A,b,Aeq,beq,lb,ub,functionConstraints,options)


%% Plot Final Position

RX=X_optim(1);
RY=X_optim(2);
RZ=X_optim(3);
TX=X_optim(4);
```

```
TY=X_optim(5);
TZ=X_optim(6);
rotmat=angle2dcm(RZ,RY,RX);
transvec=[TX,TY,TZ]';
TransMat=zeros(4,4);
TransMat(1,1)=1;
TransMat(2:4,1)=transvec;
TransMat(2:4,2:4)=rotmat;
pat_art_coords_PATRB=TransMat*[ones(length(pat_art_coords),1),pat_art_coords]';
pat_art_coords_PATRB=pat_art_coords_PATRB(2:4,:)';

figure()
hold on
plot3(fem_art_coords_PATRB(:,1),fem_art_coords_PATRB(:,2),fem_art_coords_PATRB(:,3),'ro')
plot3(pat_art_coords_PATRB(:,1),pat_art_coords_PATRB(:,2),pat_art_coords_PATRB(:,3),'bo')

%%%%%%%%%%%%%%%%%%%%%%%%%%%%%%%%%%%%%%%%%%%%%%%%%%%%
    %%%%%%%%%%%%%%%%%%%%%%%%%%%%%%%%%%%%
%%%%%%%%%%%%%%%%%%%%%%%%%%%%%%%%%%%%%%%%%%%%%%%%%%%%
    %%%%%%%%%%%%%%%%%%%%%%%%%%%%%%%%%%%%
%%%%%%%%%%%%%%%%%%%%%%%%%%%%%%%%%%%%%%%%%%%%%%%%%%%%
    %%%%%%%%%%%%%%%%%%%%%%%%%%%%%%%%%%%%
%% FUNCTION DEFINITIONS

%% Optimization Cost Function
% % function cost=costFunc(X,pat_art_coords_orig,fem_art_coords_PATRB,fem_art_elements)
% %     RX=X(1);
% %     RY=X(2);
% %     RZ=X(3);
% %     TX=X(4);
% %     TY=X(5);
% %     TZ=X(6);
% %     rotmat=angle2dcm(RZ,RY,RX);
% %     transvec=[TX,TY,TZ]';
% %     TransMat=zeros(4,4);
% %     TransMat(1,1)=1;
% %     TransMat(2:4,1)=transvec;
% %     TransMat(2:4,2:4)=rotmat;
% %     pat_art_coords_PATRB=TransMat*[ones(length(pat_art_coords_orig),1),pat_art_coords_orig]';
% %     pat_art_coords_PATRB=pat_art_coords_PATRB(2:4,:)';
% %
% %     [I,D]=knnsearch(pat_art_coords_PATRB,fem_art_coords_PATRB);
% %     cost=mean(D);
% % end

function cost=costFunc(X,pat_art_coords_orig,fem_art_coords_PATRB,fem_art_elements)
  penalty_const=100000;
  RX=X(1);
  RY=X(2);
  RZ=X(3);
  TX=X(4);
  TY=X(5);
  TZ=X(6);
```

```
    rotmat=angle2dcm(RZ,RY,RX);
    transvec=[TX,TY,TZ]';
    TransMat=zeros(4,4);
    TransMat(1,1)=1;
    TransMat(2:4,1)=transvec;
    TransMat(2:4,2:4)=rotmat;
    pat_art_coords_PATRB=TransMat*[ones(length(pat_art_coords_orig),1),pat_art_coords_orig]';
    pat_art_coords_PATRB=pat_art_coords_PATRB(2:4,:)';

    [distances]=point2trimesh('Faces',fem_art_elements,...
        'Vertices',fem_art_coords_PATRB,'QueryPoints',pat_art_coords_PATRB,...
        'Algorithm','parallel');
    square_neg_distance=distances;
    for counti=1:length(distances)
        if distances(counti)<=0
            square_neg_distance(counti)=penalty_const*(distances(counti).^2);
        end
    end
    cost=mean(square_neg_distance)
end


%% Constrain Function
% The order of X is RX,RY,RZ,TX,TY,TZ
function [c,ceq]=sphereConstraints(X,laser_coords,constraints)

    RX=X(1);
    RY=X(2);
    RZ=X(3);
    TX=X(4);
    TY=X(5);
    TZ=X(6);
    rotmat=angle2dcm(RZ,RY,RX);
    transvec=[TX,TY,TZ]';
    TransMat=zeros(4,4);
    TransMat(1,1)=1;
    TransMat(2:4,1)=transvec;
    TransMat(2:4,2:4)=rotmat;
    newpts=TransMat*[ones(4,1),laser_coords]';
    newpts=newpts(2:4,:)';
    c=[];
    ceq=constraints(newpts(1,1),newpts(2,1),newpts(3,1),newpts(4,1),...
        newpts(1,2),newpts(2,2),newpts(3,2),newpts(4,2),...
        newpts(1,3),newpts(2,3),newpts(3,3),newpts(4,3));


end
```

Appendix C

CODE for DSX DATA Processing

The following sections contains MATLAB code for the creation of the subject trial in DSX automatically, by loading in the HSSR cine files automatically, and creating the corresponding trials, by grouping together similar HSSR image data. In addition, this section contains MATLAB code to process the resulting DSX transform output data, and interpolate – based on user preference, the resulting points not tracked and perform any necessary filtering on the initial bone kinematics, prior to the final GS kinematics calculations for improved accuracy.

Create DSX Trials

```
%% createDSXTrialsForConfigurations
% Created by Thor Andreassen
% 3/18/20
% the dsx file needs to have the following lines at the very beginning, and
% the very end to work
% Beginning
%     <?xml version="1.0" encoding="utf-8"?>
%     <dxr>

% End
%     <dxr>


%% clearing
clear
close all
clc

%% SYSTEM INPUTS
% choose the filepath to the current dsx file with the cubes already
% created
dsx_subject_path=['R:\Research Common\HDL\Projects\HSSR\Data\U01\Aim 2\S193761\DSX\'];
dsx_filename=['S193761_FINAL_2'];
cubename=['Cube04'];

allcines_path=['R:\Research Common\HDL\Projects\HSSR\Data\U01\Aim 2\S193761\Cine Files\'];
allcines_path=[allcines_path,cubename,'\'];

% Define the relative path for the cine_trials, as well as tracked object
```

```
% names for the trials
dsxcine_rel_path='$(cine_trials)/';
dsxcine_filepath=[dsxcine_rel_path,cubename,'/'];
checkSide=1; % IF 0 only uses side 1

tracked_objects_R={'S193761_Femur_Right','S193761_TibFib_Right','S193761_Patella_Right'};
tracked_objects_L={'S193761_Femur_Left','S193761_TibFib_Left','S193761_Patella_Left'};



%%%%%%%%%%%%%%%%%%%%%%%%%%%%%%%%%%%%%%%%%%%%%%%%%%%%%%%%%%%%%%%%%%%%%%%
%%%%%%%%%%%%%%%%%%%%%%%%%%%%%%%%%%%%%%%%%%%%%%%%%%%%%%%%%%%%%%%%%%%%%%%
%%%%%%%%%%%%%%%%%%%%%%%%%%%%%%%%%%%%%%%%%%%%%%%%%%%%%%%%%%%%%%%%%%%%%%%
%%%%%%%%%%%%%%%%%%%%%%%%%%%%%%%%%%%%%%%%%%%%%%%%%%%%%%%%%%%%%%%%%%%%%%%
%%%%%%%%%%%%%%%%%%%%%%%%%%%%%%%%%%%%%%%%%%%%%%%%%%%%%%%%%%%%%%%%%%%%%%%BASE
CODE%%%%%%%%%%%%%%%%%%%%%%%%%%%%%%%%%%%%%%%%%%%%%%%%%%%%%%%%%%%%%%%%%%%
%% Import DSX File
dsx_filepath=[dsx_subject_path,dsx_filename];
dsx_xml_orig=xml2struct(dsx_filepath);


%% Find current cube configuration
configs=dsx_xml_orig.subject.sessions.session.configurations.configuration;
cube_index=-1;
for count_config=1:length(configs)
   tempname=configs{1,count_config}.Attributes.name;
   if testCharPresentInChar(tempname,cubename,1)==1
      cube_index=count_config;
   end
end
trials=configs{1,cube_index}.trials;
trials.trial={}

%% get list of all cinefiles
allcines=dir(allcines_path)
cine_filenames={};

counter=1;
for count_files=1:length(allcines)
   [~,~,temp_ext]=fileparts(allcines(count_files).name);
   if strcmp(temp_ext,'.cine')
%     if allcines(count_files).bytes>0
      cine_filenames{1,counter}=allcines(count_files).name;
      cine_filenames{1,counter}=cine_filenames{1,counter}(1:end-21);
      counter=counter+1;
   end
end

cine_filenames=cine_filenames(1,1:2:end)
trial_names=cine_filenames';


%% create all trial data
```

```
end_extensionA='_Cam_14201_Cine1.cine';
end_extensionB='_Cam_14202_Cine1.cine';
load('template_trial_xml.mat','templatetrial')
frequency=25;


for count_trial=1:length(cine_filenames)
   current_trial_name=cine_filenames(1,count_trial);

   if checkSide==1
      if testCharPresentInChar(char(current_trial_name),'R',0)==1 ||
testCharPresentInChar(char(current_trial_name),'Right',0)==1
         tracked_objects=tracked_objects_R;
         disp('Right Side')
      else
         tracked_objects=tracked_objects_L;
         disp('Left Side')
      end
   else
      tracked_objects=tracked_objects_R;
   end

   % create current trial value
   current_trial=templatetrial;
   %change name
   current_trial.Attributes.name=char(current_trial_name);


   % add the views to the current trial
   trial_name_camA=char([char(current_trial_name),char(end_extensionA)]);
   trial_name_camB=char([char(current_trial_name),char(end_extensionB)]);

   temp_view=createViews(frequency,dsxcine_filepath,trial_name_camA,trial_name_camB);
   current_trial.views.view=temp_view;
   % add the objects to the current trial
   temp_object=createTrackedObjects(tracked_objects);
   current_trial.trackedobjects.trackedobject=temp_object.trackedobject;
   trials.trial{1,count_trial}=current_trial;
end


%% Update original dataset

configs{1,cube_index}.trials=trials;
dsx_xml_orig.subject.sessions.session.configurations.configuration=configs;
```

```
%% Export to DSX


output_dsx_filename=['S193761_FINAL_3']
output_dsx_filepath=[dsx_subject_path,output_dsx_filename];
struct2xml(dsx_xml_orig,output_dsx_filepath)


trial_name_file=[dsx_subject_path,'S193761_Cube04_Trials.xls'];
xlswrite(trial_name_file,trial_names);



%%%%%%%%%%%%%%%%%%%%%%%%%%%%%%%%%%%%%%%%%%%%%%%%%%%%%%%%%%%%%%
%%%%%%%%%%%%%%%%%%%%%%%%%%%%%%%%%%%%%%%%%%%%%%%%%%%%%%%%%%%%%%
%%%%%%%%%%%%%%%%%%%%%%%%%%%%%%%%%%%%%%%%%%FUNCTIONS%%%%%%%%%%
%%%%%%%%%%%%%%%%%%%%%%%%%%%%%%%%%%%%%%%%

%% create view function
function view=createViews(frequency,cine_rel_path,camAcine,camBcine)
    load('template_view_xml.mat','templateview');
    cine_filenames={camAcine,camBcine}
    for count_view=1:2
        templateview.view{1,count_view}.file.Attributes.frequency=num2str(frequency);

templateview.view{1,count_view}.file.Attributes.uri=char([cine_rel_path,cine_filenames{1,count_view}]);
    end
    view=templateview.view;
end

%% create trackedObject function
function trackedobjects=createTrackedObjects(objectnames)
    load('template_tracked_object_xml.mat','templateobject');
    trackedobjects.trackedobject={};
    for count_view=1:length(objectnames)
        trackedobjects.trackedobject{1,count_view}=templateobject;
        trackedobjects.trackedobject{1,count_view}.Attributes.name=char(objectnames{1,count_view});
    end
end
```

MAIN DSX Code

```
%% Process DSX DATA Wrapper
% Created by Thor Andreassen
% Last Edited by Thor Andreassen 4/23/20


%% READ DSX Transforms
%% Clearing
clear
```

```
close all
clc


%%%%%%%%%%%%%%%%%%%%%%%%%%%%%%%%%%%%%%%%%%%%%%%%%%%%%%%%%%%
%%%%%%%%%%%%%%%%%%%%%%%%%%%%%%%%%%%
%%%%%%%%%%%%%%%%%%%%%%%%%%%%%%%%%%%%%%%%%%%%%%%%%%%%%%%%%%%
%%%%%%%%%%%%%%%%%%%%%%%%%%%%%%%%%%%
%% USER INPUT Base properties and File Paths
fluoro_frequency_filter=.5;
loadcell_frequency_filter=6;

WantFilterFluoro=1;
WantViconSync=1;
WantViconLoadCell=1;
WantLaxityData=1;
WantFilterLoadCell=1;
WantKinPlot=0;
WantLaxityPlots=0;
WantAnimate=1;
WantSaveKinData=0;
WantSaveDynData=0;

RL='L';
transform_path='R:\Research Common\HDL\Projects\HSSR\Data\U01\Aim 2\S193761\DSX\Transforms\';
results_path='R:\Research Common\HDL\Projects\HSSR\Data\U01\Aim 2\S193761\Results\';
stl_path='R:\Research Common\HDL\Projects\HSSR\Data\U01\Aim 2\S193761\STLs\';
vicon_genanalog_path='R:\Research Common\HDL\Projects\HSSR\Data\U01\Aim 2\S193761\Vicon\Force Data\';

pretrial_name='S193761_1_17_20_Cube02_';
trial_name='Internal90_06'
subject_name='S193761';

vicon_genanalog_pathname=[vicon_genanalog_path,RL,'_',trial_name,'.csv'];

loadcell_calibration=1;
%%%%%%%%%%%%%%%%%%%%%%%%%%%%%%%%%%%%%%%%%%%%%%%%%%%%%%%%%%%
%%%%%%%%%%%%%%%%%%%%%%%%%%%%%%%%%%%
%%%%%%%%%%%%%%%%%%%%%%%%%%%%%%%%%%%%%%%%%%%%%%%%%%%%%%%%%%%
%%%%%%%%%%%%%%%%%%%%%%%%%%%%%%%%%%%
%% Create base Data Processing Parameters
if RL=='L'
   RL_longname='Left';
else
   RL_longname='Right';
end

% The following lines create functions that are the calibrated Voltage -->
% Force fits for the various load cells. If a different load cell
% calibration was used, add it as a new case. and change the above load
% cell case number of loadcell=...
if WantViconLoadCell==1 && WantViconSync==1
   syms Volt
   if loadcell_calibration==1 %orange load cell
      voltfunc=-232.28*Volt+8.0679;
      loadCellVolttoForce=matlabFunction(voltfunc);
   elseif loadcell_calibration==2 %gray load cell new
      voltfunc=344.03*Volt-3.457;
      loadCellVolttoForce=matlabFunction(voltfunc);
```

```
    elseif loadcell_calibration==3 % gray load cell
        voltfunc=Volt*520.1-2.3087;
        loadCellVolttoForce=matlabFunction(voltfunc);
    else

    end
end
%% Load Tibial Transform
tibia_endfilename=[subject_name,'_TibFib_',RL_longname,'_transforms.txt'];
tibia_transform_filename=[pretrial_name,RL,'_',trial_name,'_',tibia_endfilename];
tibia_transform_filepath=[transform_path,tibia_transform_filename];
tibia_transform_data=dlmread(tibia_transform_filepath,'\t',1,0);

%% Load Femur Transform
femur_endfilename=[subject_name,'_Femur_',RL_longname,'_transforms.txt'];
femur_transform_filename=[pretrial_name,RL,'_',trial_name,'_',femur_endfilename];
femur_transform_filepath=[transform_path,femur_transform_filename];
femur_transform_data=dlmread(femur_transform_filepath,'\t',1,0);

%% Load Patella Transform
patella_endfilename=[subject_name,'_Patella_',RL_longname,'_transforms.txt'];
patella_transform_filename=[pretrial_name,RL,'_',trial_name,'_',patella_endfilename];
patella_transform_filepath=[transform_path,patella_transform_filename];
patella_transform_data=dlmread(patella_transform_filepath,'\t',1,0);

%% Determine Fluoro Frames and Times

fluoro_frame_start=max([tibia_transform_data(1,1),femur_transform_data(1,1),patella_transform_data(1,1)])
fluoro_frame_end=min([tibia_transform_data(end,1),femur_transform_data(end,1),patella_transform_data(end,1)])
fluoro_time_start=max([tibia_transform_data(1,2),femur_transform_data(1,2),patella_transform_data(1,2)])
fluoro_time_end=min([tibia_transform_data(end,2),femur_transform_data(end,2),patella_transform_data(end,2)])
if size(femur_transform_data,1)>1
    fluoro_samplerate=(fluoro_frame_end-fluoro_frame_start)/(fluoro_time_end-fluoro_time_start);
    fluoro_times=fluoro_time_start:(1/fluoro_samplerate):fluoro_time_end;
    single_frame=0;
else
    fluoro_samplerate=50;
    fluoro_times=fluoro_time_start
    single_frame=1;
end

%% Create Uninterpolated and Interpolated Transform DATA
% Despite DSX documentation, the transform file is actually Local
% coordinate system to Global Coordinate system



% Determine First and Last Common Frame

% % The following for loop is used to remove any rows that are NaN's that
% % may be gaps in the data that will not be able to be read by the rest of
% % the code. DSX can output NaN's in rows if data was not tracked at that
% % frame.
tibia_transform_uninterpolate=[];
if single_frame==0
    for counti=size(tibia_transform_data,1):-1:1
        tempnan=isnan(tibia_transform_data(counti,:));
        if ismember(1,tempnan) || tibia_transform_data(counti,1)>fluoro_frame_end ||
tibia_transform_data(counti,1)<fluoro_frame_start
```

```
            tibia_transform_data=[tibia_transform_data(1:(counti-1),:);tibia_transform_data((counti+1):end,:)];
        end
    end

    femur_transform_uninterpolate=[];
    for counti=size(femur_transform_data,1):-1:1
        tempnan=isnan(femur_transform_data(counti,:));
        if ismember(1,tempnan) || femur_transform_data(counti,1)>fluoro_frame_end ||
femur_transform_data(counti,1)<fluoro_frame_start
            femur_transform_data=[femur_transform_data(1:(counti-1),:);femur_transform_data((counti+1):end,:)];
        end
    end

    patella_transform_uninterpolate=[];
    for counti=size(patella_transform_data,1):-1:1
        tempnan=isnan(patella_transform_data(counti,:));
        if ismember(1,tempnan) || patella_transform_data(counti,1)>fluoro_frame_end ||
patella_transform_data(counti,1)<fluoro_frame_start
            patella_transform_data=[patella_transform_data(1:(counti-1),:);patella_transform_data((counti+1):end,:)];
        end
    end
end


interpolation_type=1; %1=linear, 2=spline, 3=pchip, 4=makima
for counti=1:size(tibia_transform_data,1)
    tibia_transform_uninterpolate(counti).frame=tibia_transform_data(counti,1);
    tibia_transofrm_uninterpolate(counti).time=tibia_transform_data(counti,2);
    temp=[tibia_transform_data(counti,3:6);...
        tibia_transform_data(counti,7:10);tibia_transform_data(counti,11:14);...
        tibia_transform_data(counti,15:18);];
    tibia_transform_uninterpolate(counti).transform=rotateTransMat(temp,2);

end
[~,~,Tibia_to_GCS_TransMat,Tibia_Frames]=interpolateTransMatFrames(tibia_transform_uninterpolate,interpolation
_type,WantFilterFluoro,fluoro_samplerate,fluoro_frequency_filter);

for counti=1:size(femur_transform_data,1)
    femur_transform_uninterpolate(counti).frame=femur_transform_data(counti,1);
    femur_transform_uninterpolate(counti).time=femur_transform_data(counti,2);
    temp=[femur_transform_data(counti,3:6);...
        femur_transform_data(counti,7:10);femur_transform_data(counti,11:14);...
        femur_transform_data(counti,15:18);];
    femur_transform_uninterpolate(counti).transform=rotateTransMat(temp,2);

end
[~,~,Femur_to_GCS_TransMat,Femur_Frames]=interpolateTransMatFrames(femur_transform_uninterpolate,interpolat
ion_type,WantFilterFluoro,fluoro_samplerate,fluoro_frequency_filter);

for counti=1:size(patella_transform_data,1)
    patella_transform_uninterpolate(counti).frame=patella_transform_data(counti,1);
    patella_transform_uninterpolate(counti).time=patella_transform_data(counti,2);
    temp=[patella_transform_data(counti,3:6);...
        patella_transform_data(counti,7:10);patella_transform_data(counti,11:14);...
        patella_transform_data(counti,15:18);];
    patella_transform_uninterpolate(counti).transform=rotateTransMat(temp,2);

end
```

```
[~,~,Patella_to_GCS_TransMat,Patella_Frames]=interpolateTransMatFrames(patella_transform_uninterpolate,interpolation_type,WantFilterFluoro,fluoro_samplerate,fluoro_frequency_filter);

%% Calculate Transformations
Tibia_to_Femur_TransMat=Femur_to_GCS_TransMat;
Patella_to_Femur_TransMat=Femur_to_GCS_TransMat;
Patella_to_Tibia_TransMat=Femur_to_GCS_TransMat;
for counti=1:length(Femur_Frames)
    Femur_to_GCS_TransMat(:,:,counti)=rotateTransMat(Femur_to_GCS_TransMat(:,:,counti));
    Tibia_to_GCS_TransMat(:,:,counti)=rotateTransMat(Tibia_to_GCS_TransMat(:,:,counti));
    Patella_to_GCS_TransMat(:,:,counti)=rotateTransMat(Patella_to_GCS_TransMat(:,:,counti));

Tibia_to_Femur_TransMat(:,:,counti)=inv(Femur_to_GCS_TransMat(:,:,counti))*(Tibia_to_GCS_TransMat(:,:,counti));

Patella_to_Femur_TransMat(:,:,counti)=inv(Femur_to_GCS_TransMat(:,:,counti))*(Patella_to_GCS_TransMat(:,:,counti));

Patella_to_Tibia_TransMat(:,:,counti)=inv(Tibia_to_GCS_TransMat(:,:,counti))*(Patella_to_GCS_TransMat(:,:,counti));
end

%% Calculate Kinematics

kinTF_raw=zeros(length(Femur_Frames),6);
kinPF_raw=zeros(length(Femur_Frames),6);
kinPT_raw=zeros(length(Femur_Frames),6);
for counti=1:length(Femur_Frames)
    kinTF_raw(counti,:)=calculateGSKinFromTransMat(squeeze(Tibia_to_Femur_TransMat(:,:,counti)),RL);
    kinPF_raw(counti,:)=calculateGSKinFromTransMat(squeeze(Patella_to_Femur_TransMat(:,:,counti)),RL);
    kinPT_raw(counti,:)=calculateGSKinFromTransMat(squeeze(Patella_to_Tibia_TransMat(:,:,counti)),RL);
end

%% Plotting Kinematics DATA
if WantKinPlot==1
    titles = {'TF raw FE','TF raw VV','TF raw IE','TF raw ML','TF raw AP','TF raw SI','PF raw FE','PF raw VV','PF raw IE','PF raw ML','PF raw AP','PF raw SI'};
    ylabels = {'Flexion(+)/Extension(-)','Varus(-)/Valgus(+)','Internal(-)/External(+)','Medial(-)/Lateral(+)','Anterior(+)/Posterior(-)','Superior(+)/Inferior(-)'};

    for i=1:6
        figure; hold on; set(gca,'FontSize',14);
        title(titles{i},'FontSize',14);
        plot(fluoro_times,kinTF_raw(:,i),'Color',[0.7 0 0],'LineWidth',3);
        ylabel(ylabels{i},'FontSize',14);
    end
end

%% Load Vicon Synch Data and Generic Analog/Load Cell Data
if WantViconSync==1
    [temp_vicon,vicon_data.genanalog.samplerate]=getViconFrameData(vicon_genanalog_pathname);
    vicon_data.fluoro.samplerate=vicon_data.genanalog.samplerate;
    vicon_data.fluoro.TTLdata=temp_vicon(:,2);
    vicon_data.genanalog.voltagedata=temp_vicon(:,1);

vicon_data.fluoro.falling_edge_frame=max(findThresholdLocations(vicon_data.fluoro.TTLdata,vicon_data.genanalog.samplerate,1,.1,0));
    vicon_data.fluoro.falling_edge_time=vicon_data.fluoro.falling_edge_frame/vicon_data.fluoro.samplerate;
```

```
    vicon_data.fluoro.times=[0:(1/(vicon_data.fluoro.samplerate)):((length(vicon_data.fluoro.TTLdata)-
1)/(vicon_data.fluoro.samplerate))];

    fluoro_time_start_invicon=fluoro_time_start+vicon_data.fluoro.falling_edge_time;
    fluoro_time_end_invicon=fluoro_time_end+vicon_data.fluoro.falling_edge_time;
    fluoro_times_invicon=fluoro_times+vicon_data.fluoro.falling_edge_time;

    if WantViconLoadCell==1

        vicon_data.genanalog.forcedata=loadCellVolttoForce(vicon_data.genanalog.voltagedata);
        if WantFilterLoadCell==1
            [B,A]=butter(4,(loadcell_frequency_filter/((vicon_data.fluoro.samplerate)/2)));
            vicon_data.genanalog.forcedata=filtfilt(B,A,vicon_data.genanalog.forcedata);
        end

        applied_load=interp1(vicon_data.fluoro.times,vicon_data.genanalog.forcedata,fluoro_times_invicon);
        if WantLaxityData==1

         if testCharPresentInChar(trial_name,'External',0) || testCharPresentInChar(trial_name,'Internal',0)
            torqueType=1;
            applied_load=applied_load*(2.5*2.54)/100;
         else
            torqueType=0;
         end

         if testCharPresentInChar(trial_name,'Posterior',0) || testCharPresentInChar(trial_name,'Internal',0)
            applied_load=-applied_load;
         end

        end
    end

end

%% Plot Laxity
if WantLaxityPlots==1
    figure;
    if torqueType==1
        plot(kinTF_raw(:,3),applied_load,'o');
    else
        plot(kinTF_raw(:,5),applied_load,'o')
    end
end

%% Save DATA
    % Save Dynamics Results
    if WantSaveDynData==1 && WantViconSync==1 && WantViconLoadCell==1 && WantLaxityData==1
        save([results_path,'Dynamics\',subject_name,'_',RL,'_',trial_name,'_Dynamics_DATA.mat'],...

'kinTF_raw','kinPF_raw','kinPT_raw','Tibia_to_Femur_TransMat','Tibia_to_GCS_TransMat','Patella_to_Femur_Trans
Mat',...
            'Patella_to_Tibia_TransMat','Patella_to_GCS_TransMat','Femur_to_GCS_TransMat','torqueType',...
            'vicon_data','fluoro_times','fluoro_times_invicon','applied_load');
        header={'TF F(+)E','TF VrVl(+)','TF IE(+)','TF ML(+)','TF A(+)P','TF S(+)I','PF F(+)E','PF VrVl(+)','PF
IE(+)','PF ML(+)','PF A(+)P','PF S(+)I','PT F(+)E','PT VrVl(+)','PT IE(+)','PT ML(+)','PT A(+)P','PT S(+)I'};
        if torqueType==0
            header=[header,'Load (N)'];
        else
            header=[header,'Load (N*m)'];
```

```
        end
        xlswrite([results_path,'Dynamics\',subject_name,'_',RL,'_',trial_name,'_Dynamics.xlsx'],header,'Original','A1');
        kin_lcs_cell = num2cell([kinTF_raw kinPF_raw kinPT_raw applied_load']);

xlswrite([results_path,'Dynamics\',subject_name,'_',RL,'_',trial_name,'_Dynamics.xlsx'],kin_lcs_cell,'Original','A2');

        disp(['File saved ',[results_path,'Dynamics\',subject_name,'_',RL,'_',trial_name,'_Dynamics.xlsx']])
    end

    % Save Kinematics Results
    if WantSaveKinData==1
        save([results_path,'Kinematics\',subject_name,'_',RL,'_',trial_name,'_Kinematics_DATA.mat'],...

'kinTF_raw','kinPF_raw','kinPT_raw','Tibia_to_Femur_TransMat','Tibia_to_GCS_TransMat','Patella_to_Femur_Trans
Mat',...
            'Patella_to_Tibia_TransMat','Patella_to_GCS_TransMat','Femur_to_GCS_TransMat');
        header={'TF F(+)E','TF VrVl(+)','TF IE(+)','TF ML(+)','TF A(+)P','TF S(+)I','PF F(+)E','PF VrVl(+)','PF
IE(+)','PF ML(+)','PF A(+)P','PF S(+)I','PT F(+)E','PT VrVl(+)','PT IE(+)','PT ML(+)','PT A(+)P','PT S(+)I'};
        xlswrite([results_path,'Kinematics\',subject_name,'_',RL,'_',trial_name,'_Kinematics.xlsx'],header,'Original','A1');
        kin_lcs_cell = num2cell([kinTF_raw kinPF_raw kinPT_raw]);

xlswrite([results_path,'Kinematics\',subject_name,'_',RL,'_',trial_name,'_Kinematics.xlsx'],kin_lcs_cell,'Original','A2');

        disp(['File saved ',[results_path,'Kinematics\',subject_name,'_',RL,'_',trial_name,'_Kinematics.xlsx']])
    end



%% Load stls
if WantAnimate==1
    femur_filename=[subject_name,'_Femur_Left_aligned.stl'];
    femur_filepath=[stl_path,femur_filename];
    tibia_filename=[subject_name,'_TibFib_Left_aligned.stl'];
    tibia_filepath=[stl_path,tibia_filename];
    patella_filename=[subject_name,'_Patella_Left_aligned.stl'];
    patella_filepath=[stl_path,patella_filename];

    [femur.faces,femur.vertices]=stlRead2(femur_filepath);
    [femur.faces,femur.vertices]=reducepatch(femur.faces,femur.vertices,.1);
    [tibia.faces,tibia.vertices]=stlRead2(tibia_filepath);
    [tibia.faces,tibia.vertices]=reducepatch(tibia.faces,tibia.vertices,.1);
    [patella.faces,patella.vertices]=stlRead2(patella_filepath);
    [patella.faces,patella.vertices]=reducepatch(patella.faces,patella.vertices,.1);
end
%% Animation
if WantAnimate==1
    fig=figure(200); hold on;
    view([1,0,0])
    set(fig,'color','k');
    axis off;
    counter=1;
    pat_pos=((Patella_to_Femur_TransMat(:,:,1))*[ones(size(patella.vertices,1),1) patella.vertices(:,1:3)]')';
    tib_pos=((Tibia_to_Femur_TransMat(:,:,1))*[ones(size(tibia.vertices,1),1) tibia.vertices(:,1:3)]')';
    fem_pos=([ones(size(femur.vertices,1),1) femur.vertices(:,1:3)]')';
%     tib_pos=(inv(GCS_to_Tibia_TransMat(:,:,1))*(Tibia_to_Femur_TransMat(:,:,1))*[ones(size(tibia.vertices,1),1)
tibia.vertices(:,1:3)]')';
%     fem_pos=(inv(GCS_to_Femur_TransMat(:,:,1))*[ones(size(femur.vertices,1),1) femur.vertices(:,1:3)]')';

    Femoral.handle = patch('Vertices',fem_pos(:,2:4),'Faces',femur.faces);
```

```
   % % % the following is a good color for bone
%     % "[0.992156863212585,0.917647063732147,0.796078443527222]"

set(Femoral.handle,'FaceColor',[0.992156863212585,0.917647063732147,0.796078443527222],'FaceLighting','flat','E
dgeColor','none','FaceAlpha',1.0);
   Tibial.handle = patch('Vertices',tib_pos(:,2:4),'Faces',tibia.faces);

set(Tibial.handle,'FaceColor',[0.992156863212585,0.917647063732147,0.796078443527222],'FaceLighting','flat','Edg
eColor','none','FaceAlpha',1.0);

   Patellar.handle = patch('Vertices',tib_pos(:,2:4),'Faces',patella.faces);

set(Patellar.handle,'FaceColor',[0.992156863212585,0.917647063732147,0.796078443527222],'FaceLighting','flat','Ed
geColor','none','FaceAlpha',1.0);

   light
   light('Position',[-1 0 0],'Style','infinite')
   light('Position',[0 -1 0],'Style','infinite')
   light('Position',[0 0 -1],'Style','infinite')
   lighting phong
                        view([0 1 0])%Frontal Plane View
%     view([1 0 0])%Saggital Plane View
   axis([-175,175,-175,175,-175,175]);
   for k=1:size(kinTF_raw,1)
      k
      hold off
      tib_pos=((Tibia_to_Femur_TransMat(:,:,k))*[ones(size(tibia.vertices,1),1) tibia.vertices(:,1:3)]')';
      pat_pos=((Patella_to_Femur_TransMat(:,:,k))*[ones(size(patella.vertices,1),1) patella.vertices(:,1:3)]')';
%        fem_pos=([ones(size(femur.vertices,1),1) femur.vertices(:,1:3)]')';
%        Femoral.handle.Vertices=fem_pos(:,2:4);
      Tibial.handle.Vertices=tib_pos(:,2:4);
      Patellar.handle.Vertices=pat_pos(:,2:4);

      pause(.001)

   end
end
```

Filter and Interpolate DSX DATA

```
function
[interpolated_TransAndFrames,TransMAT_raw,TransMAT_filt,frames]=interpolateTransMatFrames(Transform_data,i
nterptype,filter_YN,frequency_sampling,frequency_filter,frame_data)
% Created by Thor Andreassen
% 4/23/20
% This function takes in either matrix with row and columns for the
% Transformation and pages for each of the frames given. And a vector
% containing the corresponding frames for each of the pages in the
% Transform_data. Or it takes in a single input Transform_data, which is an
% array of structures containing in the following format.
% Transform_data(count).frame=frame#, and
% Transform_data(count).transform=TransMat.
% Note the transformation should be of the form [R,V;0,1]
```

```
    if nargin==6
        for counti=1:length(frame_data)
            transform_uninterpolate(counti).frame=frame_data(counti);
            transform_uninterpolate(counti).transform=squeeze(Transform_data(:,:,counti));
        end
    elseif nargin==5
        transform_uninterpolate=Transform_data;
    else
        error('Number of Input Arguments to Function interpolateTransMatFrames is incorrect');
    end

    if interptype==1
        interpolate_type='linear';
    elseif interptype==2
        interpolate_type='spline';
    elseif interptype==3
        interpolate_type='pchip';
    elseif interptype==4
        interpolate_type='makima';
    else
        interpolate_type='linear';
    end


    %% Create Temporary Kinematic DATA
    for counti=1:size(transform_uninterpolate,2)
        kinematics_unterpolate_frame(counti)=transform_uninterpolate(counti).frame;

[kinematics_unterpolate_angle1(counti),kinematics_unterpolate_angle2(counti),kinematics_unterpolate_angle3(counti)
]=dcm2angle(transform_uninterpolate(counti).transform(2:4,2:4),'XYZ');
        temp_vector=transform_uninterpolate(counti).transform(2:4,1);
        kinematics_unterpolate_trans1(counti)=temp_vector(1);
        kinematics_unterpolate_trans2(counti)=temp_vector(2);
        kinematics_unterpolate_trans3(counti)=temp_vector(3);
    end



    %% Interpolate Kinematic DATA
    % Interpolate angles
    if length(kinematics_unterpolate_frame)>1
        kinematics_interpolate_frame=kinematics_unterpolate_frame(1):kinematics_unterpolate_frame(end);

kinematics_interpolate_angle1=interp1(kinematics_unterpolate_frame,kinematics_unterpolate_angle1,kinematics_inter
polate_frame,interpolate_type);

kinematics_interpolate_angle2=interp1(kinematics_unterpolate_frame,kinematics_unterpolate_angle2,kinematics_inter
polate_frame,interpolate_type);

kinematics_interpolate_angle3=interp1(kinematics_unterpolate_frame,kinematics_unterpolate_angle3,kinematics_inter
polate_frame,interpolate_type);

        % Interpolate Translations

kinematics_interpolate_trans1=interp1(kinematics_unterpolate_frame,kinematics_unterpolate_trans1,kinematics_interp
olate_frame,interpolate_type);

kinematics_interpolate_trans2=interp1(kinematics_unterpolate_frame,kinematics_unterpolate_trans2,kinematics_interp
olate_frame,interpolate_type);
```

```
kinematics_interpolate_trans3=interp1(kinematics_unterpolate_frame,kinematics_unterpolate_trans3,kinematics_interp
olate_frame,interpolate_type);
   else
      kinematics_interpolate_frame=kinematics_unterpolate_frame;
      kinematics_interpolate_angle1=kinematics_unterpolate_angle1;
      kinematics_interpolate_angle2=kinematics_unterpolate_angle2;
      kinematics_interpolate_angle3=kinematics_unterpolate_angle3;
      kinematics_interpolate_trans1=kinematics_unterpolate_trans1;
      kinematics_interpolate_trans2=kinematics_unterpolate_trans2;
      kinematics_interpolate_trans3=kinematics_unterpolate_trans3;
   end


   %% Filter Kinematics DATA

   if length(kinematics_unterpolate_frame)>1 && filter_YN==1
      [B,A]=butter(4,(frequency_filter/(frequency_sampling/2)));

      % Interpolate angles
      kinematics_filter_frame=1:kinematics_unterpolate_frame(end);
      kinematics_filter_angle1=filtfilt(B,A,kinematics_interpolate_angle1);
      kinematics_filter_angle2=filtfilt(B,A,kinematics_interpolate_angle2);
      kinematics_filter_angle3=filtfilt(B,A,kinematics_interpolate_angle3);
      % Interpolate Translations
      kinematics_filter_trans1=filtfilt(B,A,kinematics_interpolate_trans1);
      kinematics_filter_trans2=filtfilt(B,A,kinematics_interpolate_trans2);
      kinematics_filter_trans3=filtfilt(B,A,kinematics_interpolate_trans3);
   end


   kinematics_interpolate_frame=kinematics_interpolate_frame-kinematics_interpolate_frame(1)+1;
   %% Create New Transformation DATA

   for counti=1:kinematics_interpolate_frame(end)
      interpolated_TransAndFrames(counti).frame=kinematics_interpolate_frame(counti);

temprotmat=angle2dcm(kinematics_interpolate_angle1(counti),kinematics_interpolate_angle2(counti),kinematics_inter
polate_angle3(counti),'XYZ');

tempvec=[kinematics_interpolate_trans1(counti);kinematics_interpolate_trans2(counti);kinematics_interpolate_trans3(
counti);];
      temptransmat=zeros(4,4);
      temptransmat(2:4,2:4)=temprotmat;
      temptransmat(2:4,1)=tempvec;
      temptransmat(1,1)=1;
      interpolated_TransAndFrames(counti).transform_raw=temptransmat;
      interpolated_TransAndFrames(counti).transform_filt=temptransmat;
      TransMAT_raw(:,:,counti)=temptransmat;
      TransMAT_filt(:,:,counti)=temptransmat;
      frames(counti)=kinematics_interpolate_frame(counti);
   end


    %% Create Filtered Transformation DATA

   if length(kinematics_unterpolate_frame)>1 && filter_YN==1
      for counti=1:kinematics_interpolate_frame(end)
         interpolated_TransAndFrames(counti).frame=kinematics_interpolate_frame(counti);
```

```
temprotmat=angle2dcm(kinematics_filter_angle1(counti),kinematics_filter_angle2(counti),kinematics_filter_angle3(co
unti),'XYZ');
        tempvec=[kinematics_filter_trans1(counti);kinematics_filter_trans2(counti);kinematics_filter_trans3(counti);];
        temptransmat=zeros(4,4);
        temptransmat(2:4,2:4)=temprotmat;
        temptransmat(2:4,1)=tempvec;
        temptransmat(1,1)=1;
        interpolated_TransAndFrames(counti).transform_filt=temptransmat;
        TransMAT_filt(:,:,counti)=temptransmat;
    end
end
```